

**A study of the influence of water and pressure on
viscosity of silicate melts**

**Eine Studie zum Einfluss von Wasser und Druck
auf
die Viskosität von silikatischen Schmelzen**

Von der Naturwissenschaftlichen Fakultät der Universität Hannover

zur Erlangung des Grades

Doktor der Naturwissenschaften

Dr. rer. nat.

genehmigte Dissertation

von

Dipl. Geol. Pierdomenico Del Gaudio

Geboren am 04.10.1969 in Catanzaro (Italien)

2005

Angestellt:

Prüfungskollegium:

Prüfungsvorsitz: Prof. Dr. Paul Heitjans

Referent: Dr. PD Harald Behrens

Korreferenten: Prof. Dr. Joachim Deubener

Prof. Dr. François Holtz

Tag der Promotion: 22.07.2005

Acknowledgements

Thanks to *Harald Behrens*, for proposing me the subject and for all the help he gave me during my work in Hannover. Thanks *Harald* for your suggestions and for nice explanation about high pressure lab and for the opportunity you gave to me.

Thanks to *Frank Schulze* which introduced me to the viscometer and for all the support he gave me to make it working.

I appreciated a lot the help given to by *Fred Blaine* in correcting in good English this Thesis. Thanks for all the help you gave to me and the time you spent with me during these four years in Hannover.

Thanks to *Francesco Vetere* and *Jan Schüssler* for sharing with me the office for all this time. Thanks *guys* for the help both of you gave to me since last day (I mean last night). Thanks *Ciccio* for all the great help I got from you. Thanks *Jan* for your nice help especially when I was fighting with your language.

I appreciated a lot the discussion and the help of *François Holtz*, *Marcus Nowak* and *Jürgen Köpcke*. Thanks to all of you.

Thanks to the entire workshop. *Willy*, *Otto* and *Bettina* you helped a lot me and I spent nice time there. I appreciated a lot your work.

I had great help from and fun with *Roman Botcharnikov*, *Kevin Klimm*, *Dominich Schreen* and *Antje Wittemberg*, *Eule*. All of you were great during this time.

Thanks *Joachim Deubener* and *Ralf Müller* for the nice suggestions you gave to me.

Thanks *Daniel Neuville* and *Pascal Richet* to giving me the possibility to come to your lab in Paris.

Grazie *Guido Ventura* e *Rosanna De Rosa* per l'aiuto e le possibilità che mi avete dato per andare avanti.

Un grazie particolare alla mia famiglia, *Teresa*, *Leonardo* la mia *mamma* e tutti gli altri per tutto quello che avete sempre fatto per me.

A special thanks to all the people I want to thanks but I forget right now. I apologize for that. Thanks!

A mio padre che purtroppo non c'è più per godersi questo felice momento con me. Grazie tanto anche a te!

Zusammenfassung

Die Viskosität silikatischer Gläser und Schmelzen ist einer der bedeutendsten physikalischen Parameter, welcher sowohl magmatische Prozesse im Erdmantel und der Erdkruste steuert als auch für die Herstellung industriell gefertigter Glasprodukte von Bedeutung ist. Die Rheologie silikatischer Gläser und Schmelzen wird vor allem durch deren chemische Zusammensetzung, Temperatur, gelöste Volatile (insbesondere Wasser), Druck und die darin verteilten Kristalle und Gasblasen beeinflusst.

Zahlreiche Arbeiten beschäftigten sich mit dem Einfluss des Druckes auf die Viskosität polymerisierter und depolymerisierter Schmelzen im Bereich niedriger Viskositäten (Kushiro 1978, Brearley et al. 1986, Mori et al. 2000, Suzuki et al. 2002, Reid et al. 2003, Tinker et al. 2004, Suzuki et al. 2005). Im Bereich hoher Viskositäten wurden nur wenige Studien durchgeführt (Schulze et al. 1999, Behrens & Schulze 2003, Liebske et al. 2003), die jedoch auf einen starken Einfluss des Druckes auf die Viskosität deuten. Ein Ziel meiner Arbeit war die Untersuchung der Druckabhängigkeit der Viskosität von Schmelzen im System Anorthit ($\text{CaAl}_2\text{Si}_2\text{O}_8$, An)–Diopsid ($\text{CaMgSi}_2\text{O}_6$, Di) im Bereich hoher Viskositäten (10^8 bis 10^{11} Pa·s) mittels eines „Parallel-Platten-Viskosimeter“ (Schulze et al. 1999).

Die Untersuchung der Druckabhängigkeit der Viskosität im Bereich 0.1 bis 400 MPa ergab einen Übergang von einer negative Druckabhängigkeit im Falle polymerisierter An-Schmelzen zu einer positive Abhängigkeit für

depolymerisierte Di-Schmelzen, vergleichbar mit Beobachtungen früherer Studien im System Albit-Diopsid (Behrens & Schulze 2003). Bei einer Temperatur von 1186 K nimmt die Viskosität einer Anorthit-Schmelze bei einer Druckänderung von 0.1 MPa auf 400 MPa um 0.32 log-Einheiten ab. Die Viskosität einer Diopsid-Schmelze erhöht sich dagegen für den selben Druckanstieg um 1.21 log-Einheiten.

Für die mittlere Zusammensetzung $An_{50}-Di_{50}$ wird die Druckabhängigkeit vernachlässigbar klein. Ein vergleichbarer Trend wurde für Alkali-reiche silikatische Schmelzen beobachtet, die eine nur schwach ausgeprägte negative Druckabhängigkeit der Viskosität für Tetrasilikat (niedriger Alkali-Gehalt) und eine schwach positive Abhängigkeit für Metasilikat (hoher Alkali-Gehalt) zeigen. Diese Ergebnisse deuten an, dass die Netzwerk-bildenden Kationen einen geringen Einfluss auf die Druckabhängigkeit der Viskosität haben; der Polymerisationsgrad ist der bedeutendste Einflussfaktor.

Die Viskosität einer Schmelze aus kommerziellem Floatglas (Firma Potters-Ballotini, Zusammensetzung in Gew%: 13.7 Na₂O – 9.8 CaO – 3.3 MgO – 0.2 FeO+Fe₂O₃ – 0.1 K₂O – 0.4 Al₂O₃ – 72.5 SiO₂) (im Bereich 10¹ bis 10¹¹ Pa·s) wurde systematisch über einen weiten Bereich bezüglich Temperatur und Wassergehalt mittels „Parallel-Platten-Viskosimetrie“ und „falling sphere“-Experimenten unter Druck untersucht. Im Allgemeinen ist der Einfluss von Temperatur und Wassergehalt auf die Viskosität der Schmelze größer als der des Druckes. Die Druckabhängigkeit wird für diese Zusammensetzung mit einem mittleren Depolymerisierungsgrad (molarer Anteil NBO nahe 0.15) als

vernachlässigbar klein angenommen (Behrens & Schulze 2003). Basierend auf einer VFT-Gleichung wurde ein neues Modell zur Voraussage der Viskosität als Funktion von Temperatur (in K) und Wassergehalt (in Gew%) entwickelt:

$$\log \eta = -3.37 + \frac{5089.5}{(T - 497.4)} - \frac{1391.1}{(T - 503.2)} \cdot \frac{w}{(w^{0.5975} - 2.6713 + 0.0035 \cdot T)}$$

Die Schmelzviskosität von Floatglas kann mit diesem Modell über den gesamten experimentellen Temperaturbereich (T_g bis 1523 K) und Wassergehalt (0 bis 4.8 Gew%) innerhalb von 0.23 log-Einheiten vorhergesagt werden. Dieses Modell findet weite Anwendungsbereiche in der industriellen Glasherstellung, deren Temperaturen und Wassergehalte innerhalb des modellierten Bereichs liegen.

Schlagerworte: Viskosität silikatischer Schmelzen, Druck, Wassergehalt

Abstract

The viscosity of silicate glasses and melts is one of the most important physical properties governing magmatic processes in Earth's mantle and crust as well as the manufacturing of glass tools. Rheology of silicate glass and melts is mainly influenced by bulk composition of the melt, temperature, dissolved volatiles (especially water content), pressure and dispersed crystals and bubbles.

Several works have looked at the effect of pressure on melt viscosity in the low viscosity range for polymerized to depolymerised melts (Kushiro 1978, Brearley et al. 1986, Mori et al. 2000, Suzuki et al. 2002, Reid et al. 2003, Tinker et al. 2004, Suzuki et al. 2005). However few studies have been done in the high viscosity range (Schulze et al. 1999, Behrens and Schulze 2003 and Liebske et al. 2003) where it is supposed pressure has a stronger effect on viscosity. The aim of my work was to investigate the pressure effect on viscosity in the high viscosity range (10^8 to 10^{11} Pa·s) for melts along the anorthite ($\text{CaAl}_2\text{Si}_2\text{O}_8$, An)–diopside ($\text{CaMgSi}_2\text{O}_6$, Di) join using a parallel plate viscometer (Schulze et al. 1999).

It was found that the pressure dependence of viscosity in the range 0.1–400 MPa varies from negative in the case of the polymerized An–melt to positive for depolymerised Di–melt, similar as observed in previous studies for the system albite–diopside (Behrens and Schulze 2003). At 1186 K viscosity of melt anorthite decreases in the order of 0.32 log units when pressure increases from ambient pressure to 400 MPa. Viscosity of diopside melt increases in the order of 1.21 log units when pressure increases from 0.1 MPa to 400 MPa.

The pressure effect becomes negligible for the intermediate composition $\text{An}_{50}\text{–Di}_{50}$. A similar trend was observed for alkali silicates melts which have only a slight negative pressure dependence of viscosity for the tetrasilicate (low alkali) to a slight positive

dependence for the metasilicate (high alkali). This result indicates that the nature of net-forming cation has a minor influence on pressure dependence of viscosity; the degree of depolymerization is the most important factor.

Melt viscosity of a commercial float glass (from Potters–Ballotini Company, composition in wt%: 13.7 Na₂O – 9.8 CaO – 3.3 MgO – 0.2 FeO+Fe₂O₃ – 0.1 K₂O – 0.4 Al₂O₃ – 72.5 SiO₂) (in the range of 10¹ to 10¹¹ Pa·s) was systematically investigated over a wide range of temperatures (593 – 1523 K) and water contents (0 to 4.82 wt.% H₂O) using parallel plate viscometry and falling sphere experiments under pressure. In general, the effects of temperature and water content on melt viscosity are much larger than that of pressure and the pressure effect on viscosity is expected to be negligible for this composition, with intermediate degree of melt depolymerization (molar fraction of NBO near 0.15) (Behrens and Schulze 2003).

A new model, based on a VFT equation, was developed for the prediction of viscosity as function of temperature (in K) and water content (in wt.%) is proposed:

$$\log \eta = -3.37 + \frac{5089.5}{(T - 497.4)} - \frac{1391.1}{(T - 503.2)} \cdot \frac{w}{(w^{0.5975} - 2.6713 + 0.0035 \cdot T)}$$

The melt viscosity of the float glass can be successfully predicted using this model, to within 0.23 log units, over the entire range of experimental temperature (T_g – 1523 K) and water contents (0 to 4.8 wt.%). This model has wide applicability in glass manufacturing where temperatures and water contents are well within this range.

Key word: Viscosity of silicate melts, pressure, water content

Content

Zusammenfassung.....	I
Abstract.....	II
1. Introduction.....	1
2. Theoretical background.....	6
2.1. Structure of glasses.....	6
2.2. Liquid to glassy state.....	9
2.3. Viscosity.....	11
2.4. Effect of H ₂ O.....	14
3. Experimental methods.....	16
3.1. Sample preparation.....	16
3.2. Determination of bulk composition.....	19
3.3. Determination of water content.....	21
3.4. Viscosity measurements (high viscosity range).....	31
3.5. Viscosity measurements (low viscosity range).....	43
4. Effect of water content on viscosity of float glass.....	47
4.1. Experimental results.....	47
4.2. Data modeling.....	55
4.3. Discussion.....	61
4.4. Application.....	67
5. Pressure dependence of viscosity of silicate melts.....	70
5.1. Experimental results.....	70
5.2. Discussion.....	81
6. Conclusion.....	84
7. Appendix.....	87

8. References.....100

1. Introduction

Knowledge about viscosity of silicate melts is important for understanding and modeling magmatic processes in the Earth's crust and upper mantle as well as for the techniques used in material science (e.g. glass science). The viscous response of magma to an applied stress controls the dynamics of magma ascent in the conduit as well as the flux of lavas after eruption. Magma generation, differentiation processes in magma chamber, phenomena of mixing of different magmas are strongly influenced by viscosity. Viscosity is also of great importance for industrial applications ranging from production of rock wool and glasses for automobiles, windows and bottles to semiconductor wafers.

The major factors controlling viscosity (hence a viscous flow) of the melt are the temperature, bulk composition, volatile content (especially H₂O, but also CO₂, sulfur species, etc.), crystal and bubble content, and pressure. With temperature viscosity varies by about 10 orders of magnitude between the liquidus and the glass transition range. Composition also has a strong effect on viscosity; at 1500 K the viscosity of pure silica is about 10 orders of magnitude higher than that of molten diopside. The viscosity range spanned by the data is wider at low temperature range than at high temperature range where they tend to converge (viscosity at $T \rightarrow \infty$ was found to be $10^{-4.3 \pm 0.74}$ Pa·s by Russell et al. 2003).

Several methods are available for melt viscosity measurements in the low and high viscosity range. For measurements in the low viscosity range, the most used are the concentric cylinder and the falling sphere method. The first method is mainly used for measurements of liquid viscosity at ambient pressure for anhydrous melts or melts containing small amount of H₂O. In this technique, a spindle is immersed in a crucible containing the melt and the viscosity is measured by imposing either a constant torque or a constant shear to the spindle. The second method is used mainly under pressure in piston

cylinder or multi anvil cell or externally and internally heated pressure vessel (Shaw 1962, Shaw 1974, Kushiro 1976, Schulze et al. 1996, Holtz et al. 1999). This method allows the viscosities of water-rich melts to be derived from the velocity of a falling sphere in the melt. This is calculated from the settling distance of a sphere and the time duration of the experiment.

In the high melt viscosity range (10^8 to 10^{11} Pa·s) the methods suitable for viscosity measurement are the creep apparatus (uniaxial compression technique), micropenetration method, and fiber elongation method. The creep apparatus can operate both at ambient pressure (Neuville and Richet 1991) and under pressure (Schulze et al. 1999). Using this device, a weight is used to apply a force on the sample and the viscosity is given by the ratio between the applied stress and the measured strain rate. The micropenetration method (Hess et al. 1995) consists of measuring the rate at which a sphere moves into the melt surface under a fixed load. In the fiber elongation method (Sakka et al. 1981, Böse et al. 2001, Goto et al. 2005) the viscosity is given by the relationship between elongation rate of a glass fiber and applied load. Viscosities of hydrous melts can be measured operating with the above methods because dehydration is very slow, however dehydration may occur in some cases.

Water is the most abundant volatile dissolved in magmas (> 0.1 wt.%) as well as in technical glasses (< 0.1 wt.%). It is well understood that even small amount of water dissolved in the melt have a tremendous effect on melt viscosity. The effect of water on melt viscosity is more pronounced than the effect of any other volatiles as well as the effect of alkali oxides (Hess et al. 1995). Previous studies already showed a large decrease of viscosity when small amount of H_2O were introduced in the melt and a continued but less pronounced decrease in viscosity as the melt becomes increasingly water-rich. The above trend has to be related to the water speciation. In support of this, studies on water speciation in glass showed the following trend: at lowest water in the glass, H_2O is mainly

dissolved as OH groups and in water-rich glass water is mainly dissolved as molecular H₂O (eg. Stolper 1982, Nowak and Behrens 2001).

The effect of dissolved water on the viscosity of technical glass (container or float glass) is not well studied. Industrial glass melted with air/gas or air/oil flame contain 0.028 – 0.035 wt.% water, if melted with oxycombustion water content may reach 0.045 – 0.065 wt.% (Deubener et al. 2003). Viscosities of commercial or technical glasses at ambient pressure in the low and high viscosity range are broadly studied. Viscosities were measured for: dry window glass by Euler et al. (1957) (low viscosity range), Zanotto et al. (1999) (calculated, which discredited the myth of flowing cathedral glasses), Priven (2001) (near the glass transition temperature), Sanditov et al. (2003) (high viscosity range); dry float glass by Prado et al. (2003) (high and low viscosity range); dry DGG standard glass by Meerlender (1974) (high and low viscosity range); dry soda-lime-silica glass by Böse et al. (2001) (high and low viscosity range) and water bearing soda-lime-silica glass by Sakka et al. (1981) (high viscosity range).

Measurements at low viscosities for water-rich melts can only be made with the falling sphere method under high pressure. When operating at ambient pressure (e.g. with concentric cylinder) vesiculation and therefore dehydration will occur. While operating in the high viscosity range it is possible to measure viscosity of water-rich melt even at ambient pressure. For instance, the duration of viscosity experiments is lower than the time required for significant diffusion of water out of the melt. Crystallization may also occur when measuring the viscosity of water-rich melt at certain $C_{water}-T$ condition depending on the composition of the melt. The difficulties to investigate hydrous glasses, especially with several weight percent of H₂O, make the knowledge of viscosities of water bearing glass more uncommon.

The effect of pressure on melt viscosity is not as strong the effects of composition, temperature and dissolved water content but it is still significant. Several studies were

performed in the low viscosity range where the pressure is supposed to have a smaller effect than in the high viscosity range (Behrens and Schulze, 2003). Above the glass transition the only method known for measuring effect of pressure on viscosity was performed by Schulze et al. (1999). A creep apparatus was build to operate under pressure (50 to 400 MPa) in an internally heated argon pressure vessel (IHPV) (Schulze et al. 1999). Viscosity was found to have a negative dependence with pressure in polymerized melts switching to a positive dependence in depolymerized melts (Behrens and Schulze 2003). Hence, viscosity will increase during the isothermal ascent of polymerized melts (e.g. anhydrous rhyolite) while it will decrease during the isothermal ascent of depolymerized melts (e.g. anhydrous to hydrous basalts). Therefore, the glass transition will be at a lower temperature for polymerized melts (e.g. anhydrous rhyolite) deep in the crust, than at the surface.

The aim of my work was to investigate and to model the effect water, as well as the effect of pressure, on viscosity of a silicate melt. A commonly used technical glass (Potters-Ballotini company) was chosen to study the effect of dissolved water on viscosity of depolymerized glass. My goal is to establish a model for determination of viscosity as function of temperature, water content. To extend the existing viscosity dataset (which includes primarily anhydrous float glass data), I provide a set of viscosity data for H₂O-bearing float glass melt (from 0.02 wt.% to 4.82 wt.%) under pressure (from 50 MPa to 400 MPa) in a wide range of temperature (from 1523 K to 593 K). In order to cover the whole range of Non-Arrhenian viscosities of the hydrous melt two methods were used for this study. High temperature viscosities were studied using falling sphere method and a creep apparatus for high viscosity range; both methods were used in an internally heated pressure (argon) vessel (IHPV).

The second part of my work was the investigation of the pressure effect on viscosity of silicate melts. In order to develop a general model to describe the pressure dependence of

melt viscosity as a function of melt polymerization, variation of viscosity along the anorthite-diopside join and on alkali silicate melts was investigated.

2. Theoretical background

2.1 Structure of glasses

A silicate glass can be considered as a frozen-in undercooled liquid, retaining the structure of the melt. The most effective theory on structure of glasses is surely Zachariasen's Theory (Scholze 1988, Shelby 2005) which asserts a very small difference of energy between glass and crystal with same chemical composition. Therefore in the glass, the same states of bonding or units of structure as in crystals should coexist.

Crystals are formed by linked $(\text{SiO}_4)^{4-}$ tetrahedrons forming 2-D and 3-D regular, ordered networks. Glasses lack the periodic long range order typical for crystals, but show only intermediate and short range order. Assuming that the same structural units are present in the glasses as in the crystals, formation of random network of such units had been proposed by Zachariasen.

On this basis Zachariasen formulated the following rules for glass formation:

- i. No oxygen is linked to more than two cations.
- ii. The coordination number of cations has to be small: 3 or 4.
- iii. Oxygen polyhedra share corners, not edges or faces.
- iv. For 3-D networks, at least three corners must be shared.

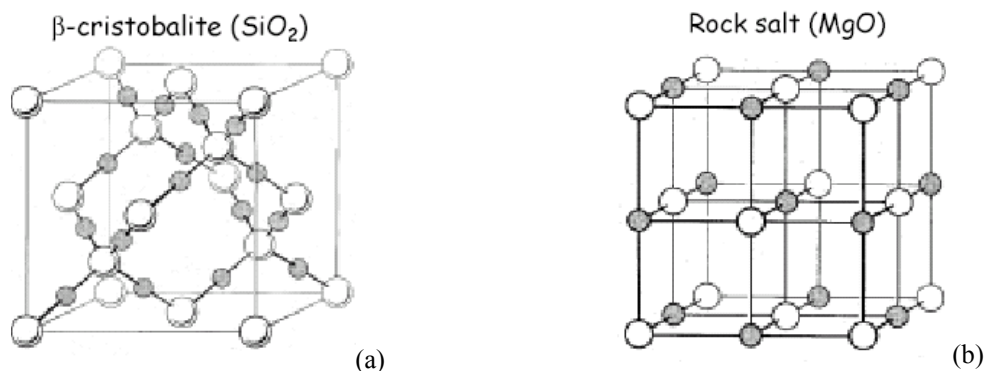


Fig.2.1. (a) In SiO_2 (β -cristobalite) no oxygen is linked to more than 2 cations, cations prefer tetrahedral bonding (small coordination number of cations), polyhedra share 4 corners; SiO_2 satisfies all Zachariasen's rules. (b) In MgO , oxygen is linked to 6 cations, cations prefer octahedral bonding, polyhedra are sharing edge; MgO does not satisfy Zachariasen's rules (Shelby 2005).

In general, glass formation occurs when all four rules are satisfied. SiO₂, B₂O₃, P₂O₅ and GeO₂ are totally following these rules, and hence are glasses formers. In contrast, MgO, CaO, Na₂O and Al₂O₃ do not form glasses, except possibly at extremely high cooling rates.

Pure SiO₂ glass is characterized by bonds between one O²⁻ and two Si⁴⁺. These oxygens are named bridging oxygens (BO), and the Si cations are named *network formers*. When an alkali oxide or an alkali earth oxide is incorporated to a random network of bridging oxygens, the alkali cation breaks the bond between one O²⁻ and one Si⁴⁺. Oxygen bonded only to one tetrahedral Si cation are named non-bridging oxygens (NBO) and the cations producing NBO are named *network modifiers*. Si⁴⁺ can be substituted by Al³⁺ and Fe³⁺ in tetrahedral sites when charge compensating cations (e.g. Na⁺, K⁺, Ca²⁺) are available. The degree of polymerization can be described in terms of the structural-chemical parameter *NBO/T*, which means the number of non-bridging oxygen per tetrahedral cation. The value of the above expression can be calculated by the following formula (Mysen et al. 1985)

$$\frac{NBO}{T} = \frac{1}{T} \cdot \sum_{i=1}^i n \cdot M_i^{n+}$$

where M_i^{n+} is the proportion of network modifying cations, “*i*”, with electrical charge n^+ .

This parameter (NBO/T) is the best indicator of the degree of polymerization in a silicate melt structure.

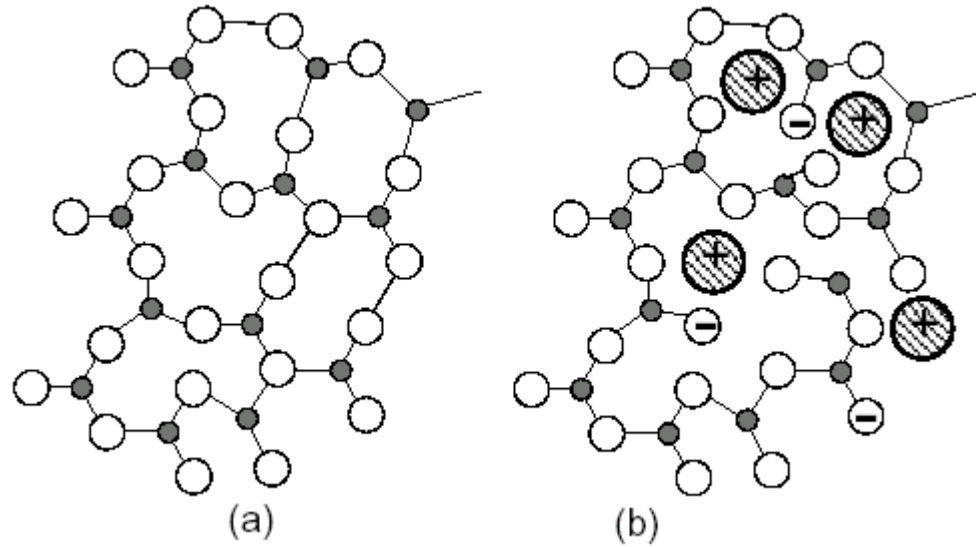


Fig.2.2. Schematic glass network. (a) SiO₂ network (Si⁴⁺ filled circles and O²⁻ white circles). (b) SiO₂ network modified through addition of Na₂O (redrawn after Shelby 2005).

The structure of the silicate network in a glass is mainly determined by the degree of polymerization of the silicate tetrahedra which can be described by abundance of different Qⁿ species, where Qⁿ denotes a tetrahedron linked by bridging oxygen atoms to n adjacent tetrahedra, thus denoting the number of bridging oxygens per tetrahedron. The range of n is between 0, for isolated tetrahedra, to 4, for a fully polymerized network.

Several methods provide insights to the structure of glass and one may draw conclusions on glass structure from the dependence of certain glass properties on composition. Chemical analysis provides structural implications only indirectly. Physical methods of structural analysis, such as X-ray scattering and absorption, better evaluate structure/composition relationships.

X-ray scattering studies of silicate glasses have provided the most widely used conceptual models of glass/melt structure. One of the major assumptions is that silicate glasses and melts have local atomic arrangements that are dictated by the same crystal chemical principles as the local atomic arrangements in silicate crystals. This assumption has proven to be true in general.

X-ray absorption spectroscopy (XAS) can be used for studying specific elements in glasses and melts when they are present in small concentration (<100 ppm). X-ray absorption near edge structure spectra (XANES) provide structural information on cations in silicate glasses and melts. These spectra are also sensitive to the oxidation state of cation.

Small amounts of water are usually present in natural glasses as well as in technical glasses. This introduces structural groups involving hydrogen and oxygen atoms. The water in glass is mainly dissolved as OH groups for small amounts of total water. At higher water contents, molecular water occurs. In highly polymerized melts (such as albite) one bridging bond (e.g. Si – O – Si) is broken for every two hydroxyl groups dissolved in the melt. This results in depolymerization of the melt with the addition of water. In this case viscosity decreases strongly when small amount of water are added to the glass and less strongly as more water is dissolved. This can be explained by the efficiency of OH groups at softening the structure of the glass, versus molecular water. The effect of small amount of water in a glass is the lowering of bridging oxygens with an increase of non-bridging oxygens.

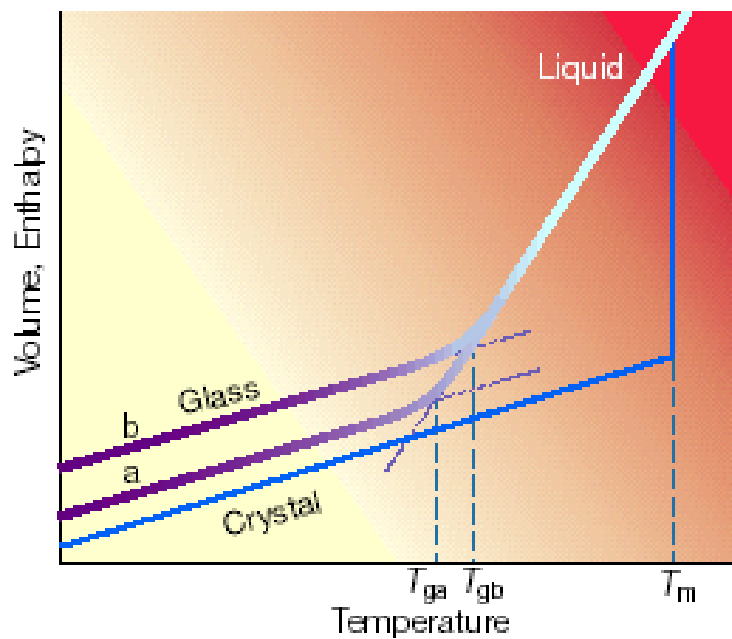
2.2 Liquid to glassy state

In general, when a silicate melt is cooled slowly from higher than T_m (melting temperature) its volume decreases gradually and decreases abruptly at T_m due to crystallization. When temperature decreases below T_m a further reduction of volume occurs but now with a lower thermal expansion coefficient. The curve liquid-crystal, in Fig.2.3, corresponds to conditions of thermodynamic equilibrium. If crystallization does not occur at T_m , the volume of the melt decreases along the curve liquid-glass. At the transition range the temperature dependence of the volume changes gradually to that of a solid. At this

point the melt becomes a solid. This happens independent of composition at uniform viscosity about 10^{12} Pa·s. It is common to designate the corresponding temperature as the glass transition temperature T_g . One can describe a glass as a solid below T_g , and as a melt above T_g . The glass transition (T_g) range is a kinetic barrier dividing the glass state from the liquid state. This range, in which transition occurs, varies with the cooling rate therefore the properties of the glass are not only depending on temperature but also on the thermal history. Slow cooling provides a lower T_g than faster cooling.

The intersection of liquid and glass trends of the volume, enthalpy versus temperature curve gives us a definition of T_g , this point usually occurs near a value of $2/3T_m$, Tammann (1933).

Fig.2.3. Scheme of the first order (e.g. enthalpy H , volume V) thermodynamic properties temperature dependence. T_m is the melting temperature. Slow cooling rate produce a glass transition at T_{ga} , faster cooling rate at T_{gb} (drawn after Debenedetti and Stillinger 2001).



2.3 Viscosity

A wide number of equations have been introduced to describe viscosity as a function of temperature and composition. The most known function which fit the data over a certain range of viscosity and temperature is the two parameter Arrhenian equation

$$\log \eta = A_a + \frac{B_a}{T}$$

where A_a is the logarithm of viscosity at infinite temperature, $B_a = E_a/R$ is the ratio between the activation energy of viscosity (E_a), which represents the magnitude of the energy threshold to be overcome, and R the gas constant while T is the temperature in Kelvin; this equation is quite good in fitting viscosity data in a narrow, low viscosity range or a narrow, high viscosity range. When both, high and low viscosity data are available the Arrhenian approach often poorly reproduces both high and low viscosities. Most melts show a deviation from Arrhenian behaviour over the whole range of temperatures. A T_g -scaled Arrhenius representation of melt viscosities (Fig.2.4) shows the Angell's strong-fragile pattern.

The Vogel-Fulcher-Tammann (VFT) is an empirical equation which provides a reasonable fit for most of glasses

$$\log \eta = A_{VFT} + \frac{B_{VFT}}{T - T_0}$$

where A_{VFT} is a constant representing the value of viscosity at infinite temperature, B_{VFT} is a constant representing the pseudo-activation energy associated with viscous flow and T_0 is the temperature (K) at which viscosity becomes infinite. This equation has no physical

meaning for $T < T_0$. For melt anorthite T_0 equals 850 K, therefore, viscosities at T lower than 850 K becomes undefined.

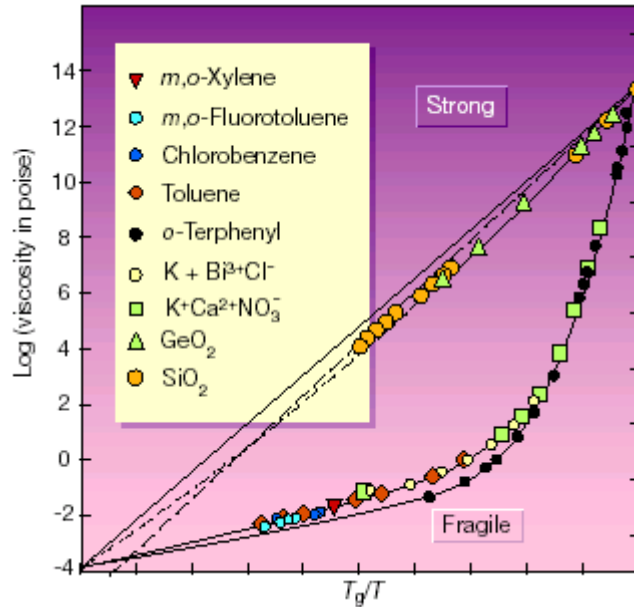


Fig.2.4 Strong-Fragile pattern after Angell et al. (2000). Strong melts approximate Arrhenian behaviour (linear relationship). Fragile melts have non-Arrhenian behaviour (drawn after Debenedetti and Stillinger 2001).

Description of viscosity in terms of Adam-Gibbs theory was proposed by Richet (1984). Since the viscosity is proportional to the relaxation times, one can deduce it by the following equation

$$\log \eta = A_e + \frac{B_e}{T \cdot S_{conf}}$$

where A_e is a constant B_e is approximately a constant related to the barrier of potential energy obstructing the structural rearrangement of the liquid, S_{conf} is the configurational entropy of the system.

The P-T dependence of viscosity can be represented by an Arrhenian equation type

$$\log \eta = A_a + \frac{E_a + V_a \cdot P}{R \cdot T}$$

in which E_a is related to the energy barrier for viscous flow and V_a may be considered as the apparent activation energy (m³/mol) or rather is related to the local volume changes during viscous flow.

The simplest modification of the Vogel-Fulcher-Tamman equation to account for pressure dependence may be to add a simply linear term to B_{VFT} which is related to local volume changes during viscous flow (Behrens and Schulze 2003).

$$\log \eta = A_{VFT} + \frac{B_{VFT} + C_{VFT} \cdot P}{T - T_0}$$

B_{VFT} is related to the energy barrier for viscous flow and C_{VFT} to the local volume changes during viscous flow.

A modified Adam-Gibbs equation which takes in account the pressure effect is proposed by Behrens and Schulze (2003). The pressure effect of viscosity is a change in the barrier for the transition from one stable structural configuration to another.

$$\log \eta = A_{AG} + \frac{B_{AG} + C_{AG} \cdot P}{T \cdot S_{conf}}$$

where C_{AG} is an analogue to the apparent activation volume or rather the volume change of a structural unit during transition between stable configurations.

2.4 Effect of H₂O

Water is dissolved in silicate melts as hydroxyl groups or molecular water. OH groups are usually bound to silicon but additional OH groups are linked to alkali earths (Xue and Kanzaki 2004). In glasses with higher total water content, H₂O can exist in molecular form. It is important to note that water impurities even at low concentrations (in the order of ppm) may have a substantial effect on the physicochemical properties of glasses. Replacement of bridging oxygens by nonbridging hydroxyl decreases the connectivity of the glass network leading to a decrease in both the viscosity and glass transformation temperature T_g and an increase in the tendency for crystallization in the glass.

Properties of glasses are much more influenced by the hydroxyl concentration than by any other modifiers. Useful methods for the measure of total water in glass are Karl-Fischer-Titration and also IR-Spectroscopy which can provide speciation information. Stuke et al. (submitted) proposed a systematic calibration of molar absorption coefficients for the near-infrared (NIR) bands for hydrous float glass and soda lime silica glass. The absorption bands at 4500 cm⁻¹ for OH groups and at 5200 cm⁻¹ for molecular water were used. For the determination of the species concentration the peak intensities of these bands were used and from the Lambert-Beer law the species concentration was determined:

$$C_{OH} = \frac{1802 \cdot A_{4500}}{d \cdot \rho \cdot \epsilon_{4500}}$$

$$C_{H_2O} = \frac{1802 \cdot A_{5200}}{d \cdot \rho \cdot \epsilon_{5200}}$$

where A denotes the absorbance (peak height), d the thickness (cm), ρ the density (g/l) and ϵ the molar absorption coefficient (L·mol⁻¹·cm⁻¹).

C_{OH} and C_{H_2O} are the concentrations of water dissolved as OH – groups and molecular H_2O , respectively.

An apparent saturation level of OH groups at 1.6 wt.% for float glasses and 2.2 wt.% in soda lime silica glasses was found at high total water content.

3. Experimental methods

3.1. Sample preparation

A technical float glass from Potters-Ballotini Company was used for the investigation of the effect of water on melts. Although the viscosity of dry float glass at ambient pressure is well known, there is a lack of viscosity data for water bearing float glass.

Glasses with water contents, in the range 0.03 - 4.82 wt.% were synthesized by melting glass spheres to which distilled water was added. Platinum capsules with an inner diameter of 6 mm and a length of 30-40 mm were used for the synthesis of the samples. To get glass with a homogeneous distribution of water three different size spheres (490-620 μm ; 100-200 μm ; 0-50 μm) were mixed in a ratio of 1:1:1, for 10-15 minutes with a shaking machine, then dried in an oven at 383 K for 30 minutes. For the synthesis of hydrous glasses the capsule was first welded at the bottom then filled stepwise with powder and water. To achieve a fully compact filling of the Pt-capsule each powder layer was compressed by a steel piston before inserting water. The capsules were sealed by arc welding to the top while the lower part of the capsules was cooled in water or with a tissue moistened with water and frozen in liquid nitrogen in order to avoid any evaporation of water during the sealing. To test for leakage, the capsules were weighed before and after annealing at 383 K for at least 60 minutes.

The synthesis of hydrous glasses was carried out in an internally heated gas (argon) pressure vessel for at least 24 h at temperature of 1523 K and under a pressure range of 200-500 MPa. Temperature was measured with four K-type thermocouples and controlled by an Eurotherm type 900 programmed controller with a precision of ± 5 K, while pressure was measured by a strain gauge manometer to a precision of ± 50 bar.

Each run was terminated by switching off the heating power while the pressure was maintained constant by automatic pumping. The initial cooling rate was about 200 K/min decreasing to about 100 K/min in the range of glass transition. This was fast enough to avoid crystallization in all samples resulting in a bubble- and crystal-free glass.

Dry anorthite ($\text{CaAl}_2\text{Si}_2\text{O}_8$), dry diopside ($\text{CaMgSi}_2\text{O}_6$) and three intermediate compositions were used to investigate the pressure effect on viscosity. Dry diopside (Di) and anorthite (An) were prepared from powdered calcium carbonate and oxides of the other components that were dried at 383 K for several hours; particular care was taken for

MgO because the powder may contain several wt% of absorbed H_2O and CO_2 . MgO and Al_2O_3 powder were heated with a ramp of 100 K/h in a 1 atm furnace up to 1073 K and then stored in a desiccator. The carbonate/oxide starting mixture was homogenised in ball mill for 10 – 15 min. To synthesize anorthite glass, a small amount of anorthite starting material was placed in a platinum crucible and melted in a furnace at 1873 K in air. After melting another small amount was added to the crucible and melted. This process was repeated until the desired amount of glass was reached. After a few hours in the furnace, the melt was quenched by pouring it on a brass plate. The resulting anorthite glass was crushed and sieved (to < 0.5 mm) and then melted again at 1873 K to improve homogeneity. After one hour the glass was quenched to room temperature inside the Pt-crucible by removing the crucible from the furnace. To allow stress relaxation the glass was annealed at ~ 1113 K for approximately one hour and then cooled to room temperature inside the crucible.

To obtain diopside glass the same procedure was used except for the quenching procedure. The glass was melted at 1873 K for one hour then quenched in a Pt-crucible to room temperature for few minutes. To allow stress relaxation the crucible was annealed at ~ 1053 K for approximately one hour and then quenched at room temperature within the crucible. After synthesis, cylindrical samples were cored from the raw anorthite and

diopside and thin sections were prepared for electron microprobe and infrared spectroscopy.

Part of the diopside and anorthite powder was crushed and mixed in appropriate proportion to produce intermediate composition ($\text{Di}_{75}\text{-An}_{25}$, $\text{Di}_{50}\text{-An}_{50}$ and $\text{Di}_{25}\text{-An}_{75}$), melted at 1873 K then quenched in air and annealed at ~ 1073 K.

The alkali silicate glasses were synthesized by melting mixtures of oxides and carbonates at 1873 K for 3 hours in a platinum crucible. In the synthesis of alkali silicate, the Pt-crucible was filled time per time by small amount of powder, as in the case with the anorthite glass. The glass was quenched by pouring the melt on a brass plate.



Fig.3.1 An example of a quenched glass (LNKS) in air, quenching was achieved by pouring the molten glass on a brass plate.

Due to the high carbonate content, the glass LNKS was synthesized by filling the Pt-crucible step-wise with small portions of powder and then melted in the furnace at 1673 K for about 30 sec. After the crucible was filled by all the powder the melt was left at temperature for 3 hours. The glass was then quenched by pouring the melt on a brass plate. In order to avoid reaction between glass surface and atmospheric water (especially in the metasilicate), the glass was stored in a desiccator. The same care was taken when

cylindrical samples where drilled, using paraffin for the cooling of the drill bit instead of water.

3.2. Determination of glass composition

The composition of float glass from Potters-Ballotini Company (72.01 SiO₂, 0.76 Al₂O₃, 0.10 Fe₂O₃, 3.92 MgO, 8.96 CaO, 13.13 Na₂O, 0.25 K₂O in wt%) was measured by Behrens and Stuke (2003).

The homogeneity and chemical composition of the glasses along the anorthite-diopside join were determined using a Cameca Cambax electron microprobe equipped with a SAMAX operating system. All data were obtained using 15 kV acceleration voltage, a defocused beam with a spot size of 15 to 20 μm, a current of 15 nA, 2 s counting time for *Na* and *K* and 5 s for the other elements. Calibration of elements is based on the following standards: *Na* on albite, *Si* and *Ca* on wollastonite, *Al* on Al₂O₃, *Mg* on MgO.

Chemical compositions for the glasses along the anorthite-diopside join are shown in Table 1a-b.

Different conditions were used to determine the composition of the glasses in the alkali silicate system. These data were obtained using 15 kV acceleration voltages, a defocused beam with a spot size of 4 to 20 μm, a current of 4 nA, 2 s counting time for *Na* and *K* and 5 s for the other elements. Calibration of the elements was the same than above. Lithium oxide was calculated by difference of the total weight percent and the rest of oxides (in wt%). The chemical compositions of the glasses are shown in table 2a-b.

Tab.1a Composition of glasses of the join An-Di in wt%

Composition in wt%					
Sample	An ₁₀₀	An ₇₅ Di ₂₅	An ₅₀ Di ₅₀	An ₂₅ Di ₇₅	Di ₁₀₀
SiO ₂	41.79	44.94	48.30	51.47	55.63
Al ₂ O ₃	35.91	28.24	20.05	10.75	0.01
MgO	0.01	3.73	7.93	12.63	17.91
CaO	21.59	22.54	23.55	24.93	26.29
K ₂ O	-	-	0.01	-	0.01
Na ₂ O	0.11	0.04	0.06	0.03	0.06
H ₂ O ^(*)	-	0.013(±0.001)	0.010(±0.001)	0.008(±0.001)	0.005(±0.001)

(*) H₂O content was measured by IR spectroscopy, the other components by electron microprobe.

Tab.1b Composition of glasses of the join An-Di in mol%

Composition in mol%					
Sample	An ₁₀₀	An ₇₅ Di ₂₅	An ₅₀ Di ₅₀	An ₂₅ Di ₇₅	Di ₁₀₀
SiO ₂	48.48	49.21	49.68	49.79	50.32
Al ₂ O ₃	24.55	18.22	12.15	6.13	0.01
MgO	0.02	6.09	12.16	18.21	24.14
CaO	26.83	26.44	25.95	25.84	25.48
K ₂ O	-	-	0.01	-	0.01
Na ₂ O	0.12	0.04	0.06	0.03	0.05
NBO/T	0.05	0.34	0.70	1.22	1.97
X _{NBO}	0.025	0.155	0.299	0.468	0.661

Tab.2a Composition of alkali silicate glasses in wt%

Composition in wt%				
Sample	LNKS/Glass1	LNK2S	LNK3S	LNK4S
SiO ₂	-	72.92	77.89	78.40
Li ₂ O	-	2.24*	2.77*	1.22*
Na ₂ O	-	9.69	7.66	7.81
K ₂ O	-	15.04	11.60	12.44
H ₂ O	-	0.020(±0.002)	0.022(±0.001)	0.015(±0.001)

(*) Calculated from difference between total oxides and 100 wt%.

Tab.2b Composition of alkali silicate glasses in mol%

Composition in mol%				
Sample	LNKS (1:1)	LNK2S (1:3)	LNK3S (1:3.8)	LNK4S (1:4.4)
SiO ₂	50.00*	75.64	79.25	81.36
Li ₂ O	16.66*	4.67	5.67	2.55
Na ₂ O	16.66*	9.74	7.55	7.86
K ₂ O	16.66*	9.95	7.53	8.23
NBO/T	1.33	0.64	0.52	0.46
X _{NBO}	0.500	0.277	0.232	0.206

(*) Nominal composition. The composition of the metasilicate was not measured because the difficulties for the preparation and analysis of a glass highly hygroscopic.

3.3. Determination of water content

Water content is an important parameter controlling various properties of silicate glasses and melts in natural systems, as well as the manufacturing of glass tools. For instance, the melt viscosity can decrease by several orders of magnitude when a few weight percent of H₂O are dissolved in the melt. Hence, a careful characterization of the water content and water speciation in the glasses is required.

Karl-Fischer titration (KFT)

The water content of water-rich glasses was measured after thermal dehydration using Karl-Fischer titration of the released H₂O:



HI and SO₃ are bonded by reagents in the titration solution (methanol, pyridinum derivates), so that the reaction proceeds quantitatively to the right hand side, with the addition of water. The necessary I₂ for the reaction is formed electrochemically in the anode of the titration cell ($\text{I}^- = \frac{1}{2}\text{I}_2 + \text{e}^-$). The amount of water participating to the reaction is correlated to the quantity of electrons used in the reaction. The reliability of the method was checked by analyzing materials with known water content (muscovite standard). The maximum error of the quantity of water is in the order of 6 – 18 µg.

The apparatus used for water determination was designed to analyze glasses with an H₂O content higher than 0.5 wt%. Therefore, the apparatus is not suitable for glasses synthesized at ambient pressure due to their low water contents (Behrens and Stuke 2003).

The major problem is the slow diffusion of water out of the melt so that the samples are not completely dehydrated during titration.

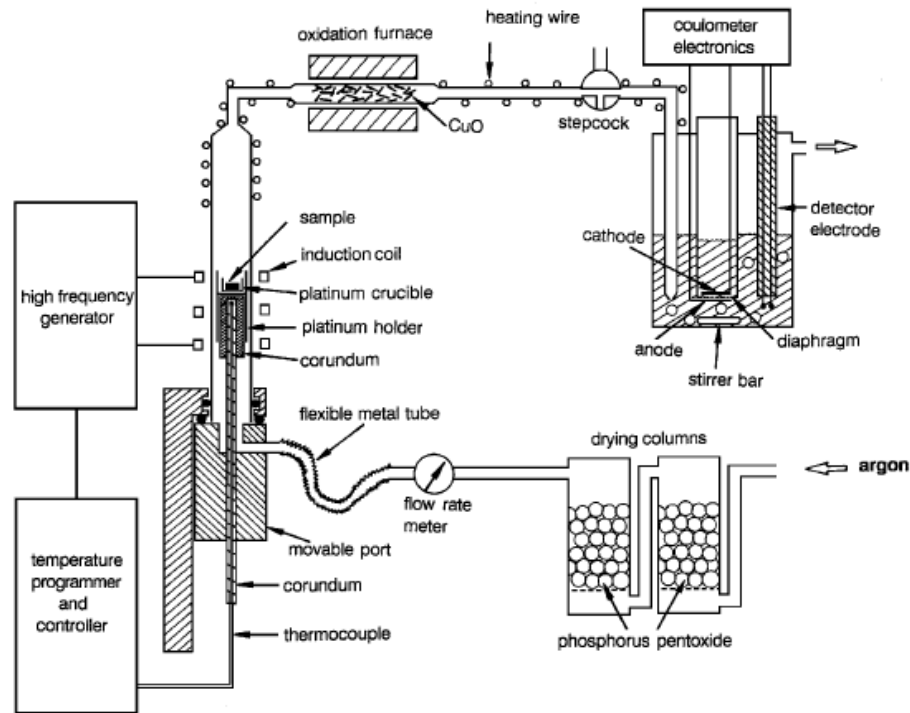


Fig.3.2 Schematic description of the Karl-Fischer titration apparatus (Behrens and Stuke 2003).

For each analysis a single piece of glass was used instead of ground glass in order to minimize the contribution of absorbed water on the glass surface. If the expected water content was more than 2 wt%, typically 10 to 20 mg were used in each analysis, if lower water contents were expected then 20 to 50 mg were used for analysis. The glasses pieces were introduced in the apparatus within a Pt-crucible. Dehydration of float glass was not explosive and hence encapsulating of the glasses was not required, as is necessary for aluminosilicate (Behrens et al. 1996). To minimize atmospheric contamination of H₂O, the apparatus was purged with a dry argon stream at a flow rate of 300 ml/min while loading of the sample and was flushed for two minutes after loading at the same rate, before starting titration. The sample was heated using a fast ramp by step-wise increasing the power of the

high frequency generator. A temperature of more than 1273 K was reached after 3 to 4 min and the titration was finished usually after 5 to 8 min. In order to correct for unextracted water a value must be added to the total water content measured with *KFT*. This value was calculated by Behrens and Stuke (2003) for Soda-Lime-Silica glasses and is 0.17 ± 0.04 wt% in samples containing less than 1.5 wt% of H₂O and 0.13 ± 0.04 wt% for glasses with higher water content.

IR spectroscopy

Slices were cut after experiments, for selected samples, from the cylinder along the major axis and also from the raw material after synthesis. The slices were doubly polished and then analyzed by IR-microspectroscopy. Thickness (50-1000 μm) was measured using a Mitutoyo micrometer with a precision of $\pm 2 \mu\text{m}$. The absorption spectra of the sections were recorded in mid-infrared (MIR) or near infrared (NIR) using a Bruker scope II IR microscope connected to an FTIR-spectrometer Bruker IFS 88.

Measurement conditions for MIR were: KBr beam splitter, 100 scans for sample and background and a spectra resolution of 2 cm^{-1} . The water concentration of samples Glas4 and FG9a were measured in the main chamber using a DTGS detector with an aperture size between 1 and 4 mm. Measurement conditions for NIR were: CaF₂ beam splitter, MCT detector, 50 scans for sample and background and a spectra resolution of 4 cm^{-1} .

The peak heights of the near-infrared absorbance at 4500 cm^{-1} (OH groups) and 5200 cm^{-1} (H₂O molecules) were used to determine the water content of hydrous glasses with an expected water content higher than 2.5wt%. The total H₂O content of hydrous glasses having lower water content than 2.5wt% was determined using mid-infrared bands at 3550 cm^{-1} and 2850 cm^{-1} caused by OH⁻ stretching vibrations of weakly and strongly H-bonding water species, respectively. The practical absorption coefficient ϵ_{pract} for the 2850 cm^{-1}

band in MIR is less sensitive to the water content than the one for 3550 cm^{-1} band in float glass as well in soda lime glass, Behrens and Stuke (2003), therefore ε_{2850} is more suitable for the determination of water content in such glasses.

The concentration of the water species and the total water content were calculated by the peak height of absorption bands with the Lambert-Beer law using absorption coefficient and density calculation from Behrens and Stuke (2003):

$$C_{\text{water}} = \frac{1801.5 \cdot A_i}{\rho \cdot d \cdot \varepsilon_i} \quad 3.2$$

C_{water} is the total water content (in wt%), A_i is the absorbance of i -band (where i is either 2850 or 3550 cm^{-1} in MIR), ρ is the density of the glass (g/l), d is the thickness (cm) of the sample and ε_i the absorption coefficient (mol/cm·l) of each i -band. The absorbance band at 2850 cm^{-1} is read and 4000 cm^{-1} is taken as background for the measurements in MIR with the following absorption coefficient: $\varepsilon_{2850} = 40.2 \pm 2.4\text{ l}\cdot\text{mol}^{-1}\cdot\text{cm}^{-1}$. The peak height of this band is calculated as the difference between the two absorbance values and is a suitable quantity for the total water determination, Behrens and Stuke (2003). Density of float glasses with different water contents was calculated after Behrens and Stuke (2003) by:

$$\rho = (2505 \pm 4) - (14.6 \pm 0.8) \cdot C_{\text{water}} \quad 3.3$$

In the NIR, using the equation 3.2, the concentrations of OH and H₂O species were calculated using the absorbance (A_i) at 4500 cm^{-1} and 5200 cm^{-1} , respectively. Total water is calculated as the sum of the concentrations of the two species. For a quantitative evaluation of the total water content, by NIR spectroscopy, the peak height of the bands at

4500 and 5200 cm^{-1} after baseline correction was used. The tangent to the curve is chosen as baseline and the following absorption coefficient are used: $\epsilon_{4500} = 0.54 \pm 0.01 \text{ l}\cdot\text{mol}^{-1}\cdot\text{cm}^{-1}$ and $\epsilon_{5200} = 1.10 \pm 0.02 \text{ l}\cdot\text{mol}^{-1}\cdot\text{cm}^{-1}$, Stuke and Behrens (submitted). The total H_2O content measured on the water bearing float glass ranges between 0.03 – 4.82 wt%. Measured water contents are shown in tables 3a and 3b.

Tab.3a Water content in float glass measured by MIR spectroscopy and KFT.

Sample	A_{2850}	thickness (cm)	density (g/l) ^(*)	Cwater (wt%)	KFT (wt%)
FG0a	0.085	0.0499	2505	0.03 ± 0.01	-
FG1	0.335	0.1366	2505	0.04 ± 0.01	-
FG2	0.073	0.0200	2505	0.06 ± 0.01	-
FG3	0.179	0.0200	2503	0.16 ± 0.02	-
FG4	0.214	0.0200	2502	0.19 ± 0.02	-
FG6a	0.220	0.0140	2501	0.28 ± 0.03	-
FG6b	1.621	0.1003	2501	0.29 ± 0.02	-
Glas2	0.164	0.0100	2500	0.29 ± 0.02	-
Glas3	0.273	0.0092	2497	0.53 ± 0.02	-
FG9a	0.353	0.0119	2493	0.53 ± 0.05	0.66 ± 0.08
FG9b	0.350	0.0093	2493	0.68 ± 0.03	-
Glas4	0.389	0.0092	2493	0.76 ± 0.09	-
FG10	0.239	0.0046	2491	0.93 ± 0.14	0.84 ± 0.16
FG11	0.479	0.0070	2487	1.23 ± 0.05	1.07 ± 0.14
FG12	0.662	0.0067	2479	1.79 ± 0.18	1.52 ± 0.07
FG13	0.919	0.0078	2474	2.14 ± 0.10	2.05 ± 0.08

Absorption coefficient: $\epsilon_{2850} = 40.2 \pm 2.4 \text{ l}\cdot\text{mol}^{-1}\cdot\text{cm}^{-1}$; FG9a was measured before experiment; FG9b was measured after experiment. ^(*) Calculated with eq. (3.3).

Tab.3b Water content in float glass measured by NIR spectroscopy and KFT.

Sample	thickness	density					Cwater	
	(cm)	(g/l) ^(*)	A_{4500}	A_{5200}	C_{OH} (wt%)	$C_{\text{H}_2\text{O}}$ (wt%)	(wt%)	KFT (wt%)
FG14a	0.0381	2468	0.049	0.058	1.72	1.02	2.74 ± 0.06	2.47 ± 0.07
FG14b	0.0385	2468	0.048	0.059	1.68	1.02	2.71 ± 0.12	-
FG18a	0.0379	2446	0.056	0.160	2.02	2.83	4.86 ± 0.19	4.66 ± 0.14
FG18b	0.0384	2443	0.054	0.166	1.93	2.89	4.82 ± 0.15	-
FG16a	0.0411	2450	0.060	0.135	2.00	2.20	4.20 ± 0.10	-
FG16b	0.0379	2450	0.054	0.134	1.95	2.37	4.32 ± 0.19	-
FG17a	0.0391	2440	0.056	0.163	1.97	2.79	4.76 ± 0.09	-
FG17b	0.0388	2446	0.056	0.146	1.98	2.52	4.49 ± 0.21	-
FG15a	0.0393	2443	0.056	0.135	1.96	2.31	4.27 ± 0.15	3.66 ± 0.12
FG15b	0.0376	2440	0.051	0.092	1.85	1.63	3.49 ± 0.06	-
FG8	0.1012	2498	0.051		0.67		0.67 ± 0.02	0.50 ± 0.09

Absorption coefficient: $\epsilon_{4500} = 0.54 \pm 0.01 \text{ l}\cdot\text{mol}^{-1}\cdot\text{cm}^{-1}$ and $\epsilon_{5200} = 1.10 \pm 0.02 \text{ l}\cdot\text{mol}^{-1}\cdot\text{cm}^{-1}$. For all the samples with suffix *a* the H₂O content is the water content before the experiment. Suffix *b* represents a measurement after experiment. ^(*) Calculated with eq. (3.3).

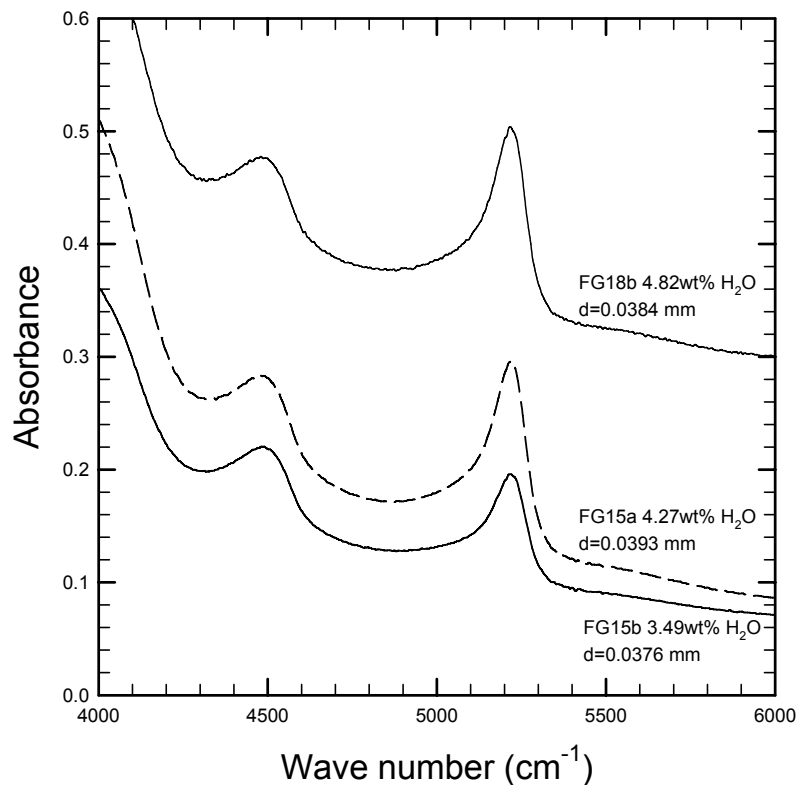


Fig.3.3 Near-infrared absorption spectra of two different float glasses. FG15a is the water content before the experiment while FG15b is the H₂O content in the same sample after the experiment. In the figure are indicated the water content (in wt%) and thickness of the section analysed.

Pre- and post-experiment water contents agree well in all but one case, indicating no significant water loss during experiments. The concentration profile of a float glass containing 0.54 wt% of H₂O (see Fig.3.4) shows no water loss after viscosity experiment. At most a rim of 20 μm in thickness was affected by desorption of water. The final water content of the sample FG15 was less (3.49 wt% instead 4.27 wt% H₂O) than before experiments. Water loss with this sample occurred during the falling sphere experiment and before the creep experiment (in chapter 4 it is shown that no water loss occurred during creep experiment, see Fig.4.2).

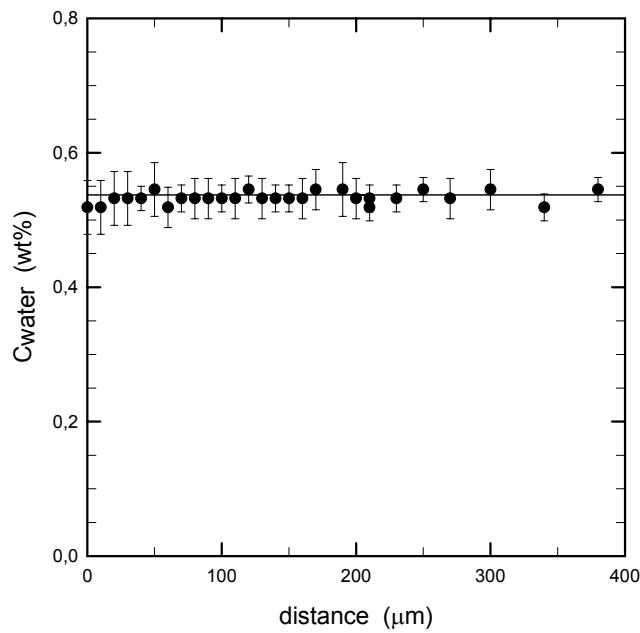


Fig.3.4 Profile of water concentration along the major axis of a float glass with a water content of 0.54 wt%.

For the calculation of the water content of the samples along the An-Di join and in the alkali silicate system the two-band model (Behrens and Stuke 2003) was used. The bands at 3550 and 2850 cm^{-1} were used to measure the fraction of OH oscillators involved in weak and strong H-bonding and the total water in silicate glasses was calculated using the following equation:

$$C_{\text{water}} = \frac{1802}{d \cdot \rho} \cdot \left(\frac{A_{3550}}{\varepsilon_{3550}} + \frac{A_{2850}}{\varepsilon_{2850}} \right)$$

The absorbance value of A_{3550} and A_{2850} were calculated by the difference between the peak height at 3550 and 2850 cm^{-1} , and the value at 4000 cm^{-1} . The absorption coefficients used for the water calculation are the following: $\varepsilon_{3550} = 71 \pm 2 \text{ l} \cdot \text{mol}^{-1} \cdot \text{cm}^{-1}$ and $\varepsilon_{2850} = 104 \pm 4 \text{ l} \cdot \text{mol}^{-1} \cdot \text{cm}^{-1}$ (Behrens and Stuke 2003). The absorbance of the anorthite was not measured because the determination of the values of A_{3550} and A_{2850} was not possible. Results for

MIR analysis are tabulated in Table 3c. Figure 3.5 and 3.6 show examples of MIR spectra obtained during analyses of various glasses.

Tab.3c Water content in An-Di and alkali silicate systems measured by MIR spectroscopy.

Sample	A_{3550}	A_{2850}	d (cm)	ρ (g/l)	C_{water} (wt%)
An ₁₀₀	-	-	-	-	-
An ₇₅ Di ₂₅	0.050	0.029	0.0502	2787	0.013 (± 0.001)
An ₅₀ Di ₅₀	0.037	0.025	0.0495	2841	0.010 (± 0.001)
An ₂₅ Di ₇₅	0.033	0.020	0.0492	2912	0.008 (± 0.001)
Di ₁₀₀	0.016	0.014	0.0489	2990	0.005 (± 0.001)
LNK2S	0.026	0.111	0.0494	2564	0.020 (± 0.020)
LNK3S	0.032	0.116	0.0501	2564	0.022 (± 0.010)
LNK4S	0.017	0.083	0.0495	2564	0.015 (± 0.012)

Density were calculated after Appen 2000.

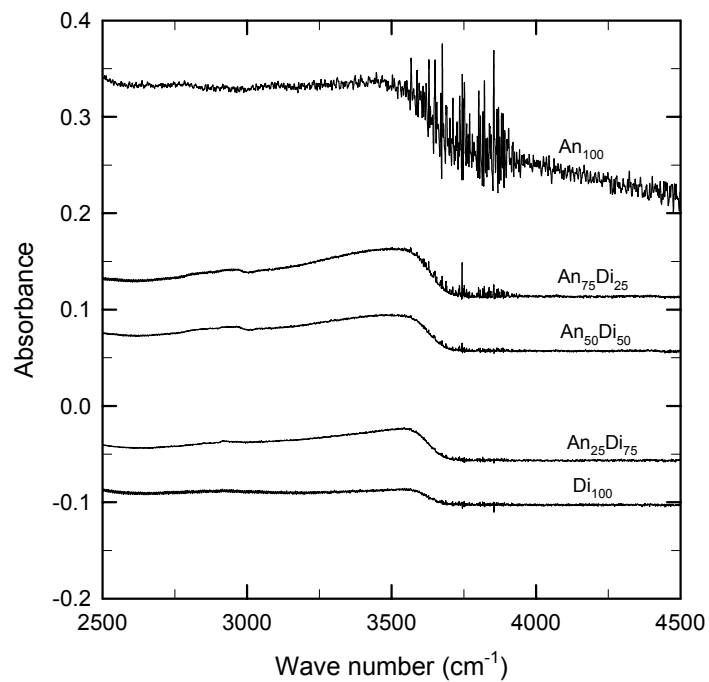


Fig.3.5 Mid-infrared absorption spectra of glasses in the system Anorthite-Diopside. Spectra are plotted with an offset for a better clarity.

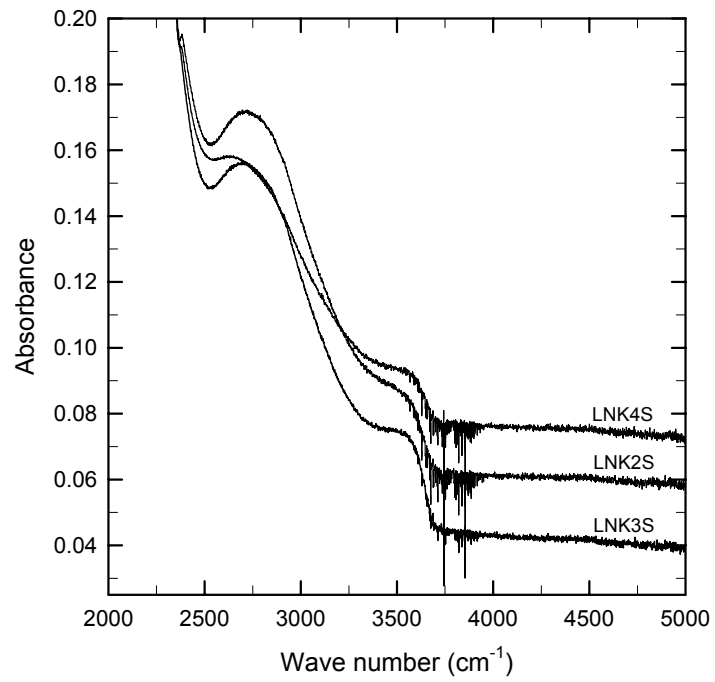


Fig.3.6 Middle-infrared absorption spectra of alkali silicate glasses. Spectra are plotted with an offset for a better clarity.

3.4. Viscosity measurements (high viscosity range)

Most of viscosity measurements were carried out using two creep apparatuses: the viscometer operating in an IHPV (Schulze et al. 1999) shown in figure 3.7, and the creep apparatus of Neuville and Richet (1991) in Paris. Using the creep apparatus the viscosity is measured by the ratio between the stress σ (Pa) and the strain rate $\dot{\varepsilon}$ (s^{-1}). In case of an elastic deformation due to shear stress, the viscosity (η) is the product between shear modulus μ and strain rate ($\eta = \mu \cdot \dot{\varepsilon}$). The normal stress is:

$$\sigma_n = E \cdot \dot{\varepsilon}$$

where E is the Young modulus. The relationship between shear modulus and Young modulus is the following:

$$\mu = \frac{E}{2 \cdot (1 + \nu)}$$

in which ν is the Poisson coefficient which equals to 0.5 in case of constant volume during deformation (Neuville PhD thesis). The shear modulus can be rewritten as $\mu = E/3$ and the shear viscosity can be written as:

$$\eta = \frac{\sigma}{\dot{\varepsilon}}$$

and for a uniaxial compression viscosity we have the following equation:

$$\eta = \frac{\sigma_n}{3 \cdot \varepsilon}$$

3.4



Fig.3.7 On the left side the viscometer sample holder is shown. Sample is within the silver sample tube on top of the silica piston. Thermocouples and glass-epoxy printed circuit board are also visible. On right part is shown the steel cover of the furnace. The inner part of the furnace consists of two heating zones made of Kanthal A1 wires (diameter of 0.6 mm) wound around a tube of sintered alumina (diameter 15 mm) (Schulze et al. 1999).

In the experiments run with a parallel plate viscometer in an IHPV the stress is the ratio between the weight (with mass M) applied to the surface S of a cylindrical glass sample.

Before each experiment the initial length L_0 , diameter S_0 and the mass M of the load are fixed. At time t the length of the sample is:

$$L(t) = L_0 - \Delta L_0$$

in which $\Delta L_0 = \sum dL_i$ that is the total change in length during the experiment. Assuming no change of volume during the experiment at time t and prevailing cylindrical shape, the surface of the sample is:

$$S(t) = \frac{S_0 \cdot L_0}{L(t)}$$

and can be rewritten as:

$$S(t) = \frac{S_0 \cdot L_0}{L_0 - \Delta L_0}$$

The expressions for stress and strain rate are:

$$\sigma = \frac{M \cdot g}{S(t)} = \frac{M \cdot g \cdot (L_0 - \Delta L_0)}{S_0 \cdot L_0} \quad 3.5a$$

$$\dot{\varepsilon} = \frac{dl}{dt} = \frac{dL_i}{L \cdot dt_i} = \frac{d(\ln L)}{dt_i} = \frac{\Delta \ln L}{\Delta t} \quad 3.5b$$

Where $\frac{dl}{dt}$ is the variation of the length with the time.

Substituting equations 3.5a and 3.5b in 3.4, the expression for the determination of the viscosity (Pa·s) is obtained as (Schulze et al. 1999)

$$\eta = \frac{M \cdot g \cdot (L_0 - \Delta L_0)}{3 \cdot S_0 \cdot L_0 \cdot \left(\frac{\Delta \ln L}{\Delta t} \right)} \quad 3.6$$

A buoyancy correction is applied to the mass of the load M because the mass was determined at ambient pressure while the viscometer operates under higher argon pressure (the minimum was 50 MPa and maximum 400 MPa). Buoyancy of the load is due to the high density of the pressure medium (argon gas). The density of argon at a given pressure was calculated using the equation given by Siewert et al. (1998)

$$\rho_{(P=const.)} = a + b \cdot T + \frac{c}{T} + d \cdot T^2 \quad 3.7$$

where ρ is the density of argon in g/cm³, T the temperature in K and a , b , c and d are regression coefficients given for a given pressure (Siewert et al. 1998). Siewert et al (1998) determined the coefficients in the pressure range of 40.5 to 253.3 MPa. Assuming the temperature at the load as 323 K than the density of the argon as function of pressure can be calculated by the following equation

$$\rho_{(T=323K)} = 0.3824 \cdot \ln P - 0.8518 \quad 3.8$$

where P is the pressure given in MPa. At experimental pressures (from 50 to 400 MPa) the density of argon is increasing from 0.644 g/cm³ at 50 MPa to 1.439 g/cm³ at 400 MPa at 323 K (see figure 3.8b). When the temperature at load is 30 K higher or lower than the

assumed one the viscosity of the DGG1 (standard glass of the *Deutsche Glastechnische Gesellschaft*) was calculated to be 0.003 log units higher or lower respectively. The weight of the load under pressure (Fig.3.8a) is given from the following equation, Schulze et al. (1999)

$$W_P = W_R - \frac{W_R \cdot \rho_{Ar}}{\rho_L} \tag{3.9}$$

where W_P is the weight of the load under pressure and W_R at ambient pressure (1033 g), ρ_{Ar} is density of argon at experimental pressure and ρ_L is density of the load (8.103 g/cm³). The weight of the load decreases from 1033 g at ambient pressure to 849 g at 400 MPa assuming a temperature of 323 K.

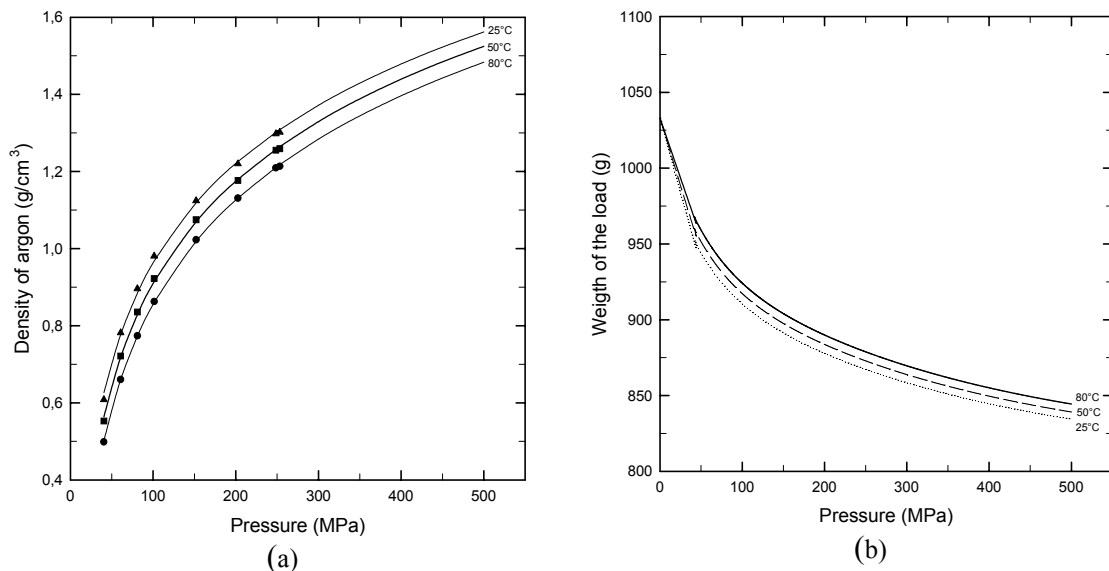


Fig.3.8a-b. Density of argon (a) affects weight of load (b). (a) Density of argon as function of pressure for different temperatures. Data are from Siewart at al. (1998). Curves are calculated using equation 3.8. (b) Example for the dependence of the weight of the load on pressure and temperature.

The dimensions of the glass cylinder ranged between 3 – 4 mm in diameter and 8 – 12 mm in length. The ends of the samples were cut and polished parallel. The initial diameter and length were measured by a micrometer (Mytutoyo, range: 0 – 25 mm) to a precision of ± 0.001 mm.

The viscosity was determined by measuring the rate deformation of the cylindrical sample with a length l as a function of an applied constant stress σ at fixed temperature, substituting equation 3.4 in 3.6, equation 3.6 can be written as follows, Neuville et al. (1991):

$$\eta = \frac{\sigma}{3 \cdot (d \ln l \cdot dt)} \quad 3.10$$

where η is the viscosity in Pa·s and t is the time at which length (l) is measured.

A pressure resistant and linear variable differential transducer (LVDT, Schaevitz 250 MHR-396) with a measuring range of 12 mm and a resolution of 0.1 μm was used to measure the position of the soft iron core (see figure 3.9a) with time. The transducer was calibrated with a height gage with a precision of 0.2 μm in order to establish the range in which relationship between the position of the core and measured voltage is linear. This was achieved by fixing the transducer to the fixed side of the gage and the core to the movable side of the gage and measuring voltage while varying position. Further calibration was required within the vessel because of shielding effects of the metallic vessel walls. In this case the transducer was inserted in the upper part of the vessel and the core was introduced from the bottom. The position of the transducer in the vessel was controlled with a portable gage. For recording all data (temperature, pressure, and transducer signal) as a function of the time the LabVIEW software was used.

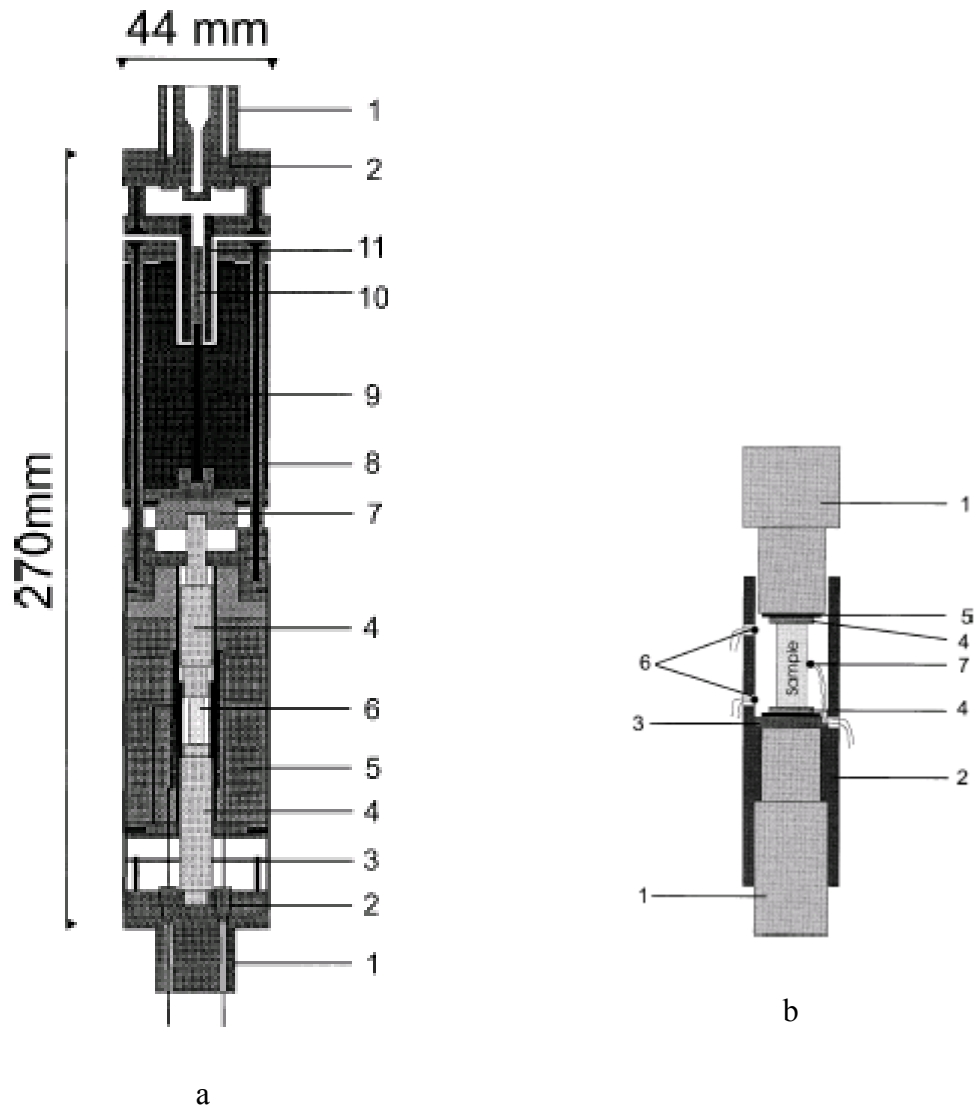


Fig.3.9a-b. (a) Schematic illustration of the viscometer: (1) closure head; (2) steel cone; (3) glass-epoxy printed circuit board; (4) silica-glass piston; (5) furnace; (6) sample; (7) ceramic shield; (8) guide bars; (9) load; (10) soft iron core; (11) linear variable differential transducer. (b) Silver sample holder: (1) silica-glass piston; (2) Ag tube; (3) ceramic disk; (4) Zn (or Al or Sn) disk; (5) Pt disk; (6) S-type thermocouples controlling the furnace; (7) S-type thermocouple measuring sample position temperature. Diagram after Schulze et al. (1999).

As is discussed in later chapters, small changes in sample temperatures induce large errors in the measurement of viscosity. To verify the temperature distribution at sample position, several calibration runs were performed using the α - β transition of quartz which increases linearly with increasing pressure (from 846 – 946 K in the pressure range 0.1 - 400 MPa, Yoder (1950)). The temperatures determined by phase transition are typically 3

– 5 K higher than the temperature recorded with the thermocouple at the sample position. During the same run aluminum disks were placed on both sides of the sample to check any thermal gradient along the sample. From the T calibration it is expected the maximum temperature uncertainty to be within ± 2 K. For all viscosity experiments, the sample temperature and thermal gradient along the sample was determined using the melting point of zinc (increasing from 692 K at 0.1 MPa to 705 K at 400 MPa), Lees et al. (1965) and Akella et al. (1973), or tin (increasing from 505 K at 0.1 MPa to 524 K at 400 MPa), Dudley et al. (1960), or aluminium (increasing from 933 K at 0.1 MPa to 958 K at 400 MPa), Lees et al. (1965), depending on temperature range for viscosity measurement.

The first step of the experiments was the pressurization of the vessel (the pressure was measured by a strain gauge manometer to a precision of ± 50 bar), to 200 MPa. Then three different consecutive ramps (40 K/min, 5 K/min, 40 K/min) were used to reach the target starting temperature. The second ramp with a lower rate was used to cover the T range near the melting point of the metal, used for T calibration, was expected. The starting (lowermost) temperature for viscosity measurements was chosen as the temperature at which the viscosity was estimated to be $10^{11.5}$ Pa·s, the highest value of viscosity measurable by this method. Temperature was maintained for 30 minutes to allow thermal expansion and mechanical relaxation of the viscometer. When the thermal conditions were stable and the LVDT signal didn't vary with the time, small temperature increases by $\pm 5 - 10$ K followed by dwells of $\approx 10 - 15$ minutes were used to measure viscosities. This time was sufficient to get steady state deformation (constant viscosity), see Fig.3.11. To finish all experiments the temperature was returned to the starting temperature and viscosity was again measured, to check for reproducibility.

The viscometer was calibrated with a standard DGG1 glass (*Deutsche Glastechnische Gesellschaft*). In the case of DGG1-a, the viscosities values measured by Schulze et al. (1999) were reproduced during calibration to within ± 0.18 log units (see Fig.3.10). The

initial measurement at 853 K was repeated once during the calibration and its viscosity was reproduced within ± 0.06 log units. A third measurement at this temperature was performed at the end of the calibration and agreed with the first measurement within 0.04 log units. Further tests were done with other DGG1 glass samples (DGG1-b, DGG1-c and DGG1-d) and the viscosities were reproduced within ± 0.20 , ± 0.08 and ± 0.08 log units, of the values given by Schulze et al (1999), respectively.

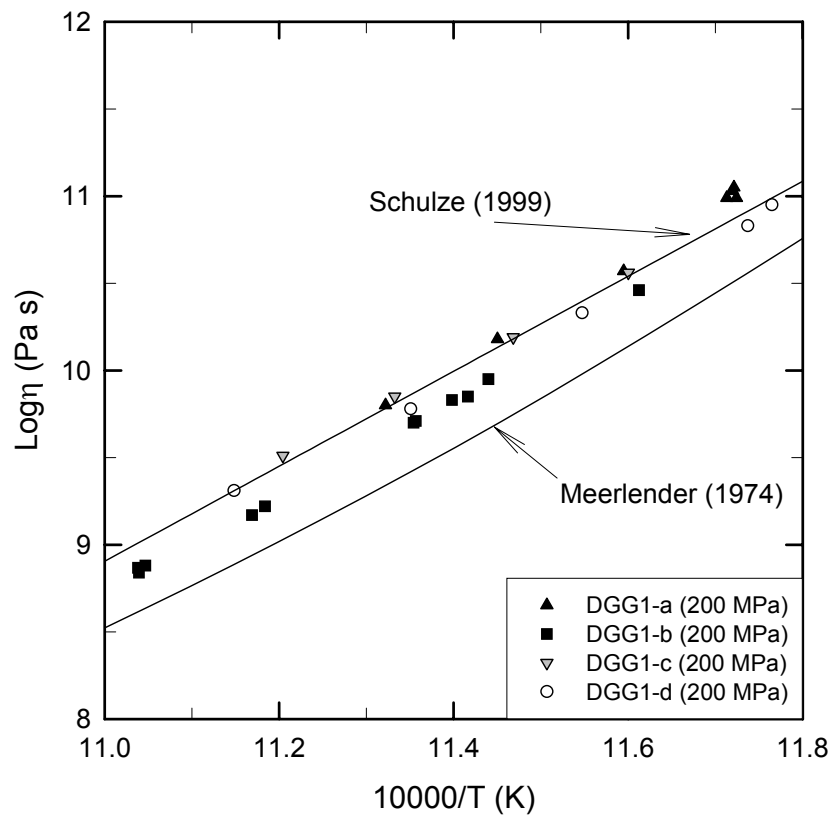


Fig.3.10 Viscosity of standard DGG1 melt. Different experiments are compared with data from Schulze et al. (1999) at 200 MPa and with data from Meerlender (1974) at 0.1 MPa.

To check the pressure dependence of the viscosity in float glass the pressure was varied at fixed $T_{(\text{Log}\eta=10)}$. Reference temperature was the temperature at which the viscosity equals 10^{10} Pa·s at 200 MPa. This procedure was used for several samples with different water contents. In addition, one glass containing 0.28 wt% of H_2O was investigated using several temperature steps at different pressures. Before changing pressure a low T was maintained

to allow pressure relaxation of the apparatus and to calculate $T_{(\text{Log}\eta=10)}$. When relaxation of the apparatus is reached and the $T_{(\text{Log}\eta=10)}$ was calculated, viscosity measurements were made over a range of 50 – 400 MPa, starting from 200 MPa. In most cases an individual experiment would end by repeating the measurement at 200 MPa to verify reproducibility. During the experiments along the An-Di join and in the system LNKS the first set of measurements was done with varying T at 200 MPa and then at constant temperature at different pressures. The variation of pressure, sample temperature and LVDT signal is shown in Fig.3.11 (float glass containing 0.28 wt% of H_2O). The figure also shows a detailed depiction of the LVDT signal during the melting point of the two zinc plates and of the LVDT signal for the viscosity measurements at a pressure of 50 MPa.

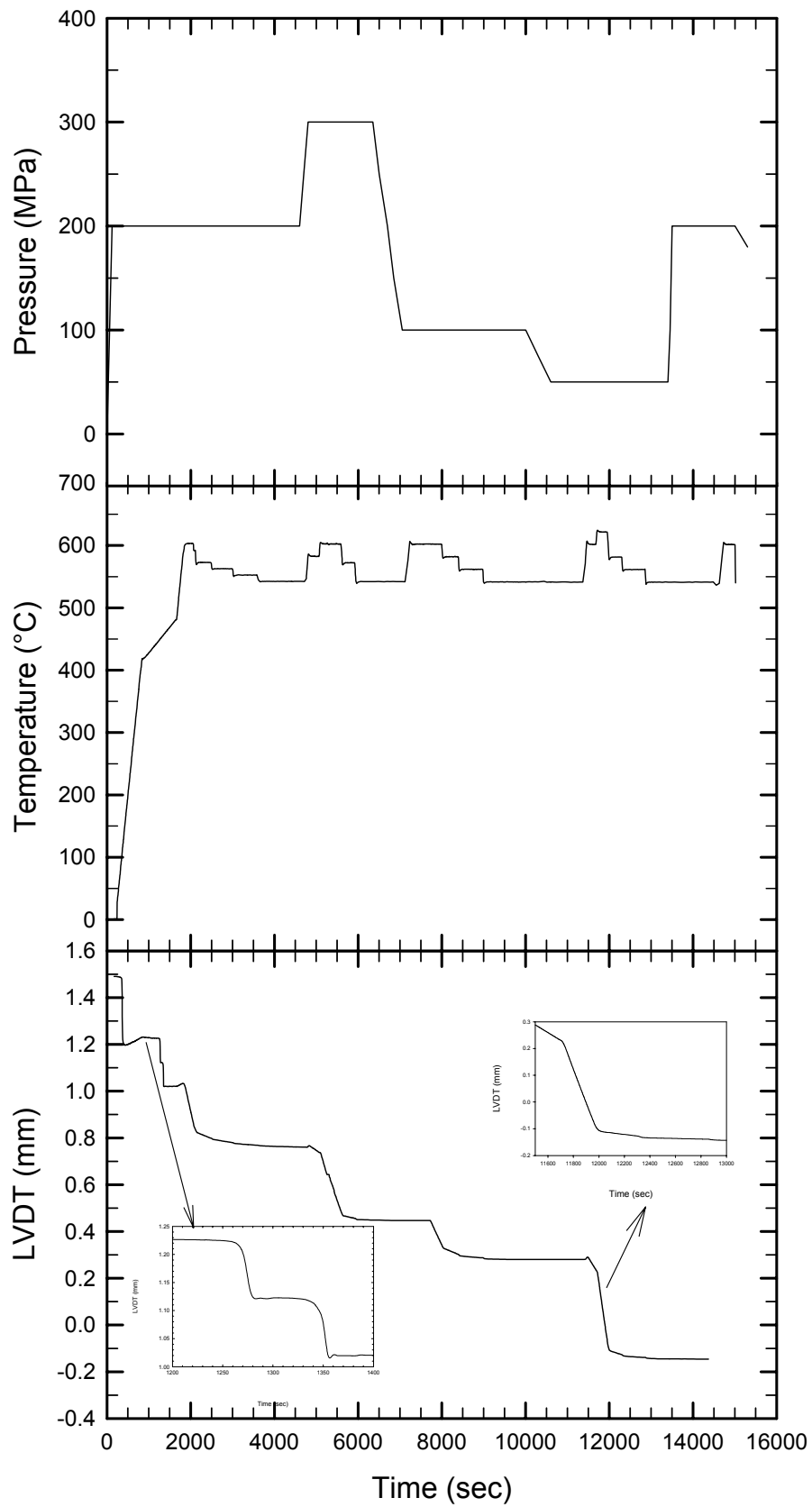


Fig.3.11 The figure shows the relationship between time, temperature, pressure and the shortening of a sample of float glass containing 0.28 wt% of H₂O (viscosities are listed in appendix).

The samples maintained a cylindrical shape during experiments indicating there is no temperature gradient during the experiment. Diopside and LNK3S samples underwent the highest shortening during the experiment.

Viscosity of anorthite, diopside and $An_{50}Di_{50}$ was measured also at ambient pressure (in the *Institut de Physique du Globe Paris Jeussieu*) using the creep apparatus described by (Neuville and Richet 1991).

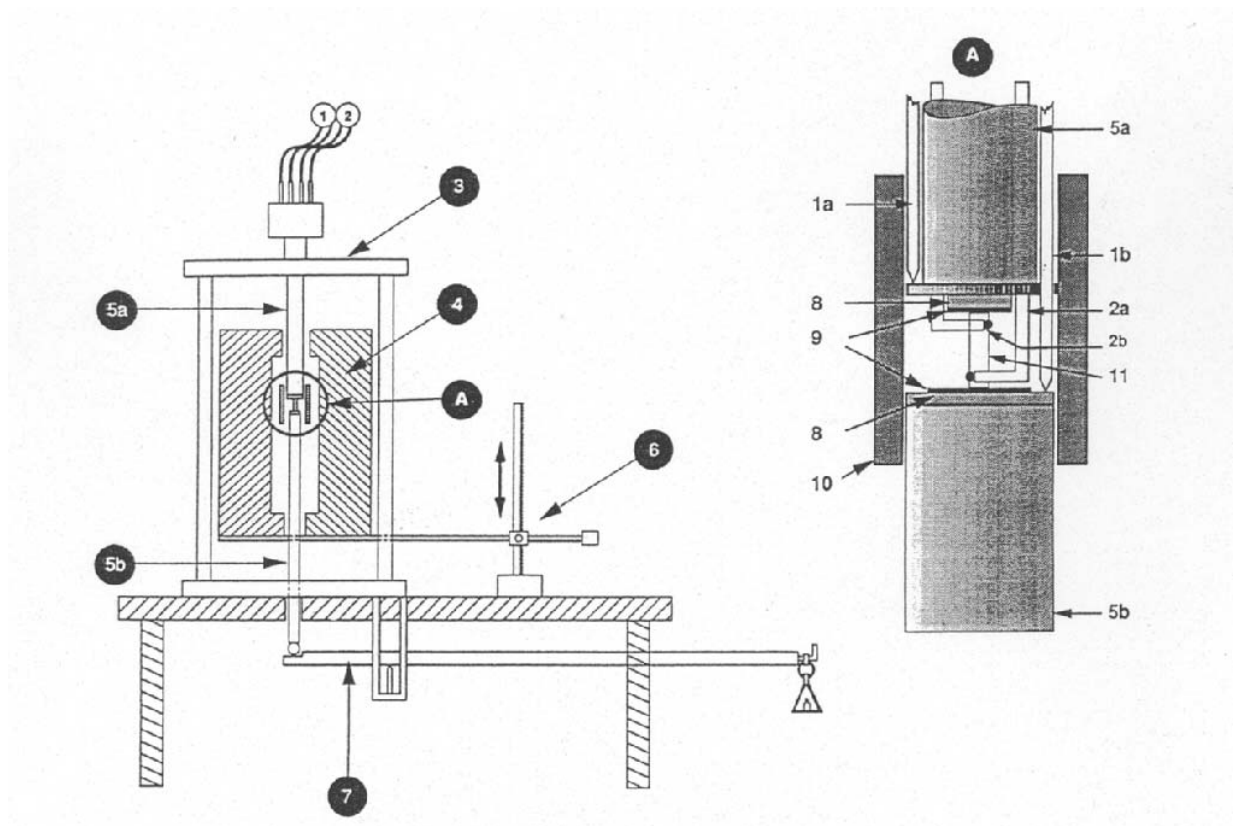


Fig.3.12 Schematic illustration of the creep apparatus of Neuville and Richet (1991). (1) LVDT; (2) S-type thermocouples; (3) frame; (4) furnace; (5) pistons; (6) jack; (7) lever; (8) alumina plates; (9) platinum foils; (10) silver cylinder; (11) sample.

In these experiments the rate of deformation of a sample of length l (see eq.3.10) is measured as a function of an applied constant stress (σ) at fixed temperature. The creep apparatus is formed by a fixed upper piston and a mobile lower piston made of hard nickel-based alloy adjusted to $1 \mu\text{m}$ to two guiding low friction slides. The sample is inserted

between two 50 μm thick platinum foils and two 5 mm thick alumina plates in contact with pistons to provide for mechanical and chemical protection. The rate of deformation of the sample is obtained by measuring the length of the sample over time. The length of the sample is measured within 2 μm by two linear variable differential transducers as difference between the positions of the lower end of two alumina rods resting on the pistons (a full description can be found in Neuville and Richet (1991)). For a given temperature, experiments were made with a variety of applied stresses while maintaining Newtonian behavior.

Viscosity is calculated by equation 3.10. With the ambient pressure viscometer was possible to measure values of viscosity varying the weight of the load (1200 – 30200 g) at constant temperature. The reported viscosities from these experiments are the averages of five to ten measurements (at constant T with varying mass). The viscosities measured at each T show a maximum deviation of 0.03 log Pa·s.

3.5. *Viscosity measurements (low viscosity range)*

Low viscosity data were measured by using the falling-sphere method. This method requires the determination of the exact position of the sphere in the glass cylinder before and after the experiment. When a sphere is accelerated by a constant force and the resistance to its motion is proportional to the velocity, the sphere will eventually attain a constant or terminal velocity such that the resistance experienced is equal and opposite of the driving force.

A cylinder (with a 4 - 6 mm diameter) was cored from the raw water bearing glass. Two pieces were cut from the cylinder, a longer one (almost 10 mm) and a smaller (1 – 2 mm) and the remaining glass was crushed. The smaller piece of glass was placed in a platinum capsule that was closed at one end with an arc-welded platinum cup (in order to

get a container with cylindrical shape) and was covered with a small amount of Pt powder in order to get a marker. The longer cylinder was then placed in the capsule and was covered with a small amount of glass powder. A platinum or palladium sphere was placed on top of the glass powder at the center of the capsule and covered with glass powder. The capsule was then crimped and sealed by welding.

The spheres used in this study were made from strands of Pt or Pd wire (thickness = $2.5 \cdot 10^{-4}$ cm) twisted together and melted by a sudden DC current. This method produces spheres with small radius (radius of 45 to 80 μm), suitable for these experiments.

The capsules were placed in an IHPV and ran at 1523 K and 200 – 500 MPa for few minutes to pre-melt the whole glass assemblage and place the sphere. The cylinders were then removed from the capsule and the position of the sphere with respect to the marker layer was determined. This was accomplished using an optical microscope equipped with an x-y stage. The glass cylinder was immersed in oil with a similar refraction index as the glass (1.622) to improve the visibility of the sphere. This position was used as the starting position for the subsequent viscosity experiment. The sample was then cleaned in acetone, dried at ambient temperature and sealed within a platinum capsule.

The capsules were loaded into the IHPV, pressure was increased to the desired pressure, and the sample was heated. The sample was heated with a ramp of 30 K/min to 1023 K and then with 70 K/min or 100 K/min to the target temperature. The duration of the experiments was in the range of 5 min to 1 h depending on the experiment viscosity. At the end of the experiment the capsules were quenched, by shutting of heating power, with a rate on the order of 200 K/min. The quenching freezes the sphere in place and the distance the sphere has travelled during the experiment can be measured, using the microscope and immersion oil technique mentioned earlier and a scaled micrometer. Terminal velocity was determined from the distance travelled and time of travel. Viscosity can then be calculated using Stokes' law:

$$\eta = \frac{2 \cdot g \cdot r^2 \cdot (\sigma - \rho)}{9 \cdot v} \cdot C_F \quad 3.11$$

where η is the viscosity (Poise), g acceleration of gravity (cm/s^2), r radius of the sphere (cm), σ density of the sphere (21.45 g/cm^3 the Pt sphere and 12.02 g/cm^3 the Pd sphere at room temperature), ρ density of molten glass (g/cm^3), v terminal velocity (cm/s) of the sphere and C_F is Faxen correction that take in account the effect of viscous drag by the capsule wall on the settling sphere. No correction is required for the differential compression and thermal expansion of the spheres because this would contribute less the 1% to the melt viscosity. Density of melt at experimental condition was calculated after Lange (1994) using the partial molar volume of water after Ochs and Lange (1999).

It is necessary to have an exact measurement of run duration, and settling distance during this time, to calculate viscosity. Especially in short experiment the contribution of the sinking of the sphere before reaching the final temperature could be significant. To consider the movement of the sphere before reaching the final temperature T_{target} the effective run duration t_{eff} was calculated in the same way as it is done for diffusion experiments, Koepke and Behrens (2001)

$$t_{eff} = \int \exp \left[\frac{-E_a}{R} \cdot \left(\frac{1}{T_m} - \frac{1}{T_{target}} \right) \right] \cdot dt \quad 3.12$$

where E_a is the activation energy (kJ/mol), R is gas constant, T_m the measured temperature in K. The method used for the estimation of activation energy is presented in chapter 4. It is clear viscosity is not necessarily Arrhenian over a wide range of temperature but for a

narrow T -range the assumption of linear variation of viscosity with reciprocal of temperature is a good approximation.

In some cases it was not possible to measure viscosities because of a large number of bubbles present in the glasses. The glass sample FG8 (0.67 wt% H₂O) was damaged in one experiment and could not be used again. Using samples with relatively high H₂O content (FG15 and FG16 see table 4.1) the run time required for each experiment was very short, in the order of 4 to 5 min. In these cases a larger error in the measure of the viscosity was obtained (see table 4.1). The major sources of error considered were: duration of each run (time correction ranged between 38 and 115 s), settling distance (measured using a scaled micrometer with a resolution of $\pm 10 \mu\text{m}$), measurements of the sphere radius (measured using a scaled micrometer with an error of the measurement of the radius of 1 to 5 μm), and temperature of the sample (precision of the temperature is $\pm 10 \text{ K}$). The errors for each viscosity measurements are included in table 4.1.

4. Effect of H₂O on viscosity of float glass

4.1 Experimental Results

Viscosities at high temperature were investigated by the falling sphere method (which is described in section 3.5) and at low temperature with a creep apparatus (described in section 3.4).

To calculate the effective runs duration for the falling sphere method requires knowledge of the activation energy (E_a) of the glass (see eq. 3.12). Especially in short experiments with water-rich melts the effective duration of the experiment is strongly influenced by a good estimation of activation energy. The E_a decreases strongly with increasing water content, in the low viscosity range, especially for low H₂O contents, Schulze et al. (1996). Furthermore, Arrhenian relationships are applicable to dry and hydrous float glass only in small T range (see Fig. 4.2). After a falling sphere experiment a first evaluation of viscosity was carried out using the dwell time only. The resulting values were then used to calculate the activation energy of the hydrous float glass. Furthermore, using the first evaluation of viscosity combined with high viscosities is possible to extract parameters to fit the whole range of viscosities. Evaluation of few low viscosities was performed and therefore calculation of E_a was possible. To verify the reliability of the falling sphere method, two experiments were duplicated at the same pressure and temperature with samples FG7 (0.29 wt.% H₂O) and FG8 (0.67 wt.% H₂O) varying the run duration. The viscosity of FG7 sample was measured at 1523 K and pressure of 200 MPa first with a run duration of 551 seconds and then with 361 seconds. The difference between the two viscosities was 0.07 log units, which was less than experimental error, see table 4.2a. Duplicated measurements with sample FG8 agree within 0.08 log units which is significantly lower than experimental error (Table 4.1). These experiments demonstrate

that steady velocity is established in these experiments and the errors introduced by the acceleration and deceleration of the spheres are negligible.

Results of falling sphere experiments are listed in Table 4.1 and of creep experiments in appendix.

Table 4.1 Experimental condition and results of falling sphere experiments with float glass melts.

Sample	H ₂ O (wt.%)	T (K)	P (MPa)	Sphere radius (μm)	Faxen Correction	Dwell time (s)	Corrected time (s)	Falling distance (cm)	Logη (Pa s)	Ea ^(*) (kJ/mol)
FG7	0.29	1523	200	(Pt) 80 ± 2.5	0.89	470	551	0.330	1.57±0.21	215
FG7		1523	200	(Pt) 80 ± 2.5	0.88	280	361	0.249	1.50±0.21	215
FG8	0.67	1523	500	(Pt) 80 ± 2.5	0.93	415	486	0.520	1.36±0.20	212
FG8		1523	500	(Pt) 80 ± 2.5	0.74	310	381	0.435	1.24±0.20	212
FG9	0.68	1523	200	(Pd) 45 ± 1.0	0.83	4500	4571	0.857	1.17±0.12	212
FG9		1473	200	(Pd) 45 ± 1.0	0.93	3600	3638	0.220	1.71±0.12	212
FG15	3.49	1523	500	(Pd) 73 ± 2.5	0.95	300	415	0.981	0.54±0.28	120
FG16	4.32	1473	500	(Pd) 53 ± 1.0	0.86	240	333	0.578	0.78±0.36	101

^(*) estimated for the range 1273 – 1523 K.

Fig.4.1 presents a plot with the results of viscosity (expressed as logarithm of viscosity) versus water content (expressed as weight percent of H₂O). The data of nominally dry melt were calculated from VFT parameters published in Prado et al. (2003). Although measurements of viscosities from Prado and from falling sphere experiments were performed at different pressures 0.1 MPa and 200 – 500 MPa, respectively, this does not significantly affect the trend (as is shown later). The viscosity of the melt decreases strongly with the addition of water to the melt. By adding 3.49 wt.% H₂O to the dry melt, viscosity at 1523 K decreases more than one order of magnitude from 1.70 Pa·s (log units) for anhydrous melt to 0.54 Pa·s (log units).

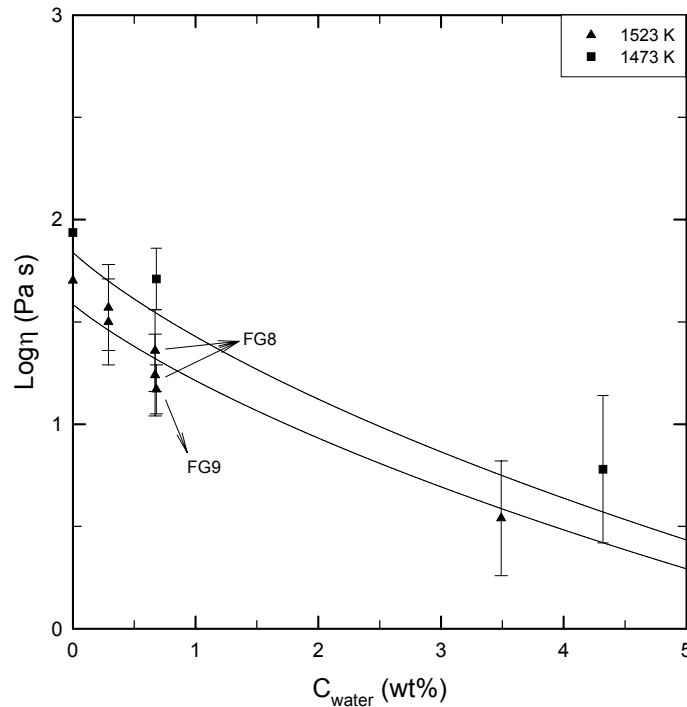


Fig. 4.1 Low viscosities of float glass. Data of dry melts were estimated after Prado et al. (2003). In two cases experiment was repeated at the same condition but varying the duration (FG7 and FG8). Viscosities of repeated measurements are reproduced within the error of the measurement. Continuous lines are trend lines, which can be used to interpolate viscosity data.

Operating with the creep apparatus allows collection of more viscosity data from each experiment. In Fig. 4.2 the viscosity data for two water rich float glasses (3.49 and 4.49 wt.%) are shown. In both experiments the scatter in the data is within ± 0.08 log units, which is comparable to that given by Schulze et al. (1999). At the end of the experiment samples were return to the starting temperature to verify whether viscosity at the beginning and at the end of the experiment were consistent. In the two cases shown in Fig. 4.2 the first measurement was reproduced at the end within ± 0.02 log units (FG17, 4.49 wt.% H₂O) and ± 0.06 log units (FG15, 3.49 wt.% H₂O). From these results it is concluded that in the range of time (more than 2 hours) necessary for these experiments water loss (see also Fig.3.6) was negligible. IR measurements after experiments support this conclusion.

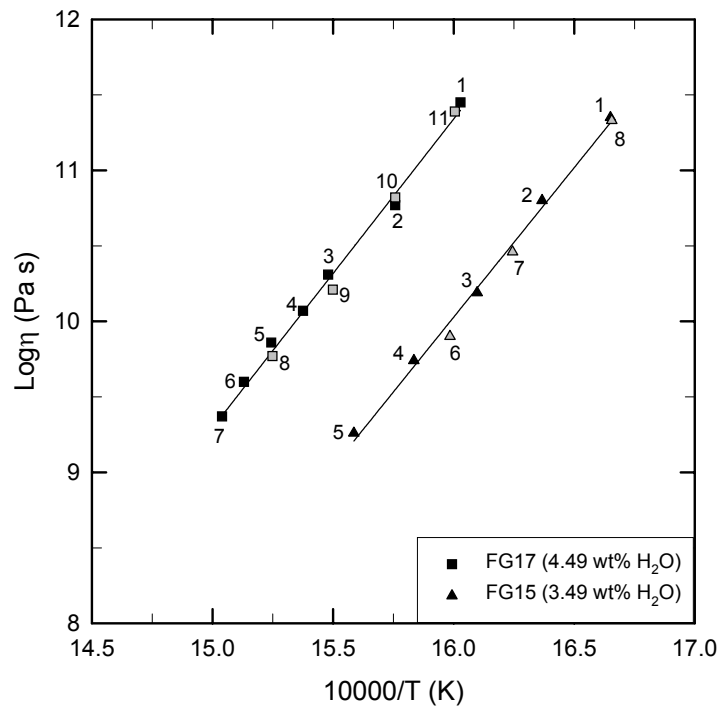


Fig.4.2 High viscosities of water bearing float glasses. The two series of viscosity measurements were done at 200 MPa. Each series consist of intervals of 10 – 15 min. at fixed T . In each series run number gives the chronological order of the measurements. Black labels represent increasing T and gray labels decreasing T .

Comparisons with literature data are possible only for ambient pressure and dry glass. In Fig. 4.3 the viscosities of float glass with 0.03 and 0.28 wt.% H₂O measured at 200 MPa (this work) are shown with data from Thies (2002) measured at 0.1 MPa and viscosities calculated after Prado et al. (2003) and Priven (2001). Deviations between the viscosities of melt containing 0.03 wt.% of water from this study and the data of Priven (2001) are within ± 0.08 log units except for the viscosity measured at 851 K. At this temperature there is a deviation of ± 0.18 log units when compared to those of Priven (2001). Comparing the data of this study to Prado et al. (2003) there is a ± 0.16 log unit deviation with a deviation of ± 0.30 log units at 851 K. The differences between the viscosities measured at 0.1 MPa (Thies 2002) and 200 MPa values are within ± 0.08 log units. The precision of the viscosity measurements is lower at high viscosity. By adding 0.28 wt.% of water to a dry glass, the viscosities decrease about 1.6 log units at 849 K.

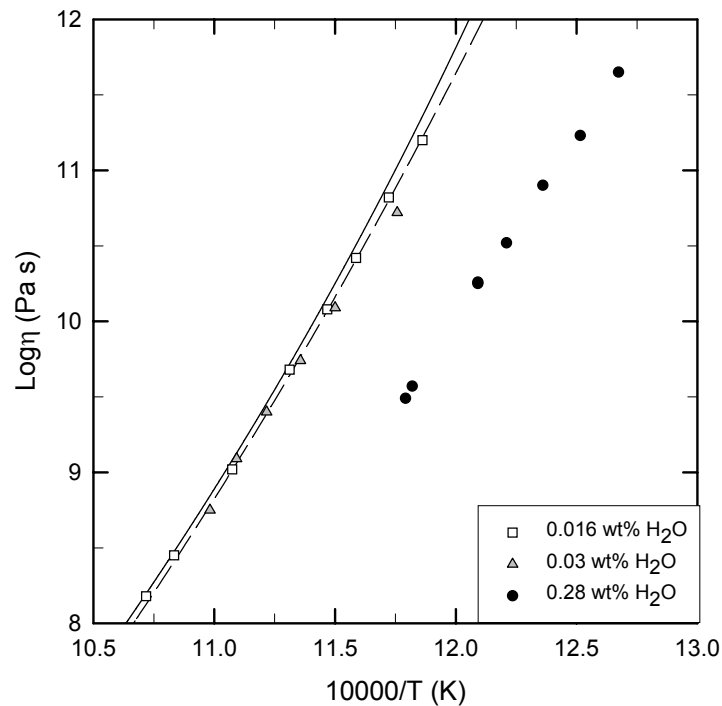


Fig.4.3 Comparison of new viscosity data for float glass with results from previous studies. Solid line is calculations after Prado et al. (2003), dashed line calculation after Priven (2001) for dry float glass. Squares are viscosity data given by Thies (PhD thesis) measured at 0.1 MPa. Triangles and circles are viscosity measured at 200 MPa (this work).

In Fig. 4.4 the data of viscosity at 200 MPa are compared with fit data of nominally dry glass (at ambient pressure), Prado et al. (2003) and Priven (2001). Water content ranges between 0.03 wt.% to 4.82 wt.% H₂O. H₂O content strongly reduces the viscosity; this influence is larger with low water contents and becomes lower for higher water content. Adding 4.82 wt.% of water to the dry melt reduces the temperature at which the viscosity of float glass equals 10^{10} Pa·s by 252 K. The influence of water is smaller at high temperature.

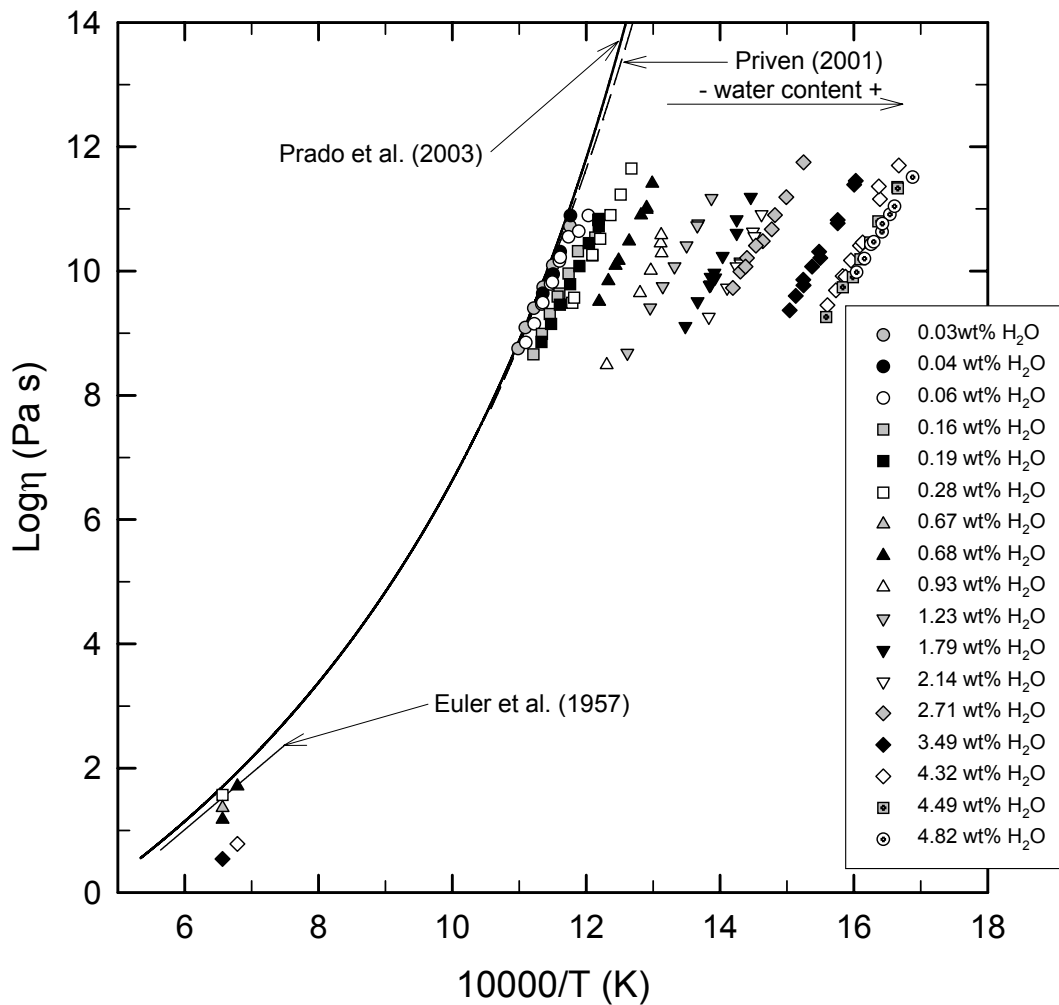


Fig.4.4 Comparison of my data for hydrous float glass in the high and low viscosity range with calculations after Prado et al. (2003) and Priven (2001) and a regression line representing the viscosity data of Euler et al. (1957). All the data collected from literature refer to dry melts.

Over a small range of temperature it is possible to consider the temperature dependence of the viscosity as an Arrhenian function of activation energy E_a (kJ/mol) and reciprocal of T (K). Activation energy was calculated for the high viscosity range using a first order linear regression of the logarithm of viscosity versus the reciprocal of temperature in the viscosity range 10^9 to 10^{11} Pa.s. Values of E_a are plotted versus water content (wt.%) in Fig.4.5. E_a shows a strong dependence on the water content of the melt, especially for low water concentrations. E_a decreases from 540 ± 7 kJ/mol for dry float glass to 358 ± 37 kJ/mol for float glass containing 1.23 wt.% of H₂O. Further increase of water content

yields no decrease of E_a (E_a is equal to 366 ± 26 kJ/mol for a glass containing 4.82 wt.% H₂O). In Fig.4.5, float glass data are compared with data of water bearing soda lime silica glass.

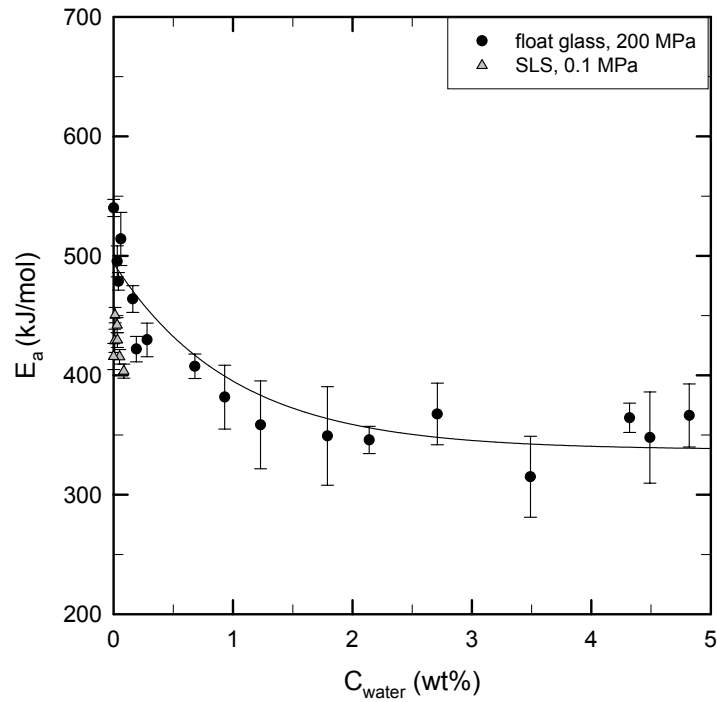


Fig.4.5 Activation energy (1σ standard error) of float glass at 200 MPa compared to values calculated from the viscosity data for anhydrous soda lime silica glass (SLS) from Böse et al. (2001) and for hydrous soda lime silica glass from Sakka et al. (1981) hydrous glass. The trend of the data is given by the solid line.

The pressure effect on viscosity of water bearing float glass is expected to be negligible for this composition with an intermediate degree of depolymerization (Behrens and Schulze 2003). Fig. 4.6 shows the pressure effect of viscosity for glasses different water contents. Experiments were carried out under different pressures (ranging between 50 to 400 MPa) for four water bearing float glass (0.04 wt.% to 2.14 wt.% of H₂O). The major variation in viscosity with increase of pressure is found in the glass with 0.28 wt.% H₂O with an increase of 0.1 log units per 100 MPa at 834 K.

When omitting the 100 MPa datum for the sample with 0.04 wt.%, the pressure dependence becomes slightly positive and all measurements together show a systematic trend in that the pressure effect becomes more negative with increasing water content. This trend is, however opposite to what is expected from results for the Ab-Di and An-Di joins, and for alkali silicate melts. Hence, it appears that dissolved water has a different effect on the pressure dependence of viscosity than alkali or alkaline earth elements.

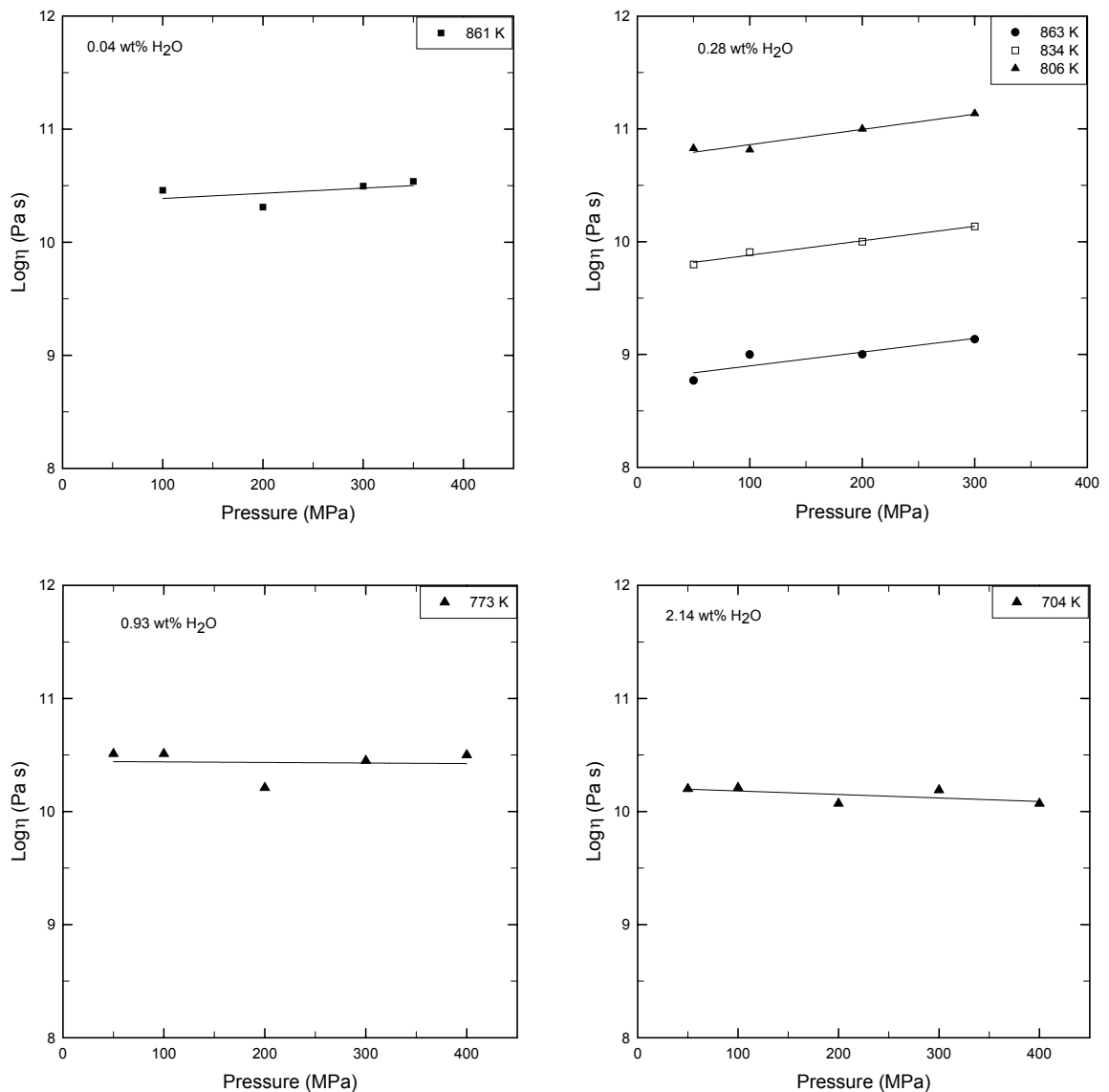


Fig.4.6 The figure shows the change in viscosity with pressure. The water content range between 0.04 wt.% and 2.14 wt.%.

4.2 Data modelling

Few models are available for prediction of viscosity as function of temperature and water content for silicate melts and no models are known for float glass melt composition. Several empirical approaches were performed to parameterize viscosity of hydrous silicate melts. The pioneering model was the one of Shaw (1972) which allows the prediction of the viscosity of hydrous silicate melts with different bulk compositions. The Shaw model considers the viscosity as having Arrhenian behaviour. However, the Arrhenian-type equation of Shaw (1972) is limited in application to the low viscosity range and can not be extended to the glass transition. Further models were proposed for specific compositions (eg: Richet et al. 1996, Schulze et al. 1996, Hess and Dingwell 1996, Holtz et al. 1999, Giordano et al. 2004) which use an extended version of the VFT equation to take into account the non-Arrhenian behaviour of viscosity as function of temperature. Zhang et al. (2003) proposed a power law model for prediction of the viscosity of rhyolitic hydrous melts as function of temperature and water content (as molar fraction). Both models reproduce quite well the viscosities in a well defined range of temperatures and water contents for a well defined composition but may fail for other compositions.

In order to create a model that can predict the viscosity of hydrous float glass, several types of equations for viscosity were tested. 203 viscosities were available in total, including data from this study at 200 MPa and data at ambient pressure from Thies (2002) and Euler et al. (1957). The input data cover a viscosity range from $10^{0.5}$ to $10^{11.5}$ Pa·s, a temperature range from 593 to 1523 K and a water content range from 0 to 4.82 wt.%. Except for one power law model, all the equations tested were VFT-equations modified by introducing a second term containing both the T parameter and the water parameter w . In this study I have also tried to constrain the first term of the equation using the VFT-parameters given by Prado et al. (2003) ($A = -2.7$, $B = 4358.44$ K and $T_0 = 533$ K) for

anhydrous melts and simultaneously fitting all data. The best results though, are obtained using equation 4.1 which is the result of fitting all the data simultaneously without constraining the VFT-parameters in the first term.

$$\log \eta = -3.37 + \frac{5089.5}{(T - 497.4)} - \frac{1391.1}{(T - 503.2)} \cdot \frac{w}{(w^{0.5975} - 2.6713 + 0.0035 \cdot T)} \quad (4.1)$$

where η is the viscosity in Pa·s, T is the temperature in K, and w is the H₂O content in wt.%. The equation 4.1 reproduces all experimental data within a standard error (1σ) of 0.23 log units (Fig4.7). The effect of pressure of viscosity is considered to be negligible as is shown in Fig.4.6; therefore equation 4.1 may be applied over the pressure range 0.1 to 400 MPa without significant error.

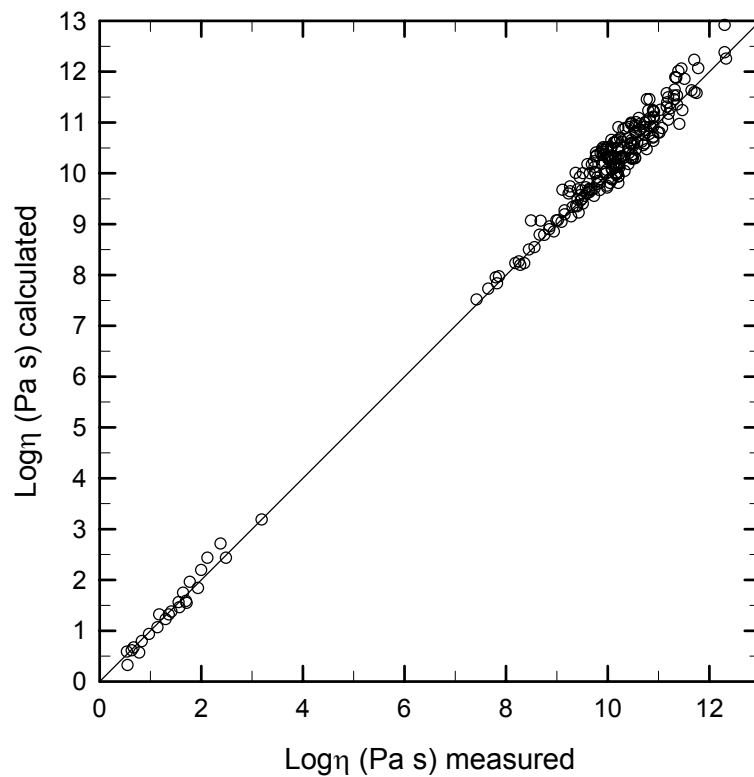


Fig.4.7. Comparison between experimental data versus calculated data from the model.

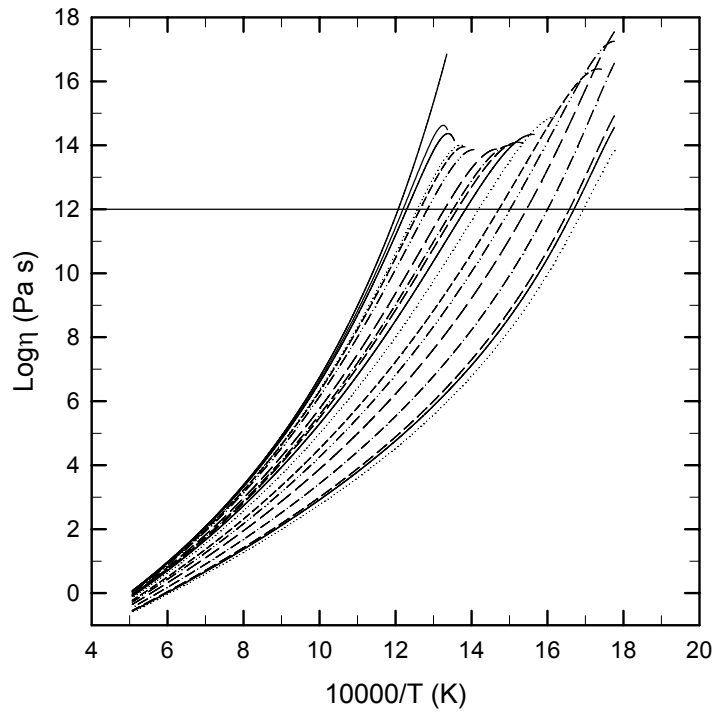


Fig.4.8a Calculated viscosities using equation 4.1 for different water contents. The fit equation is applicable for all water contents above the glass transition temperature T_g .

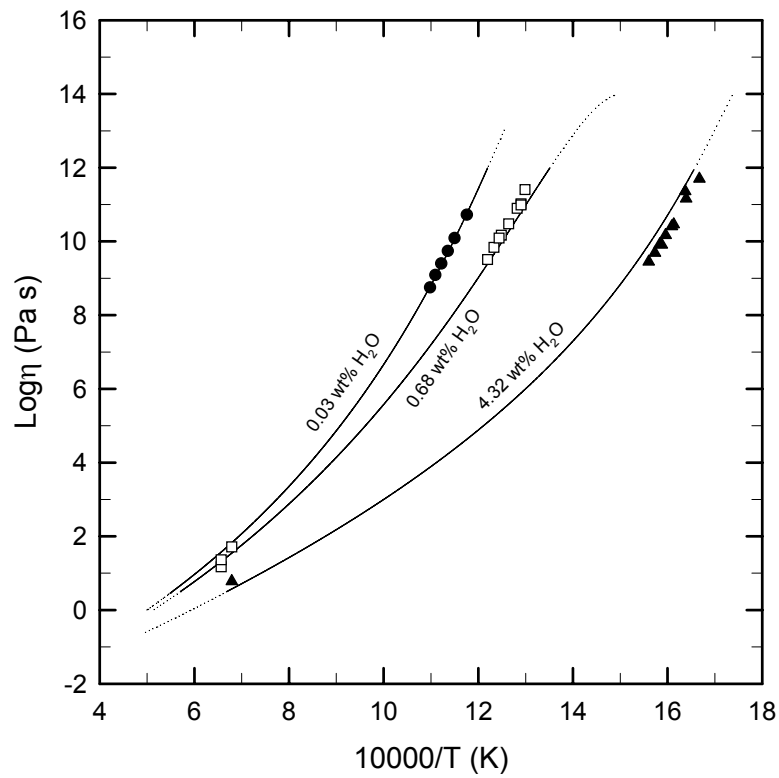


Fig.4.8b Comparison between experimental data and viscosities calculated from the model for three different water content.

For a dry melt the second term is zero and equation 4.1 reduces to a simple VFT. For a better fitting of viscosity at low and high temperatures it was required to introduce a temperature dependent expression in the last term of the equation 4.1, (Fig.4.8a-b). The extrapolation of the equation to very low temperatures is not possible without introducing significant error. In general, the model is not recommended for temperature lower than T_g since no viscosity data are available to constrain the fit for these temperatures. Moreover, at low T the fitting lines undergo an inflection (see Fig.4.8a) which gives a decreasing viscosity with decreasing temperature (dashed curves in Fig.4.8b). The inflection is at the lowest viscosity for intermediate water contents around 1 wt.%. For water poor and water rich melts the inflection point is far beyond the experimental range. The high T limits of the melt viscosity (parameters A of the VFT equation) is close to the value proposed by Russell et al. (2003) as a general value for silicate melts (-4.3 ± 0.74 Pa·s). Temperature at which viscosity becomes infinite (parameter C) and the pseudoactivation energy associated with the viscous flow (parameter B) (Russell et al., 2003) are also consistent with previous calculation.

Tab.4.2. VFT parameters for dry melt. Comparison between this work and previous model.

<i>Parameters</i>	<i>This work</i> <i>Potters-Ballotini</i>	<i>Prado et al. (2003)</i> <i>Potters</i>	<i>Priven (2001)</i> <i>window glass</i>	<i>Meerlender (1974)</i> <i>DGGI</i>
A	-3.37	-2.7	-3.66	-1.58
B (K)	5089.5	4358.4	5908	4316 ^(*)
T ₀ (K)	497.4	533	471	248 ^(*)

^(*) given in °C. Parameters after Priven are calculated only for viscosities range of 10⁸ to 10¹⁵ Pa·s.

Fig.4.7, Fig.4.8b and Fig.4.9 show how the model fits with the experimental data over the whole range of viscosities. The temperature dependence of viscosity is reduced by adding water in the melt; in Fig.4.8 and Fig.4.9 this behaviour is emphasized by the slope of the curves becoming less pronounced with increasing water contents.

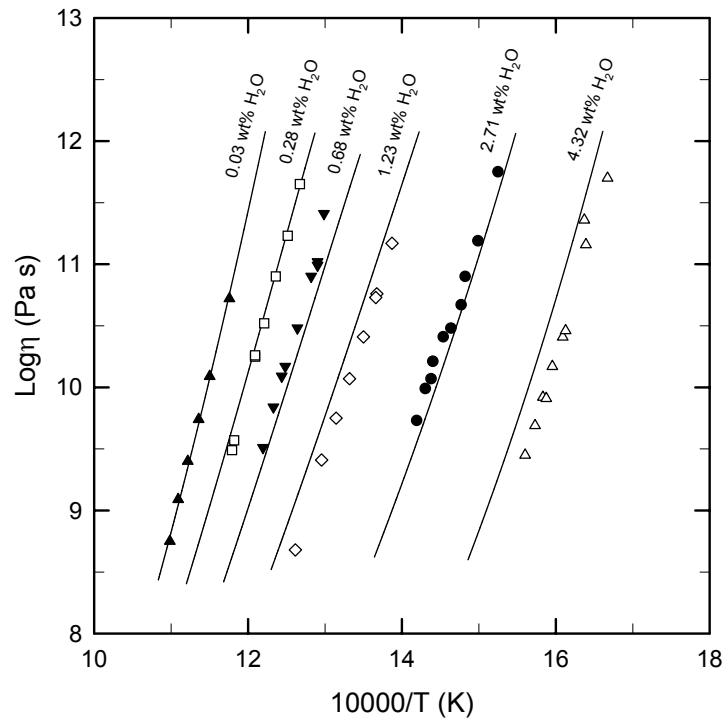


Fig.4.9. Viscosities measured by the creep apparatus at 200 MPa compared with prediction by the model (continuous lines).

Using non-linear-least-square method the VFT parameters (see appendix – II) were determined for each water content. In order to improve the fitting of melts for which low viscosities were not measured, the low viscosities of these melts (all the samples for which no measurements were done at 1523 and 1473 K) were calculated using equation 4.1.

In reproducing the experimental viscosities with the model, larger deviations were observed for the melts with 0.68, 1.23 and 4.32 wt.% of dissolved water (see Fig.4.9), though only in high viscosity range. Particularly high systematic deviations between experimental and calculated viscosities result in the melt with 4.32 wt.% dissolved H₂O for which the viscosities calculated by the model are 0.40 log units in average higher with a maximum of 0.55 log units. In the other melts deviations are not so significant and only a few measured viscosities have a deviation higher (± 0.28 log units for 1.23 wt.% water bearing melt) than the error given by the model. Deviations of single viscosities are mainly due to scattering in the experimental viscosities. Systematic and higher deviations (melt

with 4.32 ± 0.19 wt.% of dissolved water measured after experiment) may be due to the accuracy of measured water content. Another possibility is that the fit equation overestimates the dependence of water content for high water contents. Hence, an extrapolation towards higher water contents may systematically yield erroneously high viscosities.

At high temperatures differences between viscosities calculated using the model and VFT parameters are not significant. Particularly the sample 0.53 wt.% (Thies PhD thesis) gives higher viscosities calculated by VFT than the model in the isotherms plotted in Fig.4.10 with exception of the 1573 K isotherm. Viscosities of this sample were measured at low T with a different apparatus (at 0.1 MPa) and only four measurements are available. The use of limited experimental data may be the reason for the deviation in viscosities calculated by VFT parameters. Systematic deviations are found in the viscosity data of melts with 1.79, 2.71 and 4.82 wt.% of dissolved H₂O. These deviations are mainly in the viscosity range for which experimental measurements are not available (10^5 to 10^8 Pa·s) therefore, parameterisations of the model and the VFT in this range can be problematic.

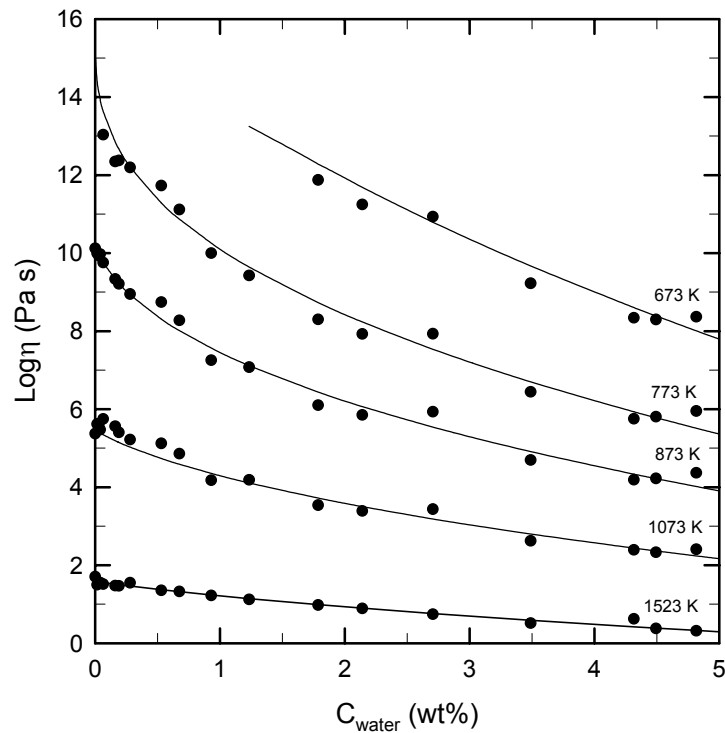


Fig.4.10. The isotherms show the comparison between the model (continuous lines) and viscosities calculated from VFT parameters (filled points).

4.3 Discussion

According to Behrens and Schulze (2003) pressure has a minor effect on viscosity (Fig.4.4) for molar fractions of non-bridging oxygen (X_{NBO}) about 0.15. Introduction of a pressure term is not required for float glass due to the negligible P -dependence of viscosity for this composition. Fig.4.10 shows the comparison between viscosities calculated by the model and by VFT parameters at fixed temperatures. A deviation occurs between viscosities calculated using VFT parameters and the equation 4.1 (see Fig.4.10) when 4.82 wt.% of water is dissolved in the melt. It is concluded that the model describes well the dependence of viscosity on water content at low viscosities but, possibly overestimates the dependence of viscosity on water content at high viscosities and high water contents. Hence, extrapolation of viscosity to high water contents is not recommended.

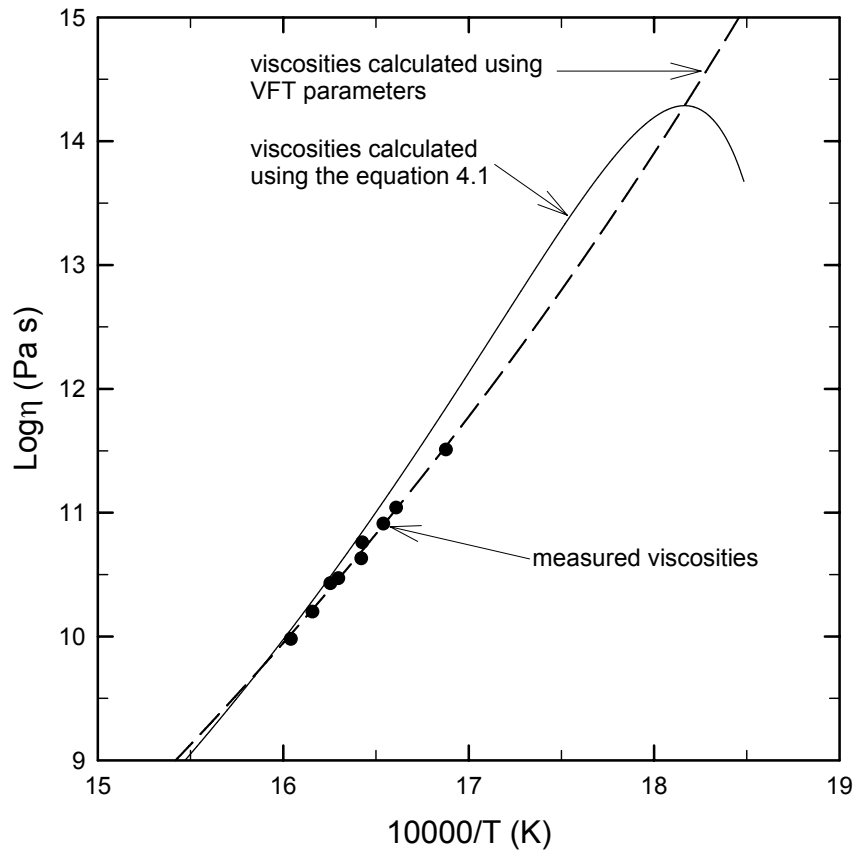


Fig.4.11 Comparison between experimental viscosities and calculated using equation 4.1 and VFT parameters for a melt glass with 4.82 wt.% of dissolved water.

Water has a profound effect on viscosity. By fixing isotherms (see Fig.4.10), viscosity is seen to be extremely sensitive to the water content in the melt. The strong decrease in viscosity is especially pronounced for small amounts of H₂O and at lower temperatures. In float glass a decrease of 2.6 log units was calculated when 1 wt.% of H₂O was added at 873 K while at 1523 K viscosity decreases by 1.3 log units when 5.0 wt.% is added.

In order to compare the T_g of different compositions as a function of water content, Deubener et al. (2003) (from geological processes to glass technology) proposed a model to calculate the reduced glass transition, T_g^* (ratio between the T_g of the melt and the glass transition temperature when the melt contains 0.02 wt.% of H₂O, T_g^{GN} such that $T_g^* = T_g / T_g^{GN}$). This model predicts the glass transition temperature of water bearing glasses

as a weighted combination of different contributing factors controlling T_g , dry glass, OH groups and molecular water

$$T_g^* = \frac{C_G \cdot 1.01 + A \cdot C_{OH} \cdot 0.22 + B \cdot C_{H_2O} \cdot 0.22}{C_G + A \cdot C_{OH} + B \cdot C_{H_2O}}$$

$C_G = (1 - C_w)$, C_{H_2O} and C_{OH} are the corresponding weight fractions ($C_i = c_i / 100\%$) of anhydrous glass and water dissolved as H₂O molecules and OH groups, respectively, C_w is the total water. A and B are parameters weighting the influence of hydroxyl and molecular H₂O on T_g^* , respectively. The reduced glass transitions for float glass were calculated as the ratio between the T_g (defined by a viscosity of 10¹² Pa·s, calculated using VFT parameters) and the T_g of a float glass containing 0.02 wt.% of total water (which is 822 K). Calculation of the T_g^* for the float glass studied in this work are consistent with results reported in Deubener et al. (2003). The reduced glass transition decreases with increasing total water content especially for low water content where H₂O is mainly dissolved as OH groups. The effect of total water content has less effect on the T_g^* for water-rich melts where molecular water becomes dominant.

Parameters A and B for float glass (using H₂O speciation data after Stuke et al. (submitted)) were calculated by fitting all T_g^* data simultaneously. The parameter A , which is weighting the influence of hydroxyl groups, was found to be 23.7 for a depolymerized float glass. This is significantly lower than the values found by Deubener et al. (2003), who found the A parameter to be 30 for depolymerized glass. The parameter B , which is weighting the influence of molecular water, was found to be 6.8, significantly *higher* than the value found by Deubener et al. (2003) who found a B value of 5 for depolymerized glasses. In both cases (this study and Deubener et al. 2003) it indicates that hydroxyl groups have larger influence on reduced glass transition of float glass than molecular

water. However, when comparing ratios of the influence of OH vs. molecular H₂O between studies, it is found that the influence of OH groups is still larger but is less significant in float glass. In a depolymerized float glass, hydroxyl groups have a weighting parameter (A) only 3.5 times more than the molecular water (B), as compared to a ratio (A/B) of 6 from Deubener et al. (2003). Therefore, for a depolymerized float glass, molecular water has more significant effect on T_g^* , when compared to the effect of OH-groups, than in other depolymerized glasses.

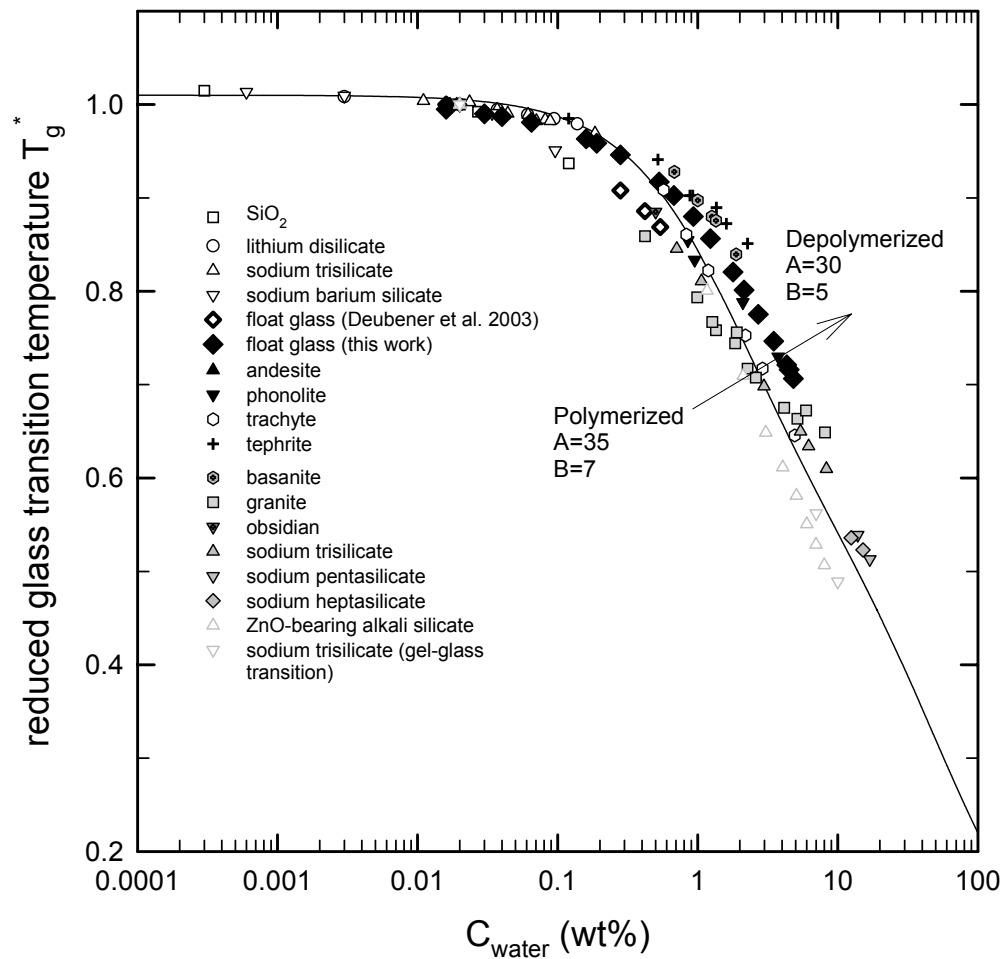


Fig.4.12. Reduced glass transition temperature as a function of total water content (wt.%) (from Deubener et al 2003). The data of float glass (this study), obtained from VFT equation for each water content, well fit with the model.

Fig.4.13 shows a comparison of the variation of the calculated glass transition temperature T_g with the dissolved water in float glass and several natural compositions from literature. Differences in composition do not produce different trends; all the T_g show a strong decrease for low total water content and a smaller decrease for high total water content.

In the polymerized albite melt, extensive depolymerization occurs as water is initially dissolved in the melt. The strong depolymerization is due to the fact that most of the water is dissolved as hydroxyl groups at low water content. With increasing water content further depolymerization occurs but less water is occurring as OH groups in the melt and the effect is not as strong.

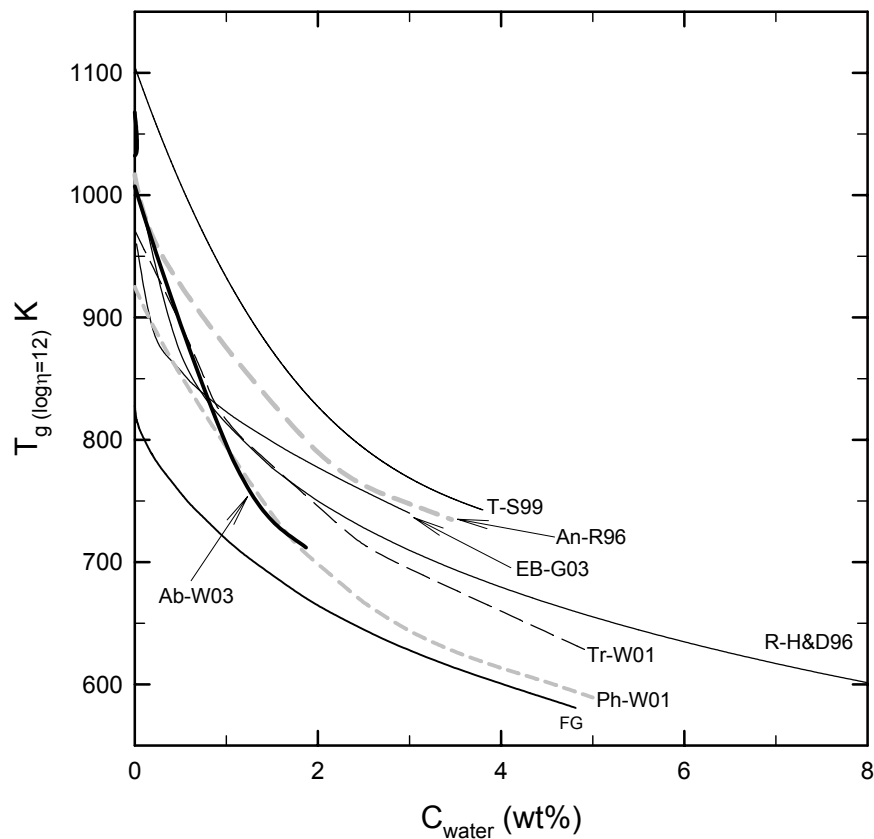


Fig.4.13 Comparison between glass transition temperatures of float glass with other silicate melts from literature. Ab=Albite (Whittington et al. 2003), An=Andesite (Richet et al. 1996), EB=Etna-Basalt (Giordano et al. 2003), FG=float glass (this work), Ph=Phonolite (Whittington et al. 2001), R=Rhyolite (Hess and Dingwell 1996), T=Tonalite (Schulze et al. 1999), Tr=Trachyte (Whittington et al. 2001).

The isokom of a depolymerized Etna basalt (Giordano et al. 2003) also shows a strong depression (temperature decreases by 70 K) when 0.2 wt.% of H₂O is added. All the glass transitions in Fig.4.13 decrease with an increase in water content, approach linearity at high water contents, and remain concave-up. However, depolymerized as well as polymerized melts show a strong influence of water on T_g when water is dissolved as hydroxyl groups. The effect of water at low water contents is lower for partially depolymerised melts such as float glass, due to the smaller influence of OH-groups on T_g in such glasses (as opposed to more polymerized melts), but is still strong.

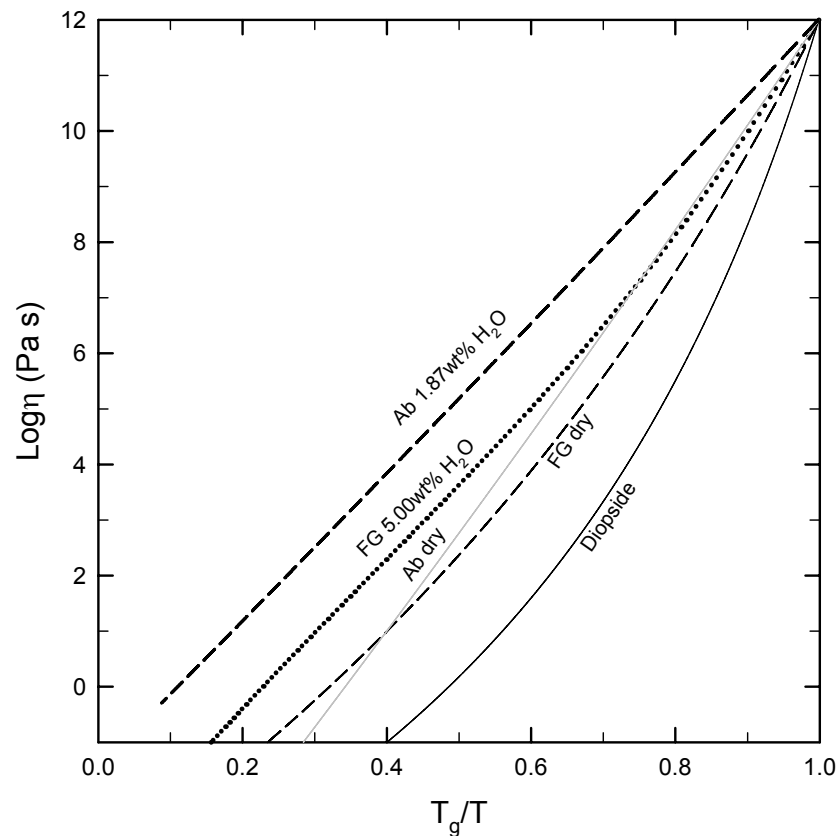


Fig.4.14 Fragility of dry float and anhydrous glass (this study) compared with dry albite (Ab) and diopside (Di) (Russell et al. 2003) and with water bearing albite (Whittington et al. 2003).

The degree of Non-Arrhenian behaviour can be quantified by the fragility of the melt (Angell et al. 2000). Fragile melts have strongly non-Arrhenian viscosity-temperature

relationships. Fragility increases from polymerised albite (Ab) to depolymerised diopside (Di). In Fig.4.14 the fragility of anhydrous and hydrous float glass are plotted with fragility calculated for anhydrous albite and diopside (Russell et al. 2003) and hydrous albite (Whittington et al 2003). It can be seen that both hydrous and anhydrous albite show a linear trend, showing no change in fragility with the addition of water to the melt. In contrast, the dry float glass melt shows a stronger curvature, increased fragility, compared to hydrous melt, indicating a decrease in fragility with the addition of water.

4.4 Application

In recent years the replacement of traditional air-fuel mixtures by oxygen-fuel mixtures for heating the tanks for melting glass has created a necessity for a better understanding of the reaction of water vapor with the molten glass. This is because the tank atmosphere is no longer diluted by nitrogen from air when pure oxygen is used and the partial pressure of water vapor in the tank atmosphere increases. The amount of chemically bound water, in the form of hydroxyl groups, in the glass increases as a square root of the increase in partial pressure of water vapor. As result glasses produce using oxygen-fuel firing contain a major amount of hydroxyl compared to the same glasses produced using air-fuel firing. Therefore, the influence of H₂O on the properties of water bearing technical glass especially at low water contents (technical glass contain usually <0.1wt.% of H₂O) must be well understood.

In glass manufacturing certain reference points, such as working point and softening point, are determined as function of viscosity. Fig.4.15 shows the variation of the working point (*WP*), softening point (*SP*) and glass transition temperature (*T_g*) with water content.

- The *WP* is the temperature at which the molten glass can be formed/manipulated; the viscous material is deformed into the final desired

shape. The working range is between 10^3 and $10^{6.6}$ Pa·s and a glass is named “long glass” when the working range is large or “short glass” when the working range is small. Viscosity is low enough ($\eta = 10^3$ Pa·s) for some shear processing (pressing, blowing, etc.) but high enough to retain some shape after shear is removed.

- The *SP* is the temperature at which glass will deform under its own weight. The Littleton softening point ($\eta = 10^{6.6}$ Pa·s) is measured by a standard fiber elongation test (1mm/min).
- T_g is the temperature at which viscosity is $\eta = 10^{12.3}$ Pa·s (in earlier work considered to be 10^{12} Pa·s). This value was chosen because at that viscosity the relaxation time equals the time necessary to measure macroscopic properties (thermodynamic properties) of the glass.

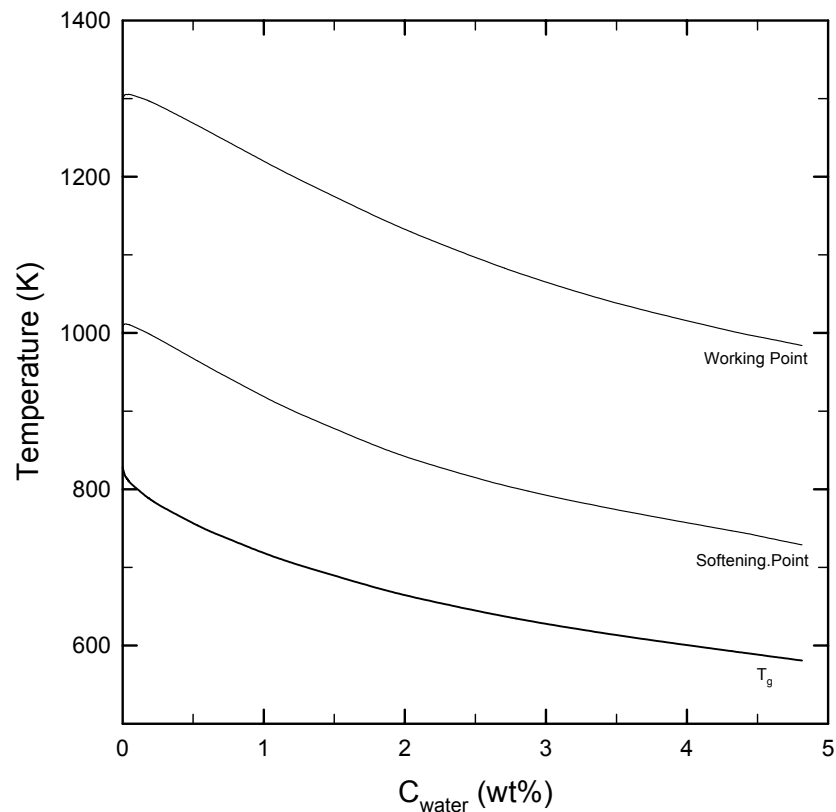


Fig.4.15 Variation of the most important reference points with the water content in the glass.

In Fig.4.15 is shown the variation of T_g , SP and WP as a function of water content calculated using VFT parameters. The three curves are more or less parallel indicating that the variations of the value of these points approximately have the same change with changing water content. While the glass transition temperature shows a continuous decrease with increasing the water content, the working point and the softening point show no variation of temperature for water contents lower than 0.1 wt.% and with higher water contents they start to decrease. Adding 4.82 wt.% water the value of each point decreases by about 200 K.

5. Pressure dependence of viscosity

5.1 Experimental results

Viscosity data obtained for melts along the An-Di join are summarized in the Appendix. Within the investigated temperature range, the viscosities can be described at each pressure by an Arrhenian relationship. The viscosities of melt Di_{100} are compared to literature data (Schulze et al. 1999) in Fig.5.1. These data at 200 MPa correspond well to previous data (highest deviation is ± 0.08 log units) except the viscosity measured at 1027 K ($\log\eta = 10.97$ Pa·s) which is 0.17 log units higher than that of Schulze et al. (1999). Viscosities at 300 MPa are systematically higher than the viscosities of Schulze et al. (1999). The new data are 0.47 log units higher at 1047 K and 0.50 log units at 1066 K. In order to have a larger pressure range than previous study, additional measurements were carried out at 400 MPa.

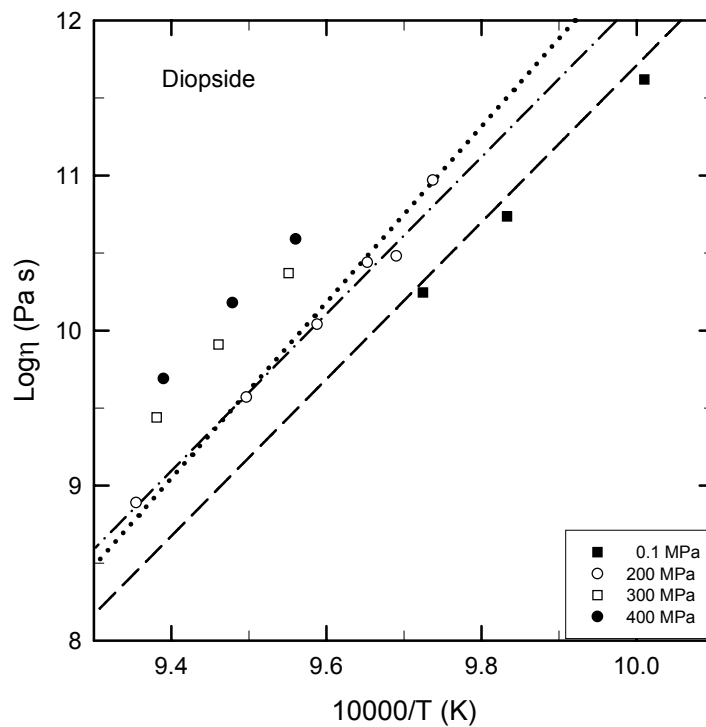


Fig.5.1 Arrhenian plot for melt viscosity of diopside at different pressures. Lines are fits from Schulze et al. 1999 for 0.1 MPa (dashed lines), 200 MPa (dashed-dotted line) and 300 MPa (dotted line).

After experiments at 400 MPa the shrinkage of the sample was about 40% (final length was approximately 50% of the minimum starting length of 8mm suggested by Schulze et al. 1999). As a result of the high amounts of shrinkage further sets of viscosity measurements at 100 MPa or 50 MPa was not possible. In both this study and that of Schulze et al. (1999) the same apparatus was used for viscosity experiments. Viscosity was also measured at ambient pressure using the creep apparatus of Neuville and Richet (1991). This data correspond to the data from Schulze et al. (1999) within ± 0.08 log units. As shown in Fig.5.1 the data at 0.1 MPa are consistent with the high pressure measurements, even considering that when using the creep apparatus of Neuville and Richet (1991) the applied load is 30 times greater. For reference temperatures, the temperatures at which the logarithm of melt viscosity at 200 MPa equals 9, 10 and 11 were chosen. In this study the logarithm of the viscosity of melt diopside equals 9 at 1066 K, 10 at 1044 K and 11 at 1024 K. The predictions of Behrens and Schulze (2003) (grey lines) are plotted for comparison at the same temperatures. The pressure dependence of viscosity (of diopside melt) determined in this work is consistently higher than that given by Behrens and Schulze (2003).

At a P-T condition of 300 MPa and 1066 K the logarithm of viscosity is 9.01 from Schulze et al. (1999), 8.97 from Behrens and Schulze (2003) and 9.45 from this study. This difference is less at 300 MPa and 1024 K condition at which the logarithm of viscosity is 11.18 from Schulze et al. (1999), 10.95 from Behrens and Schulze (2003) and 11.55 from this study. The viscosities measured at 0.1 MPa are higher than the ones calculated with parameters given by Behrens and Schulze (2003) between 0.09 log units at 1024 K and 0.12 log units at 1066 K. Small differences in composition (0.23 wt% higher MgO and 0.65 wt% lower CaO in this study) can not explain the differences between the two sets of data.

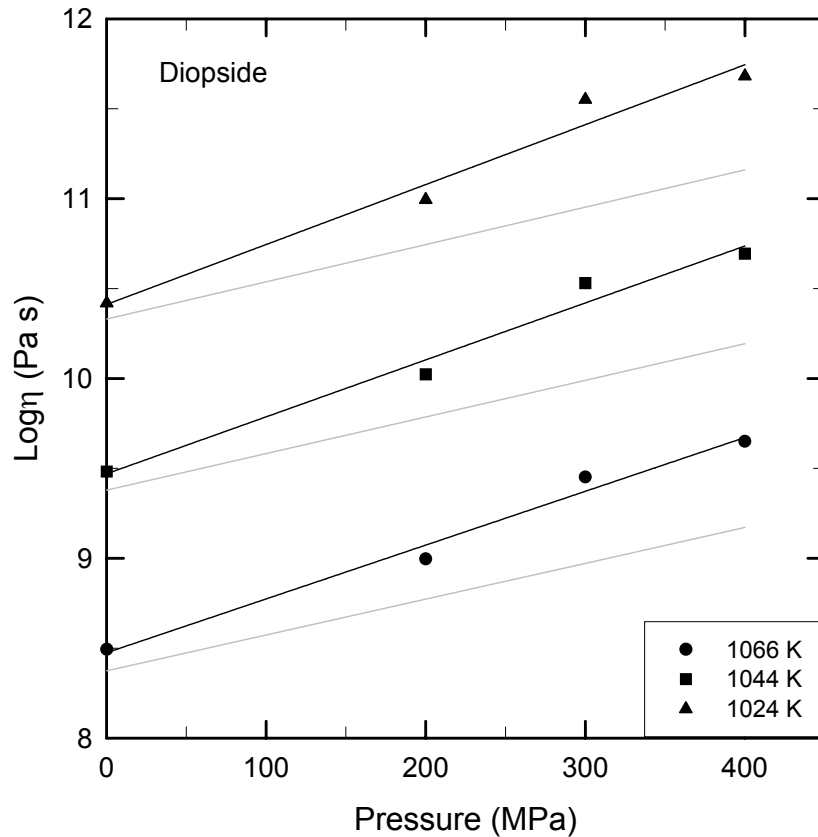


Fig.5.2 Viscosity of diopside melt measured as a function of pressure. Data at 0.1 MPa were measured in a creep viscometer in Paris (Neuville and Richet, 1991). Solid lines are linear regression of the data and grey lines are reporting viscosity as function of pressure calculated after Behrens and Schulze (2003) for some temperature.

A combination between the scattering of the data and the shorter pressure range of the investigation done by Behrens and Schulze (2003) may be the source of their lower pressure effect.

The viscosity of anorthite melt was measured at 0.1 MPa in the creep apparatus of Neuville and Richet (1991) and under pressure (range 50 – 400 MPa) with creep apparatus of Schulze et al. (1999). Data at 0.1 MPa correspond well with data from Taniguchi (1992) within ± 0.25 log units and with Russell et al. (2003) within ± 0.05 log units (Fig.5.3). It was only possible to investigate a narrow range of temperatures (1128 -1158 K) under pressure because the range of glass transition for anorthite melt is too close to the upper temperature limit of the viscometer. While the scatter of the measurements with respect to

the regression line at fixed pressure is less than ± 0.08 log units for anorthite melt, the scatter of calculated viscosities at fixed temperature (1186, 1163 and 1140 K) is higher (± 0.18 log units at 1186 K). The measured viscosities at 50 and 200 MPa are lower than values given by the linear regression. However, negative pressure dependence of viscosity, already observed in the polymerized albite melt (Behrens and Schulze 2003), is also evident for polymerized anorthite melt. At 1186 K in melt anorthite viscosity decreases by 0.32 log units when pressure increases from 0.1 MPa to 400 MPa while at 1140 K the decrease is 0.45 log units (see Fig.5.4). The pressure dependence of viscosity becomes positive in $An_{75}Di_{25}$ with an increase of 0.28 log units at 1112 K as a result of a pressure increase from 50 MPa to 400 MPa (temperature at which the logarithm of viscosity is 10 at 200 MPa).

The pressure dependence of viscosity was also measured in four alkali silicate melts (a metasilicate, tetrasilicate, trisilicate and a disilicate). The viscosity of the metasilicate melt was determined in the pressure range from 50 to 340 MPa (only one measurement at 340 MPa and temperature of 626 K because of technical problems with the viscometer).

At 638 K, the temperature at which the viscosity of the metasilicate melt equals 10^{10} Pa·s at 200 MPa, viscosity increases by 0.39 log units when pressure is increased from 50 to 300 MPa. An experimental problem also occurred using the tetrasilicate so that only one measurement was carried out at 300 MPa and 733 K. After completion of the viscosity experiment with the sample LNK3S (trisilicate) the shrinkage was too high (43%). The viscosities at 50 MPa were the last measured for this sample and it is believed that the high shrinkage is the source of the apparently high viscosity values at 50 MPa, especially at higher temperatures. For this reason the set of measurement at 50 MPa was neglected in Fig.5.6 and in the evaluation of pressure dependence. A full set of viscosity data was obtained for the disilicate melt.

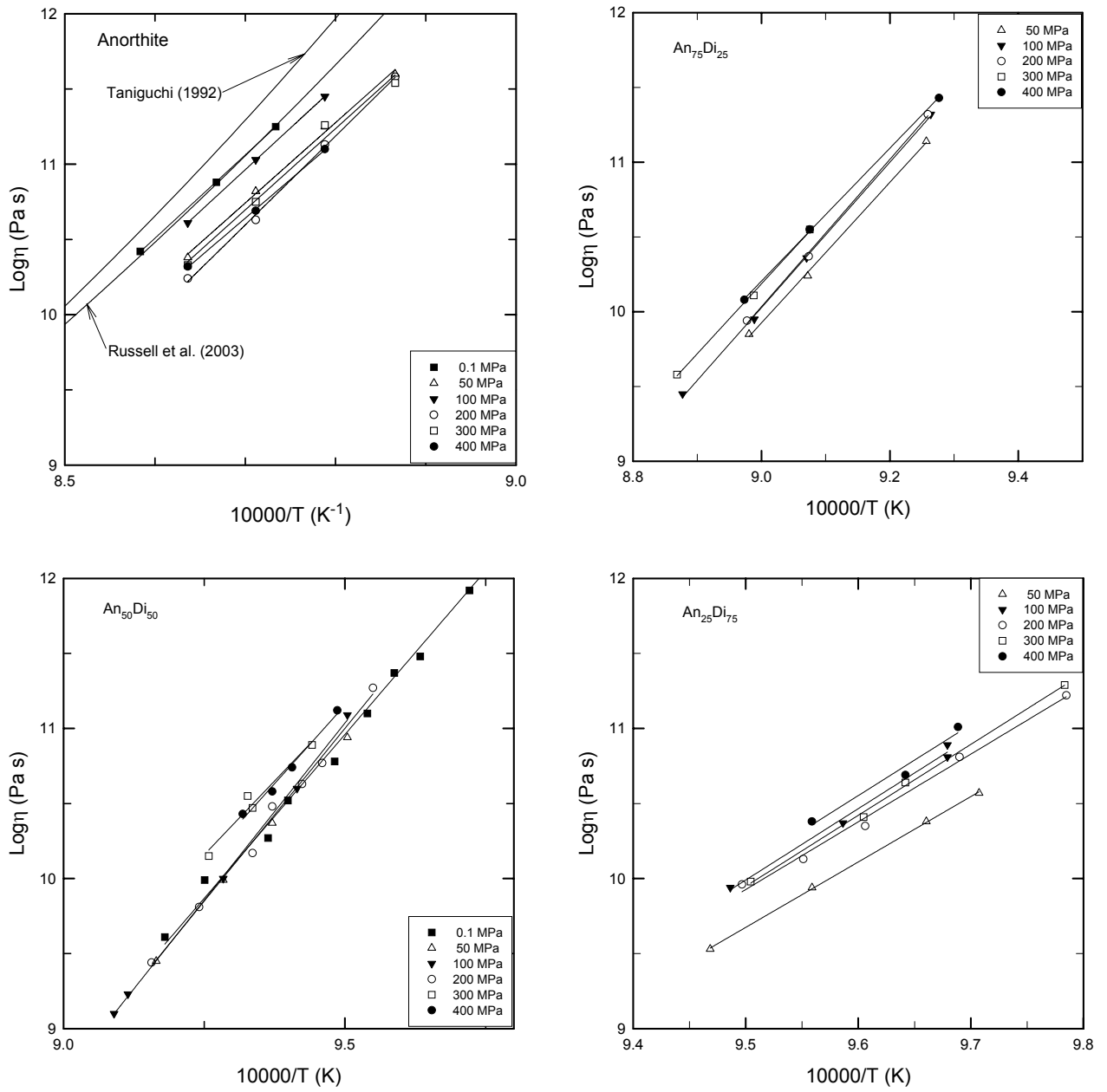


Fig.5.3 Arrhenius plots for melt viscosity along the join An-Di at various pressures.

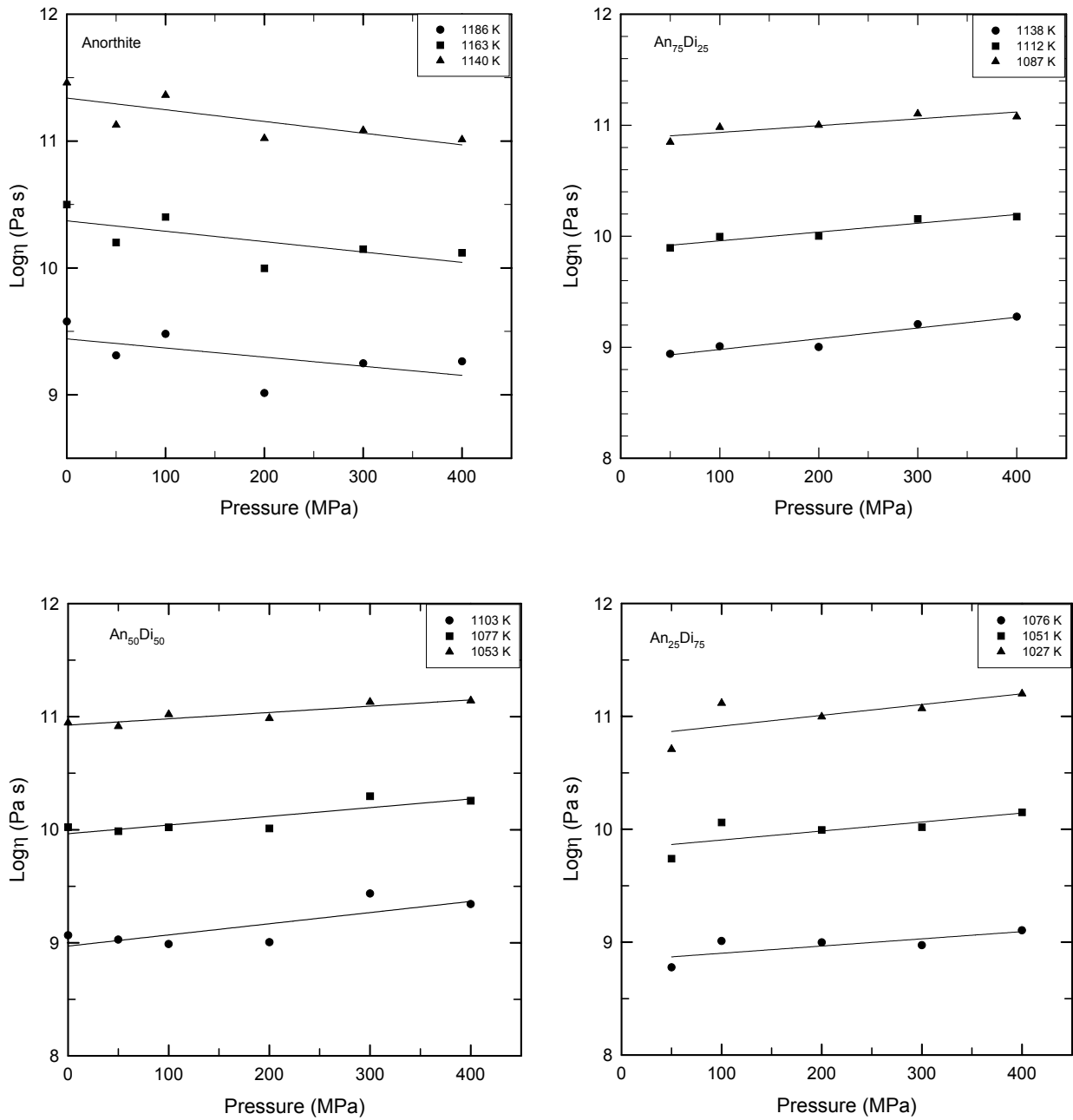


Fig.5.4 Pressure dependence of melt viscosity in the system An-Di. Isotherms are plotted for reference temperatures at which the melt viscosity at 200 MPa equals 10^9 Pa·s (filled circles), 10^{10} Pa·s (filled squares) and 10^{11} Pa·s (filled triangles).

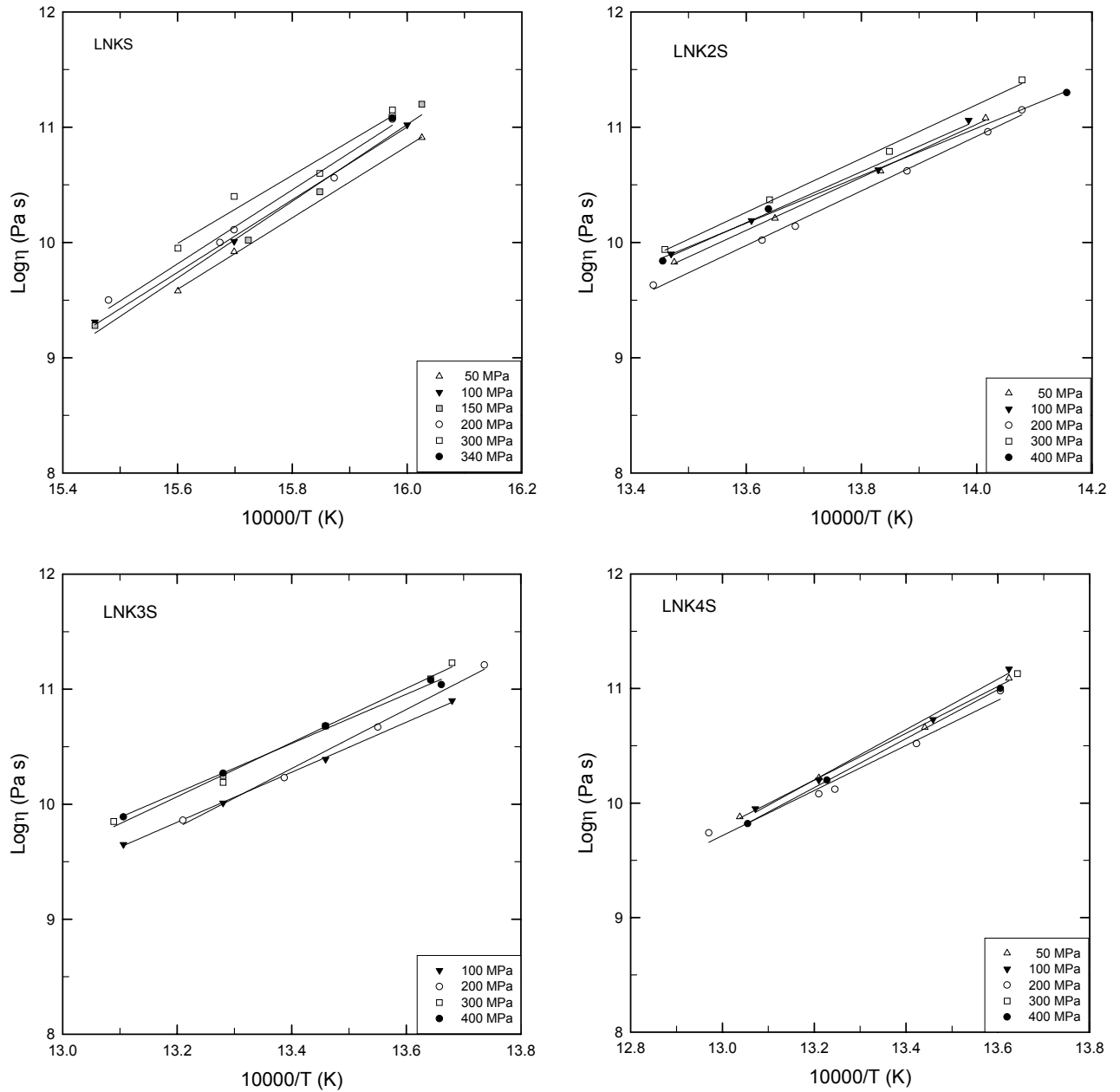


Fig.5.5 Temperature dependence of viscosity of alkali silicate under several pressures.

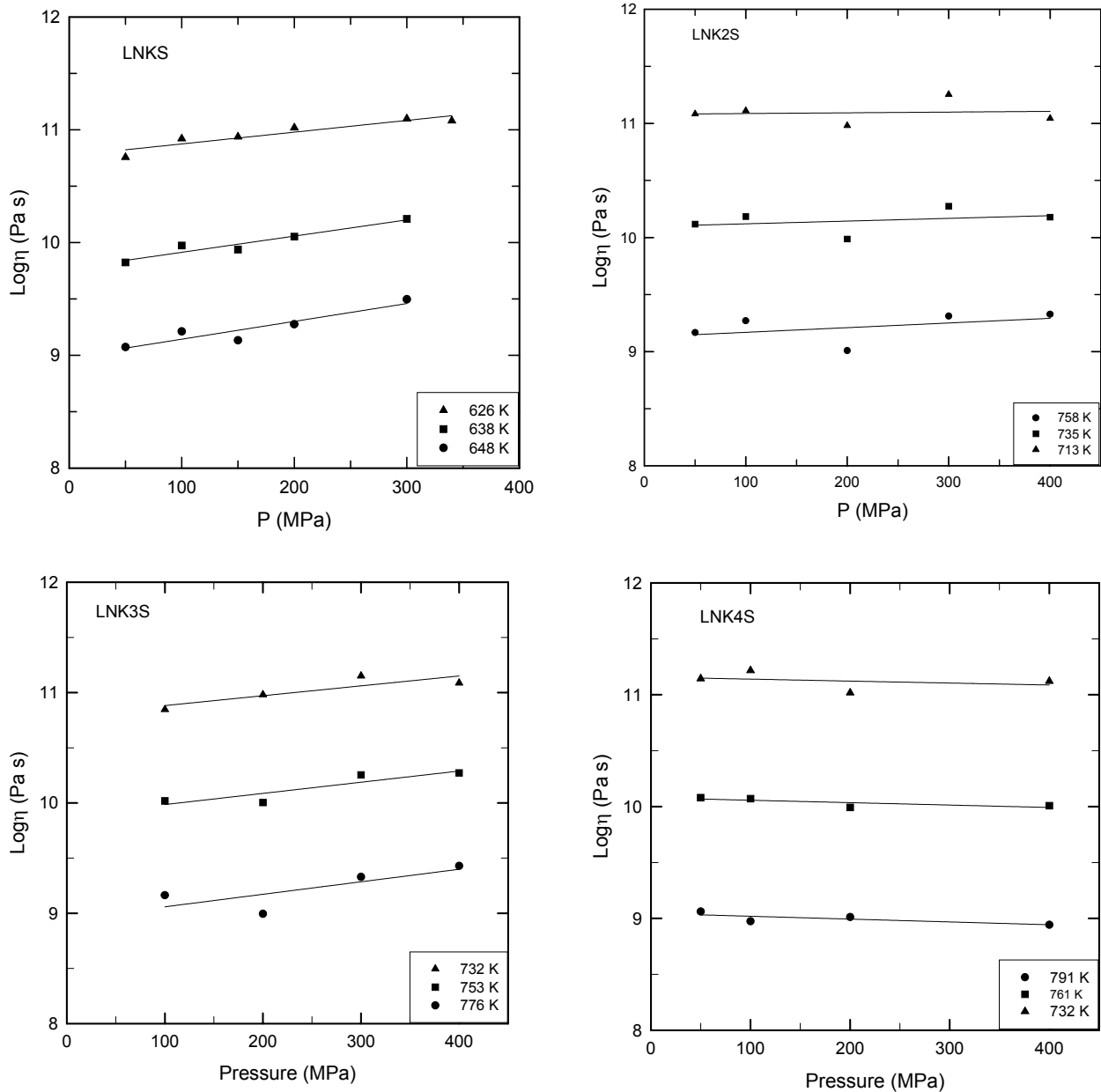


Fig.5.6 Pressure dependence of viscosity of alkali silicate.

For each composition the value of the apparent activation volume (V_a) as $V_a = 2.303 \cdot R \cdot T \cdot (\partial \log \eta / \partial P)$ was calculated using linear regressions of $\log \eta$ versus pressure at constant temperature (Behrens and Schulze 2003). In order to compare the data of the An-Di system and alkali silicate melts (investigated in this work) with other melt composition V_a was related to the X_{NBO} (molar fraction of non bridging oxygen atoms). X_{NBO} (which is equals to $NBO / (NBO + BO)$, NBO are non bridging oxygen atoms and BO

bridging oxygen atoms) is suitable as the main compositional variable in graphical representation. X_{NBO} was preferred over NBO/T (ratio between non bridging oxygen atoms to tetrahedral cations) because it is a valid thermodynamic compositional variable for a two oxygen mixing model, in contrast to NBO/T which has no ultimate thermodynamic justification. Furthermore, the degree of melt polymerization can be quantified in terms of X_{NBO} where $X_{NBO}=0$ in case of completely polymerized melts and $X_{NBO}=1$ for completely depolymerised melts. In Fig.5.7 third-order polynomials are used to illustrate the compositional trend of V_a in the system albite-diopside (Behrens and Schulze 2003). The An_{100} melt viscosity shows a negative pressure dependence of over the entire temperature range investigated. The V_a values vary slightly with temperature from -16.3 ± 11.3 cm^3/mol at 1186 K to -20.1 ± 8.7 cm^3/mol at 1140 K (the uncertainty of V_a corresponds to the 1σ standard deviation in the regression). The pressure dependence of viscosity is positive for all Di-bearing compositions. The V_a values in Di-bearing compositions of the join An-Di increases with decreasing temperature as well as in the system Ab-Di from Behrens and Schulze (2003). An exception is $An_{50}Di_{50}$ which has a V_a value at 1103 K of 20.8 ± 8.4 cm^3/mol and 11.2 ± 2.1 cm^3/mol at 1053 K. The V_a for Di melt is higher than the one from Behrens and Schulze (2003). However, the scatter is higher in the new measurements and real compositions are slightly different in both studies. In the case of alkali silicate the pressure effect is not significant and does not vary with temperature in LNK4S (average V_a value of -3.15 ± 3.0 cm^3/mol , X_{NBO} of 0.206). With the increase of alkali content V_a becomes increasingly positive. In contrast to the observation in the system An-Di as well in the system Ab-Di, V_a does not vary significantly with temperature in the alkali silicate.

The variation of V_a with composition in the system An-Di similar to that found in the system Ab-Di (Behrens and Schulze 2003) while in the alkali silicate system at a given X_{NBO} , V_a is slightly smaller.

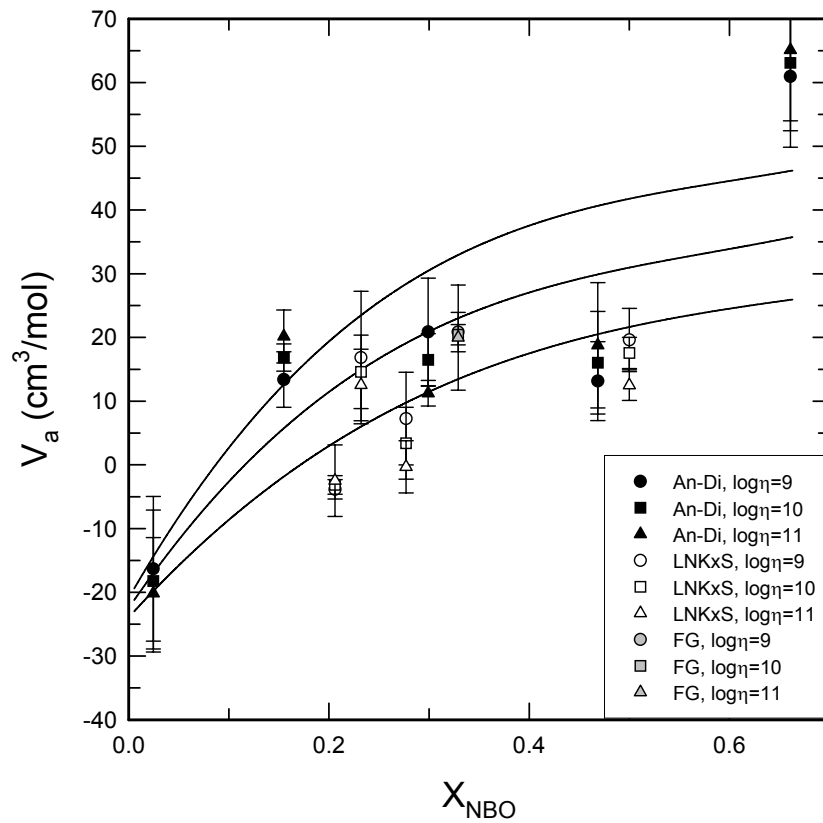


Fig.5.7 Variation of the apparent activation volume (V_a) for viscous flow with mol fraction of non-bridging oxygen (X_{NBO}). Error bars correspond to 1σ standard deviation of the linear regressions shown in figures 5.4 and 5.6. Lines are fits by third-order polynomials to illustrate the compositional trend of V_a in the system albite-diopside (Behrens and Schulze 2003).

Tab.5.1 Results of combined P - T fitting using equation 5.1.

Sample	X_{NBO}	T (K)	P (MPa)	$Log\eta_0$ (Pa·s)	E_a (kJ/mol)	V_a ($10^{-6} m^3/mol$)
An ₁₀₀	0.025	1128 – 1158	0.1 – 400	-33.4 (2.87)	975.8 (63.0)	-17.5 (4.3)
An ₇₅ Di ₂₅	0.155	1100 – 1127	50 – 400	-31.7 (0.85)	886.0 (18.1)	14.5 (2.0)
An ₅₀ Di ₅₀	0.299	1047 – 1067	0.1 – 400	-31.7 (0.70)	858.7 (14.2)	13.3 (2.0)
An ₂₅ Di ₇₅	0.468	1033 – 1054	50 – 100	-33.7 (2.77)	875.6 (55.3)	17.2 (4.3)
Di ₁₀₀	0.661	1027 – 1069	0.1 – 400	-39.4 (1.39)	975.5 (26.8)	64.1 (4.9)
FG (0.28 wt% H ₂ O)	0.329	504 – 577	50 – 300	-18.5 (0.47)	450.2 (73.3)	21.7 (2.3)
LNKS	0.500	626 – 646	50 – 340	-39.3 (1.59)	599.8 (19.5)	15.4 (2.6)
LNK2S	0.277	713 – 744	50 – 400	-19.3 (1.52)	414.5 (21.2)	1.7 (2.7)
LNK3S	0.232	720 – 773	100 – 400	-18.8 (1.92)	412.6 (27.5)	18.2 (4.7)
LNK4S	0.206	735 - 771	50 – 400	-17.8 (0.90)	405.8 (13.8)	-2.9 (1.9)

In parenthesis 1σ standard error of estimate.

A combined P - T fitting using the following equation (Behrens and Schulze 2003)

$$\log\eta = \log\eta_0 + \frac{E_a + V_a \cdot P}{2.303 \cdot R \cdot T} \quad 5.1$$

also reproduces the measured viscosities in (Table 5.1). The parameters derived by combined P - T fitting represent average values of V_a and E_a in the investigated viscosity range. A fundamental assumption in this fitting is that E_a and V_a do not vary with pressure and temperature. No additional parameters such as temperature derivatives of E_a and V_a using combined P - T fitting of our data and previous data can be constrained because the error of the experimental viscosity data is too high. There is a possible trend of increasing V_a with decreasing T , however due to scatter it can not be proven with any statistical certainty. In Fig.5.8 the average values of V_a are plotted for An-Di, alkali silicate and float glass melts (containing 0.28 wt% H₂O) and compared with best fit line of the Ab-Di join from Behrens and Schulze (2003). The values of V_a for the Ab-Di join and for the standard glass DGG (Schulze 2000) are also plotted. The An-Di system, Ab-Di system and LNK3S all show a similar variation in V_a . The V_a values of the other alkali silicate melts are always slightly lower. The calculated V_a value for a diopside melt is 64.1 ± 4.9 cm³/mol versus 40.7 ± 2.3 cm³/mol given by Behrens and Schulze (2003).

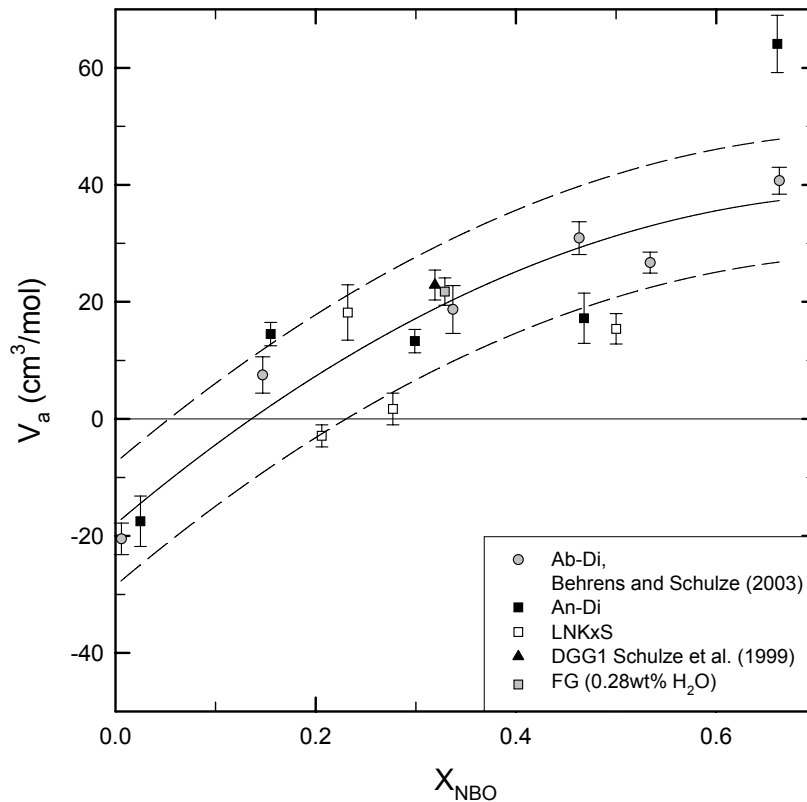


Fig.5.8 Comparison of V_a values for melts of the join An-Di (filled squares) with LNKxS system (open squares) and continuous line reproduces the Ab-Di system from Behrens and Schulze (2003) and dashed lines the 1σ standard deviation. Error bars represent 1σ standard deviation.

5.2 Discussion

In the high pressure range (10^9 to 10^{11} Pa·s), the pressure dependence of the melt viscosity is determined mainly by the degree of melt polymerization and less by the specific composition of the melt. Melts such as albite (containing alkali metals) and melts such as anorthite (containing alkali earths) have similar negative values of V_a of -20.5 ± 2.6 and -17.5 ± 4.9 cm³/mol, respectively. This indicates that V_a is mainly dependent on the degree of polymerization and is not sensitive to compositional variations in this case. A similar value (-22.2 ± 6.7 cm³/mol) was found for a tonalitic composition ($\text{QZ}_{33}\text{Ab}_{33}\text{An}_{33}$) by Schulze et al. (1999). All data in the An-Di and Ab-Di systems show negative pressure dependence for fully polymerized melts going to zero pressure dependence around a value

of 0.17 for X_{NBO} and positive pressure dependence for partially and fully depolymerized melts above this value. Results for alkali silicate melts are consistent with the trend of increasing V_a with increasing melt depolymerization found in the An-Di and Ab-Di systems, although the dependence appears to be less pronounced.

Combined effect of pressure and water content was investigated in hydrous float glass. The effect of water content on viscosity is greater than that of pressure. For instance, the highest pressure effect on viscosity of float glass was found in the glass containing 0.28 wt% of H_2O where viscosity increases by 0.10 log units per 100 MPa at temperature of 834 K. In comparison adding only 0.10 wt% water to a dry float glass, at 200 MPa and 834 K, viscosity will decrease by 0.84 log units.

The change of calculated glass transition temperature T_g as function of pressure for anorthite is higher (-3 K/100 MPa when pressure is increased from 200 to 300 MPa) than the one calculated by Taniguchi (1992) (-0.39 K/100 MPa) for the same composition. This difference can be due to the different methods of calculation of T_g , in this work it is calculated by linear regression fitting of the viscosity data (high viscosity range) at each pressure (ranging between 0.1 to 400 MPa). Taniguchi calculated it using the Williams-Landel-Ferry (WLF) equation modified for the calculation of T_g (Taniguchi, 1992). With this method T_g is also calculated by fitting viscosities data but only low viscosities (Taniguchi 1992) were available under pressure (range 0.1 MPa-2GPa). The T_g calculated by WLF-modified by Taniguchi (1992) for diopside gives a positive pressure dependence and equals 3.4 K/100 MPa, in comparison the pressure dependence of glass transition temperature calculated in this work is 6 K/100 MPa.

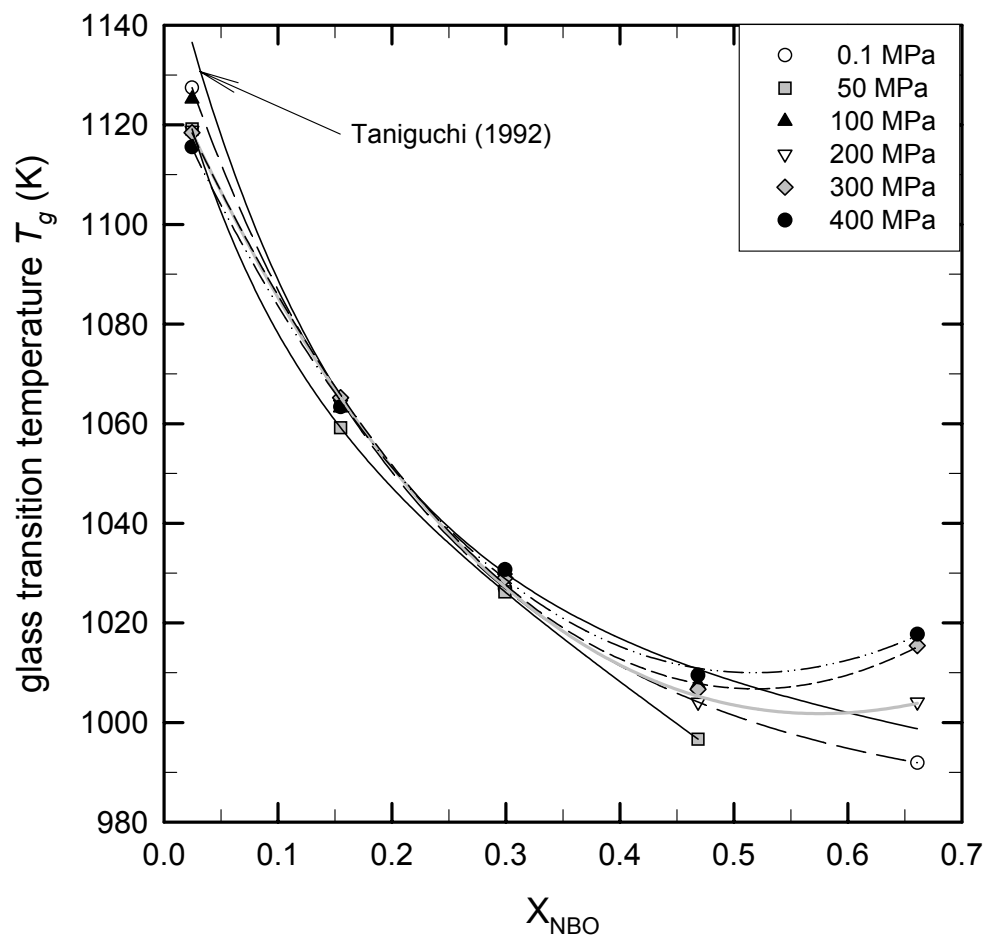


Fig.5.9 Glass transition temperatures T_g along the join An-Di in the range of pressures 0.1 to 400 MPa compared to literature data at 0.1 MPa (Taniguchi 1992).

Conclusion

Newtonian viscosities of silicate melts were investigated over a wide range of pressures (0.1 to 400 MPa) and temperatures (573 to 1523 K). Viscosities of water bearing float glass (0 to 4.82 wt% H₂O) were extensively studied at constrained pressure of 200 MPa. Experiments were performed on selected hydrous float glasses varying the pressure (50 to 400 MPa). The effect of temperature and water content on viscosity is much larger than that of pressure in particular at low H₂O contents. There was no effect of pressure on viscosity in *quasi*-dry (0.03 wt%) and water bearing melts (up to 2.14 wt%), consistent with results of melts having similar molar fraction of non-bridging oxygen $X_{NBO} = 0.15$ (Behrens and Schulze 2003). The maximum pressure effect measured in float glass was in a glass with 0.28 wt% of H₂O dissolved. With this composition an increase in pressure by 200 MPa can be compensated by a decrease of 10 K in temperature. At low water contents water is mainly dissolved as hydroxyl groups (chemically dissolved water). These hydroxyl groups break bridging oxygen bonds explaining the decrease of viscosity.

The glass transition temperature T_g in float glass decreases by 247 K when 4.82 wt% of H₂O is added to the melt, a similar trend occurs with other compositions. The T_g of float glass is lower than many natural liquids but the trend is the same. The reduced glass transition T_g^* (Deubener et al. 2003) is consistent with the T_g^* of the other melts. There is a large decrease in T_g^* with the addition of water at low water contents, at higher water contents this effect becomes less pronounced. The large decrease in T_g^* at low water content is generally explained by the preferential incorporation of OH-groups over molecular water which occurs less at higher water contents. However, the influence of OH

groups on T_g^* in depolymerized float glass is less than suggested by Deubener et al. (2003) for some other depolymerized melts.

In order to calculate viscosities of water bearing float glass as function of temperature and H₂O content a new model is presented, applicable in the T -range $T_g - 1523$ K and H₂O-range dry - 4.82 wt%. Using this model over the stated range viscosities can be predicted to within 0.23 log units (1σ).

The effect of pressure on viscosity was investigated in the high viscosity range along the anorthite-diopside join and in alkali metal silicate melts. Viscosity of diopside melt fit well with the previous study of Schulze et al. (1999) at 0.1 and 200 MPa, while the viscosities measured at 300 MPa are 0.40 log units higher than the measurements of Schulze et al (1999).

In a narrow T -range viscosity can be expressed as function of activation energy E_a and apparent activation volume V_a . In order to compare the pressure effect on viscosities of different melt compositions, V_a was related to the molar fraction of non-bridging oxygens X_{NBO} [$X_{NBO}=0$ in polymerized melts (An) and $X_{NBO}=1$ in completely depolymerized melts (Di)]. The apparent activation volume varies along the join An-Di from a negative value in polymerized anorthite to positive in fully depolymerized diopside the same trend was also observed along the join Ab-Di (Behrens and Schulze 2003). Higher value of V_a were found for the diopside melt compared to previous work (64.1 ± 4.9 cm³/mol instead 40.7 ± 2.3 cm³/mol), this may be due to the larger range of pressure investigated in this study compared to the previous work.

The variation of viscosities with varying pressure in the alkali silicate system is also consistent with previous result of Behrens and Schulze (2003) with a slightly negative pressure dependence of viscosity in partially depolymerized tetrasilicate melts to positive in more polymerized metasilicate melts.

By comparing the results of this work with the previous results (Behrens and Schulze 2003) it is concluded that the pressure dependence of melt viscosities is more dependant on the degree of melt polymerization and less on the specific melt composition. Along the anorthite-diopside join, at same X_{NBO} , the higher values of V_a occur at lower temperature (the effect of pressure becomes higher with decreasing the temperature) this was also observed in the system Ab-Di (Behrens and Schulze 2003).

Tab.1. Composition of float glass and DGG1 melts (in wt%)

	Float Glass (Potters-Ballotini company)	DGG1
SiO ₂	72.01 ± 0.55	71.72
Al ₂ O ₃	0.76 ± 0.06	1.23
Na ₂ O	13.13 ± 0.28	14.95
CaO	8.96 ± 0.18	6.73
MgO	3.92 ± 0.12	4.18
K ₂ O	0.25 ± 0.05	0.38
BaO	-	-
Fe ₂ O ₃	0.10 ± 0.09	0.19
B ₂ O ₃	-	-
TiO ₂	-	0.14
ZrO ₂	-	-
SO ₃	-	0.44
P ₂ O ₅	-	-

Composition of float glass after Behrens and Stuke (2003).

Composition of DGG1 after Schulze (2000)

Tab.2. Composition of float glass and DGG1 (in mol%)

	Float Glass (Potters-Ballotini company)	DGG1
SiO ₂	71.39 ± 0.54	70.92
Al ₂ O ₃	0.44 ± 0.03	0.72
Na ₂ O	12.62 ± 0.27	14.33
CaO	9.51 ± 0.19	7.13
MgO	5.80 ± 0.18	6.16
K ₂ O	0.16 ± 0.03	0.24
BaO	-	-
FeO/Fe ₂ O ₃	0.04 ± 0.04	0.07
B ₂ O ₃	-	-
TiO ₂	-	0.10
ZrO ₂	-	-
SO ₃	-	0.33
P ₂ O ₅	-	-

Tab.3. VFT parameters for water bearing float glass

C_{water} (wt%)	A	B	T_0
0.00	-3.37	5089.5	497.4
0.03	-3.75	5644.7	461.4
0.04	-2.48	3938.7	554.4
0.06	-4.82	7337.6	369.1
0.16	-4.88	7526.1	341.8
0.19	-3.96	6082.1	408.1
0.28	-3.46	5416.9	431.2
0.68	-3.80	5845.7	382.4
0.93	-2.04	3417.1	488.4
1.23	-3.29	5123.8	366.7
1.79	-2.33	3679.9	419.2
2.14	-2.34	3627.6	409.2
2.71	-3.43	5024.5	323.9
3.49	-2.28	3257.3	386.2
4.32	-1.87	2664.7	405.2
4.49	-2.28	3071.0	375.1
4.82	-2.81	3744.6	331.6

VFT parameters were calculated by fitting simultaneously measured high viscosities and measured and calculated (by the model) low viscosities.

Tab.4. Viscosity of DGG1 melts.

DGG1-a	T (K)	Log η (Pa·s)
	853	11.03
	852	10.99
	853	11.05
	862	10.57
	873	10.18
	883	9.80
	853	10.99
DGG1-b	861	10.46
	875	9.85
	877	9.83
	874	9.95
	880	9.71
	880	9.70
	894	9.22
	895	9.17
	905	8.84
	905	8.88
	905	8.86
	913	8.59
DGG1-c	862	10.56
	871	10.19
	882	9.85
	892	9.51
DGG1-d	850	10.95
	866	10.33
	881	9.78
	897	9.31
	852	10.83

All the viscosities were measured at 200 MPa.

Tab.5. Viscosity of float glass melts.

Sample	C _{water} (wt%)	P (MPa)	T (K)	Log η (Pa·s)
FG0a	0.03	200	851	10.72
	0.03	200	870	10.09
	0.03	200	881	9.74
	0.03	200	892	9.40
	0.03	200	902	9.09
	0.03	200	911	8.75
FG1	0.04	100	861	10.46
	0.04	200	850	10.89
	0.04	200	861	10.31
	0.04	200	869	9.95
	0.04	200	881	9.64
	0.04	300	861	10.50
	0.04	350	861	10.54
FG2	0.06	200	831	10.89
	0.06	200	852	10.55
	0.06	200	862	10.16
	0.06	200	872	9.79
	0.06	200	882	9.47
	0.06	200	891	9.15
	0.06	200	901	8.85
	0.06	200	881	9.49
	0.06	200	870	9.82
	0.06	200	861	10.22
	0.06	200	841	10.64
	FG3	0.16	200	821
0.16		200	842	10.32
0.16		200	852	9.96
0.16		200	862	9.64
0.16		200	873	9.31
0.16		200	882	8.99
0.16		200	892	8.66
0.16		200	864	9.59
0.16		200	824	10.54
FG4	0.19	200	821	10.84
	0.19	200	831	10.45
	0.19	200	841	10.08
	0.19	200	851	9.79
	0.19	200	862	9.46
	0.19	200	872	9.15
	0.19	200	883	8.86
	0.19	200	821	10.72

FG6a	0.28	50	831	9.89
	0.28	50	850	9.23
	0.28	50	813	10.55
	0.28	50	794	11.30
	0.28	100	837	9.76
	0.28	100	817	10.47
	0.28	100	798	11.16
	0.28	100	777	11.78
	0.28	200	848	9.49
	0.28	200	819	10.52
	0.28	200	809	10.90
	0.28	200	799	11.23
	0.28	200	789	11.65
	0.28	200	827	10.25
	0.28	200	827	10.26
	0.28	200	846	9.57
	0.28	300	847	9.64
	0.28	300	819	10.73
	0.28	300	790	11.71
FG7	0.29	200	1523	1.57
FG8	0.67	200	1523	1.36
FG9	0.68	200	770	11.41
	0.68	200	775	11.02
	0.68	200	780	10.90
	0.68	200	791	10.48
	0.68	200	801	10.17
	0.68	200	811	9.84
	0.68	200	820	9.51
	0.68	200	804	10.09
	0.68	200	775	10.99
	0.68	200	1473	1.71
	0.68	200	1523	1.17
	FG10	0.93	50	771
0.93		100	771	10.08
0.93		200	813	8.49
0.93		200	762	10.29
0.93		200	771	10.01
0.93		200	781	9.65
0.93		200	763	10.45
0.93		200	762	10.58
0.93		300	771	10.14
0.93		400	771	10.17

FG11	1.23	200	731	10.76	
	1.23	200	721	11.17	
	1.23	200	741	10.41	
	1.23	200	751	10.07	
	1.23	200	761	9.75	
	1.23	200	772	9.41	
	1.23	200	732	10.73	
	1.23	200	793	8.68	
FG12	1.79	200	722	9.77	
	1.79	200	702	10.83	
	1.79	200	692	11.19	
	1.79	200	712	10.24	
	1.79	200	722	9.90	
	1.79	200	732	9.51	
	1.79	200	742	9.11	
	1.79	200	722	9.78	
	1.79	200	702	10.61	
	1.79	200	719	9.97	
	1.79	200	718	9.89	
	FG13	2.14	50	702	10.20
2.14		100	702	10.21	
2.14		200	690	10.63	
2.14		200	699	10.15	
2.14		200	709	9.73	
2.14		200	699	10.12	
2.14		200	689	10.56	
2.14		200	684	10.91	
2.14		200	702	10.07	
2.14		200	723	9.26	
2.14		300	702	10.19	
2.14		400	702	10.07	
FG14		2.71	200	667	11.19
		2.71	200	677	10.67
	2.71	200	683	10.48	
	2.71	200	688	10.41	
	2.71	200	694	10.21	
	2.71	200	699	9.99	
	2.71	200	705	9.73	
	2.71	200	696	10.07	
	2.71	200	675	10.90	
	2.71	200	656	11.75	

FG15	3.49	200	624	11.45
	3.49	200	635	10.77
	3.49	200	646	10.31
	3.49	200	650	10.07
	3.49	200	656	9.86
	3.49	200	661	9.60
	3.49	200	665	9.37
	3.49	200	656	9.77
	3.49	200	645	10.21
	3.49	200	635	10.82
	3.49	200	625	11.39
	3.49	200	1523	0.54
FG16	4.32	200	600	11.70
	4.32	200	610	11.16
	4.32	200	622	10.41
	4.32	200	627	10.17
	4.32	200	632	9.92
	4.32	200	636	9.69
	4.32	200	641	9.45
	4.32	200	630	9.91
	4.32	200	620	10.46
	4.32	200	611	11.36
	4.32	200	1473	0.78
	FG17	4.49	200	601
4.49		200	611	10.80
4.49		200	621	10.19
4.49		200	632	9.74
4.49		200	642	9.26
4.49		200	626	9.90
4.49		200	616	10.46
4.49		200	601	11.33
FG18	4.82	200	605	10.91
	4.82	200	609	10.63
	4.82	200	615	10.43
	4.82	200	619	10.20
	4.82	200	623	9.98
	4.82	200	614	10.47
	4.82	200	609	10.76
	4.82	200	602	11.04
	4.82	200	593	11.51

Tab.6. Viscosity of melts along the anorthite-diopside join

Sample	T (K)	Log η (Pa·s)	P (MPa)
An ₁₀₀	1154	10.88	0.1
	1145	11.25	0.1
	1165	10.42	0.1
	1128	11.60	50
	1138	11.25	50
	1148	10.82	50
	1158	10.38	50
	1138	11.45	100
	1148	11.03	100
	1158	10.61	100
	1128	11.58	200
	1138	11.13	200
	1148	10.63	200
	1158	10.24	200
	1128	11.54	300
	1138	11.26	300
	1148	10.75	300
	1158	10.33	300
	1138	11.10	400
	1148	10.69	400
1158	10.32	400	
An ₇₅ Di ₂₅	1080	11.14	50
	1102	10.24	50
	1114	9.85	50
	1080	11.32	100
	1103	10.36	100
	1113	9.95	100
	1127	9.45	100
	1080	11.32	200
	1102	10.37	200
	1114	9.94	200

	1102	10.55	300
	1113	10.11	300
	1128	9.58	300
	1078	11.43	400
	1102	10.55	400
	1114	10.08	400
An ₅₀ Di ₅₀	1055	10.78	0.1
	1068	10.27	0.1
	1038	11.48	0.1
	1029	11.92	0.1
	1048	11.10	0.1
	1018	12.41	0.1
	1008	12.86	0.1
	1043	11.37	0.1
	1064	10.52	0.1
	1081	9.99	0.1
	1089	9.61	0.1
	1052	10.94	50
	1067	10.37	50
	1077	9.99	50
	1091	9.45	50
	1052	11.09	100
	1062	10.60	100
	1077	10.00	100
	1097	9.23	100
	1100	9.10	100
	1047	11.27	200
	1057	10.77	200
	1061	10.63	200
	1071	10.17	200
	1082	9.81	200
	1092	9.44	200
	1067	10.48	200
	1059	10.89	300
	1072	10.55	300
	1080	10.15	300
	1071	10.47	300
	1067	10.58	400
	1073	10.43	400
	1063	10.74	400
	1054	11.12	400

An ₂₅ Di ₇₅	1030	10.57	50
	1046	9.94	50
	1056	9.53	50
	1035	10.38	50
	1033	10.89	100
	1043	10.37	100
	1054	9.94	100
	1033	10.81	100
	1032	10.81	200
	1041	10.35	200
	1047	10.13	200
	1053	9.96	200
	1022	11.22	200
	1022	11.29	300
	1037	10.64	300
	1052	9.98	300
	1041	10.41	300
	1037	10.69	400
	1046	10.38	400
	1032	11.01	400
Di ₁₀₀	1017	10.74	0.1
	1028	10.25	0.1
	999	11.62	0.1
	989	12.06	0.1
	979	12.75	0.1
	1032	10.48	200
	1043	10.04	200
	1053	9.57	200
	1069	8.89	200
	1036	10.44	200
	1027	10.97	200
	1047	10.37	300
	1057	9.91	300
	1066	9.44	300
	1046	10.59	400
	1055	10.18	400
1065	9.69	400	

Viscosities at 0.1 MPa were measured with the creep apparatus of Neuville and Richet (1991)

Tab.7. Viscosity of alkali silicate melts

	T (K)	$\log\eta$ (Pa·s)	P (MPa)
LNKS	624	10.91	50
	637	9.92	50
	641	9.58	50
	625	11.02	100
	637	10.01	100
	647	9.31	100
	624	11.20	150
	631	10.44	150
	636	10.02	150
	647	9.28	150
	626	11.07	200
	637	10.11	200
	630	10.56	200
	626	11.10	200
	638	10.00	200
	646	9.50	200
	626	11.15	300
	631	10.60	300
	637	10.40	300
	641	9.95	300
626	11.08	340	
LNK2S	714	11.08	50
	723	10.62	50
	733	10.21	50
	742	9.83	50
	715	11.06	100
	735	10.19	100
	742	9.90	100
	723	10.63	100
	721	10.62	200
	731	10.14	200
	713	10.96	200
	734	10.02	200
	744	9.63	200

	733	10.37	300
	743	9.94	300
	722	10.79	300
	706	11.30	400
	733	10.29	400
	743	9.84	400
LNK3S	731	10.90	100
	743	10.39	100
	753	10.01	100
	763	9.65	100
	728	11.21	200
	738	10.67	200
	747	10.23	200
	757	9.86	200
	753	10.19	300
	731	11.23	300
	743	10.68	300
	753	10.25	300
	764	9.85	300
	733	11.09	300
	732	11.04	400
	743	10.68	400
	753	10.27	400
	763	9.89	400
	733	11.08	400
LNK4S	734	11.09	50
	757	10.22	50
	767	9.88	50
	744	10.66	50
	734	11.17	100
	757	10.20	100
	765	9.95	100
	743	10.73	100
	735	10.98	200
	745	10.52	200
	755	10.12	200
	757	10.08	200
	771	9.74	200

	733	11.13	300
	735	11.00	400
	756	10.20	400
	766	9.82	400

References

- Akella, J., Ganguly, J., Grover, R., and Kennedy, G., (1973) Melting of lead and zinc to 60 kbar. *Journal of Physics and Chemistry of Solids*, 34, 631-636.
- Angell, C.A., Ngai, K.L., McKenna, G.B., McMillan, P.C. and Martin, S.W., (Sep. 2000). Relaxation in glass forming liquids and amorphous solids. *Journal of Applied Physics*, 88 n.º6, 3113-3157.
- Behrens, H., Schulze, F., (2003) Pressure dependence of melt viscosity in the system $\text{NaAlSi}_3\text{O}_8 - \text{CaMgSi}_2\text{O}_6$. *American Mineralogist*, 88, 1351-1363.
- Behrens, H., Stuke A., (2003) Quantification of H_2O contents in silicate glasses using IR spectroscopy – a calibration based on hydrous glasses analyzed by Karl-Fisher titration. *Glass Sci. Technol.*, 76 n.º.4, 176-189.
- Behrens, H., Romano, C., Nowak, M., Holtz, F., Dingwell, D.B. (1996). Near-infrared spectroscopy determination of water species in glasses of the system MAI_3O_8 (M=Li, Na, K): an interlaboratory study. *Chemical Geology*, 128, 41-64.
- Böse, N., Klingenberg, G., and Meerlender, G., (2001). Viscosity measurements of glass melts – Certification of reference material. *Glastechnische Berichte Glass Sci. technol.*, 74, n.º.5, 115-126.
- Brearley, M., Dickinson, J.E., and Scarfe, C.M., (1986). Pressure dependence of melt viscosities on the join diopside-albite. *Geochimica et Cosmochimica Acta*, 50, 2563-2570.
- Brückner, R., Yue, Y., and Habeck A. (1994). Determination of the rheological properties of high-viscous glass melts by cylinder compression method. *Glastechnische Berichte Glass Sci. technol.*, 67 n.º5, 114-117.
- Debenedetti, P. G., and Stillinger, F. H., (March 2001). Supercooled liquid and the glass transition. *Nature*, 410, 259-267.

- Deubener, J., Müller, R., Behrens, H., and Heide, G., (2003). Water and the glass transition temperature of silicate melts. *Journal of Non-Crystalline Solids*, 330, 268-273.
- Dingwell, D. B., and Webb S., (1990). Relaxation in silicate melts. *European Journal of Mineralogy*, 2, 427.
- Dudley, J. D., and Hall, H. T., (1960) Experimental Fusion Curves of Iridium and Tin to 105,000 Atmospheres. Reprinted from *The Physical Review*, 118, n°5, 1211-1216, June 1.
- Euler von, R., Winkler, G. F., and Lahn, M., (1957). Über die viskositäten von gesteins- und silikatschmelzen. *Glastechnische Berichte Glass Sci. technol.*, 30 n° 8, 325-332.
- Giordano, D., Dingwell, D.B., (2003). Non-Arrhenian multicomponent melt viscosity: a model. *Earth and Planetary Science Letters*, 208, 337-349.
- Giordano, D., Romano, C., Papale, P., and Dingwell, D.B., (2004). The viscosity of trachytes, and comparison with basalts, phonolites, and rhyolites. *Chemical Geology*, 213, 49-61.
- Goto, A., Taniguchi, H. and Kitakaze A., (2005). Viscosity measurements of hydrous rhyolitic melts using fiber elongation method. *Bulletin of Volcanology*, online first DOI: 10.1007/s00445-004-0401-7
- Hess, K.U., Dingwell, D.B., and Webb, S.L., (1995). The influence of excess of alkalis on the viscosity of a haplogranitic melt. *American Mineralogist*, 80, 297-304.
- Hess, K.U., and Dingwell, D.B., (1996). Viscosities of hydrous leucogranitic melts: A non-Arrhenian model. *American Mineralogist*, 81, 1297-1300.

- Holtz, F., Roux, J., Ohlhorst, S., Behrens, H., and Schulze, F., (1999). The effect of silica and water on the viscosity of hydrous quartzofeldspathic melts. *American Mineralogist*, 84, 27-36.
- Koepke, J. and Behrens, H., (2001). Trace element diffusion in andesitic melts: An application of synchrotron X-ray fluorescence analysis. *Geochimica et Cosmochimica Acta*, 65, 1481-1498.
- Kuryaeva, R. G., (2004). Degree of polymerization of alluminosilicate glasses and Melts. *Glass Physics and Chemistry*, 30 n°2, 157-166.
- Kushiro, I., Yoder, H.S and Mysen, B.O. (1976). Viscosities of basalt and andesite melts at high pressure. *Journal of Geophysical Research*, 31/35, 6351-6356.
- Kushiro, I (1978). Density and viscosity of hydrous calc-alkalic andesite magma at high pressure. *Geophysical Laboratory Carnegie Institution*.
- Lange, R.A., The effect of H₂O, CO₂ and F on the density and viscosity of silicate melts, *Rev. Mineralogy*, 1994, 30, 331 – 369.
- Lees, J., and Williamson, B.H.J., (1965) Combined very high pressure high temperature calibration of the tetrahedral anvil apparatus, fusion curves of zinc, aluminium, germanium, and silicon to 60 kilobars. *Nature*, 208, 278-279.
- Liebske, C., Behrens, H., Holtz, F., and Lange, R., (2003). The influence of pressure and composition on the viscosity of andesitic melts. *Geochimica et Cosmochimica Acta*, 67, 473-485.
- Mazurin O.V., Startsev, Y.K. and Stoljar S.V., (1982). Temperature dependence of viscosity of glass-forming substances at constant fictive temperatures. *J. Non-Cryst. Solid* 53, 105–114.
- Meerlender, G., (1974). Viskositäts-Temperatur-Verhalten des Standardglases I der DGG. *Glastechnische Berichte Glass Sci. technol.*, 47, n°1, 1-3.

- Mesko, M.G. and Shelby, J.E., (2001). Water solubility and diffusion in alkali silicate melts. *Phys. Chem. Glasses*, 42, 173-178.
- Mori, S., Ojami, E., Suzuki, A., (2000). Viscosity of albite melt to 7 GPa at 2000 K. *Earth and Planetary Science Letters*, 175, 87-92
- Mysen, B.O., Virgo, D. and Seifert, F.A., (1985). Relationship between properties and structure of aluminosilicate melts. *American Mineralogy*, 70, 88-105.
- Neuville, D.R, Etude des propriétés thermodynamiques et rhéologiques des silicates fondus. Thèse de doctorat de l'Université Paris 7.
- Neuville, D.R., and Richet, P., (1991). Viscosity and mixing in molten (Ca, Mg) pyroxenes and garnets. *Geochimica et Cosmochimica Acta*, 55, 1011-1019.
- Nowak, M., and Behrens, H., (2001). Water in rhyolitic magmas: getting a grip on a slippery problem. *Earth and Planetary Science Letters*, 184, 515-522.
- Ochs, F.A., Lange, R.A., (1999). The density of hydrous magmatic liquids , *Science*, 283 (5406), 1314.
- Prado, M. O., Fredericci, C., and Zanutto, E. D., (2003). Isothermal sintering with concurrent crystallization of polydispersed soda-lime-silica-glass beads. *Journal of Non-Crystalline Solids*, 331, 145-156.
- Prado, M. O., Fredericci, C., and Zanutto, E. D., (2003). Non-isothermal sintering with concurrent crystallization of polydispersed soda-lime-silica-glass beads. *Journal of Non-Crystalline Solids*, 331, 156-167.
- Priven, A. I., (2001). Calculation of temperature dependences of the viscosity and volume relaxation time for oxide glass-forming melts from chemical composition and dilatometric glass transition temperature. *Glass Physics and Chemistry*, 27 n° 6, 527-542.
- Rapp, D.B. and Shelby, J.E., (2003). Water diffusion and solubility in soda-lime-silica melts. *Phys. Chem. Glasses*, 44, 394-400.

- Reid, J.E., Suzuki, A., Funakoshi, I.K., Terasaki, H., Brent, P., Rubie, D.C., Ohtani, E., (2003). The viscosity of CaMgSi₂O₆ liquid at pressure up to 13 GPa. *Physics of the Earth and Planetary Interiors*, 139, 45-54.
- Richet, P., (1984). Viscosity and configurational entropy of silicate melts. *Geochimica et Cosmochimica Acta*, 48, 471-483.
- Richet, P., Lejeune, A.M., Holtz, F., and Roux, J., (1996). Water and the viscosity of andesite melts. *Chemical Geology*, 128, 185-197.
- Richet, P., (2002). Enthalpy, volume and structural relaxation in glass-forming silicate melts. *Journal of Thermal Analysis and Calorimetric*, 69, 739-750.
- Russell, J.K., Giordano, D., Dingwell, D.B., (2003). High-temperature limits on viscosity of non-Arrhenian silicate melts. *American Mineralogist*, 88, 1390-1394.
- Sakka, S., Matusita, K., Watanabe, T., and Kamiya, K., (1981). Effects of small amounts of water on the viscosity, glass transition temperature and Vickers Hardness of silicate glasses. *Yogyo-Kyokai-Shi*, 89, 577-584.
- Sanditov, D. S., Badmaev, S. S., Tsydypov, S. B., and Sanditov, mB. D., (2003). A model of fluctuation free volume and the valence-configurational theory of viscous flow of alkali silicate glasses. *Glass Physics and Chemistry*, 29 n°. 1, 2-6.
- Scherer, G. W., (1984). Use the Adam-Gibbs equation in the analysis of structural relaxation. *Journal of the American Ceramic Society*, 67, 504-511.
- Scholze, H., (1988) *Glas: Natur, Struktur und Eigenschaften*. Springer Verlag.
- Schulze, F., (2000). Untersuchung zum Einfluß von druck und gelöstem Wasser auf die Viskosität silikatischer Schmelzen – Anwendung eines "parallel-plate"-viscosimeter unter hohen Drücken. PhD thesis.
- Schulze, F., Behrens, H., Holtz, F., Roux, J., and Johannes, W., (1996). The influence of H₂O on viscosity of haplogranitic melt. *American Mineralogist*, 81, 1155-1165.

- Schulze, F., Behrens, H., and Hurckuck W., (1999). Determination of the influence of pressure and dissolved water on viscosity of high viscous melts-application of a new parallel-plate viscometer. *American Mineralogist*, 84, 1512-1520.
- Shaw, H.R., (1962). Obsidian-H₂O viscosities at 1000 and 2000 bars in the temperature range 700 to 900°C. *Journal of Geophysical Research*, 68(23), 6337-6343.
- Shaw, H. R., (1972). Viscosities of magmatic silicate liquids: An empirical method of prediction. *American Journal of Science*, 272, 870-893.
- Shelby, J.E. (2005). *Introduction to glass science and technology*. 2nd edition, Springer.
- Siewert, R., Büttner, H., and Rosenhauer M., (1998). Experimental investigation of thermodynamic melting properties in the system NaCl-KCl at pressures of up to 7000 bar. *Neues Jahrbuch für Mineralogie Abhandlungen*, 172, 2/3, 259-278.
- Solvang, M., Zue, Y. Z., Jensen, S. L., Dingwell, D. B., (2004). Rheological and thermodynamic behaviours of different calcium aluminosilicate melts with same non-bridging oxygen content. *Journal of Non-Crystalline Solids*, 336, 179-188.
- Stebbins, J.F., McMillan, P.F., and Dingwell, D.B., (1995). Structure, dynamics and properties of silicate melts. *Mineralogical Society of America. Reviews in Mineralogy*, 32.
- Stolper, E.M., (1982). The speciation of water in silicate melts. *Geochim. Cosmochim. Acta* 46, 2609-2620.
- Stuke, A., Behrens, H., Schmidt, B. and Dupree, R. (submitted). H₂O speciation in float glass and soda lime silica glass. *Chemical Geology (Special issue)*.
- Suzuki, A., Ohtani, E., Funakoshi, K., and Terasaki, H., (2002). Viscosity of albite melt at high pressure and high temperature. *Physics and chemistry of minerals*, 29, 159-165.

- Suzuki, A., Ohtani, E., Terasaki, H., and Funakoshi, K., (2005). Viscosity of silicate melts in CaMgSi₂O₆-NaAlSi₂O₆ system at high pressure. *Physics and Chemistry of Minerals*, DOI 10.1007/s00269-005-0452-0.
- Tammann, G., (1933). *Der Glaszustand*. Voss, Leipzig, pg. 123.
- Taniguchi, H., (1995). Universal viscosity equation for silicate melts over wide temperature and pressure ranges. *Journal of Volcanology and Geothermal Research*, 66, 1-8.
- Taniguchi, H., (1992). Entropy dependence of viscosity and the glass-transition temperature of melts in the system diopside-anorthite. *Contrib. Mineral Petrol.*, 109, 295-303.
- Thies, M., (2002). *Herstellung un rheologische Eigenschaften von pörosen Kalk-Natron-Silicatschmelzen*. PhD thesis, Technischen Universität Berlin.
- Tinker D., Lesher, C.E., Baxter, G.M., Uchida, T., and Wang Y., (2004). High-pressure viscometry of polymerized silicate melts and limitations of the Eyring equation. *American Mineralogist*, 89, 1701-1708.
- Xue, X. and Kanzaki, M., (2004). Dissolution mechanisms of water in depolymerized silicate melt: Constraints from ¹H and ²⁹NMR spectroscopy and ab initio calculations. *Geochimica et Cosmochimica Acta*, 68, 5027-5057.
- Yoder, H.S., Jr. (1950). High-low quartz inversion up to 10000 bars. *Trans. Am. Geophys. Un.* 31, 827-835.
- Witthington, A., Richet, P., Behrens, H., Holtz, F. and Scaillet, B., (2003). Experimental temperature-X(H₂O)-viscosity relationship for leucogranites and comparison with synthetic silicic liquids. *Trans. of the Royal Soc. of Edinburgh: Earth Sciences*, 95, 59-71.

- Witthington, A., Richet, P. and Holtz, F., (2000). Water and viscosity of depolymerized aluminosilicate melts. *Geochimica et Cosmochimica Acta*, 64, 3725-3736.
- Witthington, A., Richet, P., Linard, Y. and Holtz, F., (2001). The viscosity of hydrous phonolites and trachytes. *Chemical Geology*, 174, 209-224.
- Zanutto, E. D., Gupta, P. K., (1999) Do cathedral glasses flow? Additional remarks. *American Journal of Physics*, 67 (3), 260-262.
- Zhang, Y.X., Xu, Z.J. and Liu, Y., (2003). Viscosity of hydrous rhyolitic melts inferred from kinetic experiments, and a new viscosity model. *American Mineralogist*, 88, 1741-1752.